Molecular beacon nanosensors for live cell detection and tracking differentiation and reprogramming

Ilieva, Mirolyuba

Publication date:
2013

Document Version
Publisher's PDF, also known as Version of record

Technical University of Denmark

Molecular beacon nanosensors for live cell detection and tracking differentiation and reprogramming

Mirolyuba Ilieva

DTU Nanotech
Department of Micro- and Nanotechnology

PhD Thesis

April 2013

Mirolyuba Simeonova Ilieva

Molecular beacon nanosensors for live cell detection and tracking differentiation and reprogramming

PhD Thesis

April 2013

Supervisor Assoc. Prof. Martin Dufva

Co-supervisor Professor Jenny Emnéus

Department of Micro- and Nanotechnology Technical University of Denmark

Abstract

High-sensitive and high-affinity methods to measure gene expression inside living cells have proven to be invaluable in regards to understanding fundamental processes such as cell differentiation, reprogramming, regeneration and cancer genesis. One tool for transcription visualization on single cell level is molecular beacons (MBs). They are stem-loop structured antisense oligonucleotide probes labelled with a reporter fluorophore at one end and with quencher at the other end. Upon hybridization with complementary target, hydrogen bonds between stem nucleotide bases brake, resulting in separation of fluorophore from quencher and thereby emission of a fluorescent signal that can be detected.

In this project the usability and applicability of MBs for live cell detection and tracing of gene expression was demonstrated. MBs library targeting gene markers for pluripotent stem cells as well as markers for different stages of cell differentiation into the three germ lineages were designed. The focus was on stem cell differentiation into neuronal lineage as well as reprogramming into a more immature state after plasmid transfection or under the influence of the environment and growth conditions. We have been able to detect gain of expression of neuronal markers during differentiation of embryonic mesencephalon derived cells (LUHMES) into dopamine neurons. Loss of expression of stem cell markers was also observed suggesting that MBs are able to dissociate from target mRNA and regenerate from open to closed state within living cells. Using MBs targeting pluripotent stem cell markers we demonstrated reverse into a more immature state of LUHMES induced by neurosphere-like growth conditions. Moreover, we have been able to trace localisation of this particular population during differentiation and thus demonstrate the usability of MBs for monitoring cell behaviour within 3D clusters. Finally, MBs detection of expression of human pluripotent markers after reprograming of adult somatic cells with plasmid codding for mouse transcription factors was demonstrated.

In conclusion, the method of using transfected MBs is an easy and rapid way to detect gene expression. Target cells do not need to be genetically modified. Furthermore, MBs are able to detect both up- and down regulation of gene expression on the single cell level and dynamic tracing of specific cell populations within 3D clusters.

Resumé

Metoder med høj følsomhed og høj affinitet til at måle genekspression i levende celler har vist sig at være uvurderlige med hensyn til at forstå fundamentale processer, såsom celledifferentiering, -reprogrammering og -regenerering samt cancer genesis. Et redskab for visualisering af transkription på enkelcelle niveau er molekylære beacons (MBs). Det er antisense oligonukliotide prober med en hårnålestruktur mærket med en reporter fluorofor i den ene ende og en quencer i den anden ende. Ved hybridisering med komplimentær target, brydes hydrogenbindingerne mellem nukleotid baserne i de to parallelle strenge i hårnålestukturen, resulterende i adskillelse af fluorofor fra quencer og dermed emission af et fluorescerende signal, der kan detekteres.

I dette studie er brugbarheden og anvendeligheden af MBs for detektion og sporing af genekspression demonstreret. Et bibliotek af MBs, målrettet genmarkører for pluripotente stamceller såvel som markører for forskellige stadier af celledifferentiering til de tre kimcellelinier, er designet. Focus var på stamcelledifferentiering til neuronale linier såvel som reprogrammering til mere umodne stadier efter plasmid transfektion eller under indflydelse af miljø og vækstbetingelser. Vi har været i stand til at detektere stigning i ekspression af neuronale markører under differentiering af embyonale mesencephalon udledte celler (LUHMES) til dopamin neuroner. Tab af ekspression af stamcellemarkører blev også observeret tydende på, at MBs er i stand til at dissociere fra target mRNA og regenerere fra åbent til lukket stadie i levende celler. Ved brug af MBs målrettet pluripotente stamcellemarkører demonstrerede vi tilbagevending til et mere umodent stadie af LUHMES induceret ved neurosphere-lignende vækstbetingelser. Derudover har vi været i stand til at spore lokalisering af *den* bestemte population under differentiering og dermed demonstrere brugbarheden af MBs for monitorering af celle opførelse indeni 3D klynger. Endelig blev detektion af ekspression af humane pluripotente markører efter reprogrammering af voksen somatiske celler med plasmid kodende for mussetranskriptionsfaktorer demonstreret ved brug af MBs.

Afslutningsvis kan det konkluderes, at metoden med brug af MBs er en let og hurtig måde til at bestemme genekspression. Målcellerne behøver ikke at blive genetisk modificeret. Yderligere er MBs i stand til at detektere både op- og nedregulering af genekspression på enkelcelle niveau samt dynamisk sporing af specifikke cellepopulationer i 3D klynger.

Preface

The work described in this thesis has been carried out in the Fluidic Array Systems and Technology (FAST) group at the Department of Micro- and Nanotechnology (DTU Nanotech), Technical University of Denmark (DTU) in the time period from May 2010 to April 2013. The work has been supervised by main supervisor assoc. prof. Martin Dufva and co-supervisor prof. Jenny Emnéus, Bioanalytics group, DTU Nanotech. The work was supported by FTP grant 09-070568.

The thesis consists from seven chapters. Chapter IV and Chapter VII are based on the findings described in more details in submitted manuscripts applied as Appendix 1 and 2.

Acknowledgements

Here is the place to express my gratitude to all people that have been part of my life during this project. First, I would like to thank my supervisor Martin Dufva for the opportunity to finally start a PhD study, for being positive always when I have been in pessimistic mood when the results are not as I expected, and to stay calm when I fulminate against journal editors, reviewers and other staff. Thanks to Mette - for taking care of the cells when I was absent, for the help with translation, and together with Maciej for the help with the microscope imaging. Without you beacons would never shine. I would like to thank to prof. Ole Hansen for the patience to listen to my popular explanations of biological events for physicists. Thanks to Paolo – my project mate - for the beacons *in vitro* characterization and presentation of my poster to Hawaii conference. Thanks to the lab technicians – Ina, Ole, Lotte, and Lene – for the daily help and for that they always smile and say "Hi". Thanks to my office mates for keeping peaceful and silent atmosphere in the office and to endure the open window when my brain needed oxygen and outside was -10.

Thanks to my family – my daughter Iliana (who allays sent greetings to the cells-it works!) and my husband Dimitar for the patience (shopping, babysitting and good cooking), my mother and brother – for keeping competitive spirit in me, and all friends for supporting me during this study.

Finally, I would like to thank two people who I lost recently – my sister who always believed in me more than myself, and my father – who always wanted to have a "Doctor" in the family. I did it!

Mira

Table of contents

List of figures

List of Abbreviations

Abbreviation	Description
AP	alkaline phosphatase
ASC	adipose derived stem cells
CAT	chloramphenicol acetyltransferase
cDNA	complementary DNA
DM	differentiation medium
DMEM	Dulbecco's modified Eagle medium
DPBS	Dulbecco's phosphate-buffered saline
EB	embryoid body
ESC	embryonic stem cells
FBS	fetal bovine serum
FGF	fibroblast growth factor
GAPDH	glyceraldehyde 3-phosphate dehydrogenase
GDNF	glial cell derived neurotrophic factor
GFP	green fluorescent protein
GM	growth medium
GUS	β-glucuronidase
hGH	human growth hormone
HIF	hypoxia induced factor
iPSC	induced pluripotent stem cells
Klf4	Kruppel-like factor 4
LUHMES	Lund human mesencephalic cell line
MAP2	microtubule-associated protein 2

MB	molecular beacon
MEF	mouse embryonic fibroblasts
MSC	mesenchymal stem cells
NeuN	neuronal nuclei antigen
p-L-o	poly-L-ornitine
qRT-PCR	quantitative reverse transcription polymerase chain reaction
ROI	region of interest
S/N	signal-to-noise ratio
SEM	standard error of the mean
SHH	sonic hedgehog
SLO	streptolysin O
TCEP	tris(2-carboxyethyl)phosphine
TH	tyrosine hydroxylase

Publication list

Submitted Manuscripts (part of thesis)

1. Dynamic tracking of expression of neuronal markers in living human neurons detected using molecular beacons. **Ilieva M.**, Della Vedova P., Hansen O., Dufva M. Submitted manuscript to Biomaterials (Appendix 1)

2. Sox2 and Oct4 mRNA-expressing cells, detected by molecular beacons, localize to the centre of neurospheres during differentiation. Ilieva M., Dufva M. Submitted manuscript to PLoS One (Appendix 2)

Peer-reviewed conference proceedings (part of thesis)

1. Molecular Beacon Technology Based Sensor for Real-Time Detection and Tracking Neural Stem Cell Differentiation. **Mirolyuba Ilieva**, Paolo Della Vedova, Martin Dufva. 2012 IEEE-EMBS Micro and Nanotechnology in Medicine Conference, The Westin Maui Resort and Spa, Ka'anapali, Hawaii (Appendix 3)

2. Nanomachine Based Optical Sensors. Paolo Della Vedova, **Mirolyuba Ilieva**, Ole Hansen, Martin Dufva 2012. IEEE-EMBS Micro and Nanotechnology in Medicine Conference, The Westin Maui Resort and Spa, Ka'anapali, Hawaii (Appendix 3)

Conference contribution (part of thesis)

1. Molecular beacon – tool for real time studying gene activity in stem cells. **Ilieva M.**, Dufva M. EMBL Conference Stem cells in cancer and regenerative medicine. 29 Aug – 1 Sep 2012. Heidelberg, Germany

Manuscripts in preparation (to some extent part of thesis)

1. Biochemical characterization of RNA and DNA based molecular beacons. Paolo Della Vedova, **Mirolyuba Ilieva**, Ole Hansen, Martin Dufva

2. Actuating molecular beacon hybridization status by an external radio frequency field. Paolo Della Vedova, **Mirolyuba Ilieva**, Martin Dufva, Ole Hansen

3. Signal amplification using nested molecular beacons. Paolo Della Vedova, **Mirolyuba Ilieva**, Ole Hansen, Martin Dufva

Chapter I. Methods for detecting gene expression

1. Introduction

Gene expression is the process by which information from a gene is used in the synthesis of a functional gene product. The products of gene expression are proteins and in non-protein coding genes the product is a functional RNA (ribosomal, transfer, small nuclear RNA). Gene expression is the most fundamental level at which the genotype gives rise to phenotype. The thousands of genes expressed in a particular cell determine what that cell can do. Each step in the flow of information from DNA to RNA to proteins provides the cell with a potential control point for self-regulating its functions by adjusting the amount and type of proteins it produces.

The amount of particular protein in a cell reflects the balance between protein synthetic and degradative biochemical pathways. Protein production starts at transcription (DNA to RNA) and continues with translation (RNA to proteins). The control of these processes plays a critical role in determining what proteins are present in the cell, in what amount, and on what time. The way in which a cell processes its RNA transcripts and newly made proteins also influences protein levels.

The amount and types of mRNA molecules in a cell reflect the function of that cell. RNA transcription point makes an efficient control point because many proteins can be made from a single mRNA molecule. Transcript processing provides an additional level of regulation for eukaryotes – transcripts are modified in the nucleus before they are exported to the cytoplasm for translation. The primary transcripts in eukaryotes contain intervening sequences called introns, and they are removed before the mature mRNA leaves the nucleus. The remaining regions of the transcript, which include the protein-coding regions (exons), are splice together to produce mature mRNA. Due to alternative splicing – a process in which particular exons of a gene may be included within, or excluded from the final, processed mRNA from that gene – different isoforms of the protein may exist. Eukaryotic transcripts are also modified at their ends, which affects their stability and translation.

On the degradative side of the balance, cells can rapidly adjust their protein levels through the enzymatic breakdown of RNA transcripts and existing protein molecules. Both of these actions results in decreased amounts of certain proteins. Often this breakdown is related to specific events in the cell such as cell dividing and differentiation.

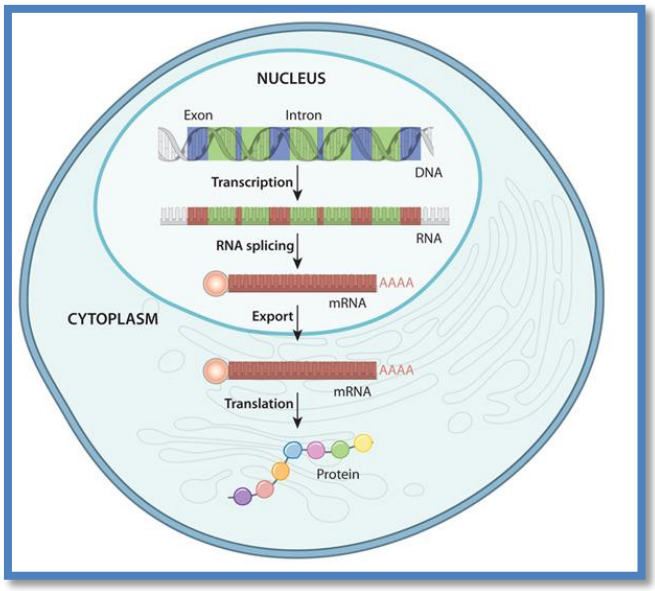

Figure 1. An overview of the flow of information from DNA to protein in a eukaryotic cell (Nature Education, 2010)

The variety of gene expression profiles characteristic of different cell types arise because these cells have distinct sets of transcription regulators. Some of these regulators work to increase transcription, whereas others prevent or suppress it.

Transcription begins when an RNA-polymerase binds to a promoter sequence on the DNA molecule. Other DNA sequences, known as enhancer sequences, also play an important role in transcription providing binding sites for regulatory proteins that affect RNA polymerase activity. Binding of regulatory proteins to an enhancer sequence causes a shift in chromatin structure that either promotes or inhibits RNA polymerase and transcription factor binding.

Some regulatory proteins affect the transcription of multiple genes. This occurs because multiple copies of the regulatory protein binding sites exist within the genome of a cell. Regulatory proteins can have different roles for different genes, and this is one mechanism by which cells can coordinate the regulation of many genes at once.

Different cell types express characteristic sets of transcriptional regulators. As multicellular organisms develop, different sets of cells within these organisms turn specific combinations of regulators on and off. Such developmental patterns are responsible for the variety of cell types present in the mature organism.

Regulation of the two main steps of protein production – transcription and translation – is critical to this adaptability. Cells can control which genes get transcribed and which transcripts get translated.

The ability to quantify the level at which a particular gene is expressed within a cell, tissue or organism promise to impulse the advancement in molecular biology, medical research, diagnostics and therapy. Many methods have been developed to measure gene expression levels between different cell populations. This chapter describes the commonly used methods for gene expression detection.

2. Northern Blotting (NB)

NB is a technique that is used for detection of RNA where the total cellular RNAs are extracted and fractioned according to size by gel electrophoresis. The RNAs are transferred to a filter and detected by hybridization with radioactive probe [1]. The principle of the method is present in figure 2.

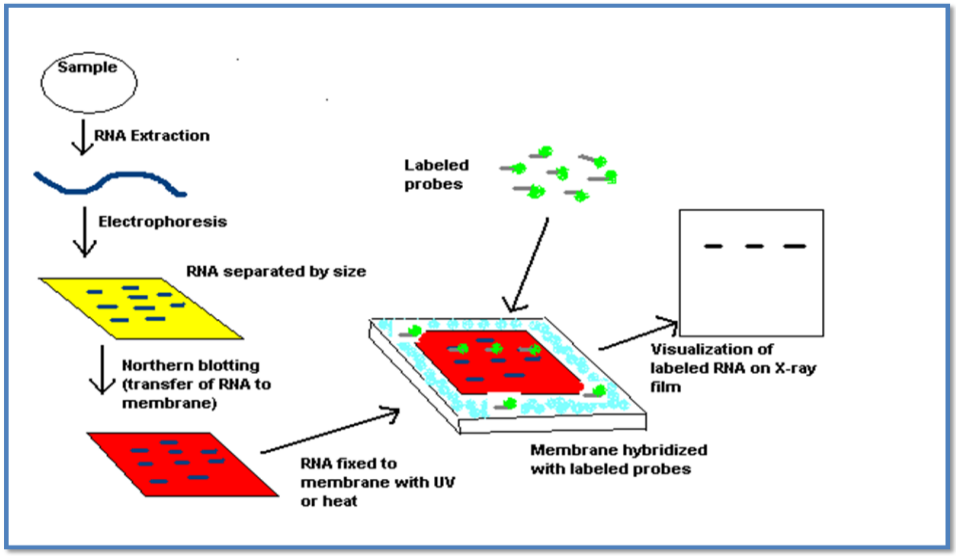

Figure 2. Schematic presentation of Northern blot technique (Wikipedia)

With NB it is possible to observe cellular control over structure and function by determining the particular gene expression levels during differentiation, morphogenesis,

as well as abnormal or diseased conditions [2]. Standard NB procedure is less sensitive than nuclease protected assays and RT-PCR. Approximately 100 000 copies of RNA sequence are required for detection by blot hybridization. It is also highly sensitive to RNA degradation method. The quality of the data and the ability to quantitate expression are severely impaired if RNA samples are even slightly degraded. Multiple probe analysis is also problematic. To detect more than one target it is usually necessary to strip the initial probe before hybridizing with a second probe. Thus results derived from progressive rounds of blotting may be less accurate, since harsh treatment is required to strip conventional probes from blots. Moreover NB does not measure transcription rates or RNA stability, only steady state mRNA accumulation levels. Last but not least the chemicals which are used in this technique can be harmful for the researcher's health because they contain formaldehyde, ethidium bromide, radioactive material and ultra violet light.

3. FISH

Fluorescent in situ hybridization is a cytogenetic technique that was first used to detect and localize the presence of specific DNA sequences on chromosomes [3]. This method can also be used to detect and localize RNA targets - mRNA, lncRNA, miRNA in cells and tissue samples [4, 5].

In this technique, samples are fixed and then hybridization is performed using a set of fluorescently labeled oligonucleotides, each complementary to a unique part of the target RNA. The principle of the method is present on figure 3.

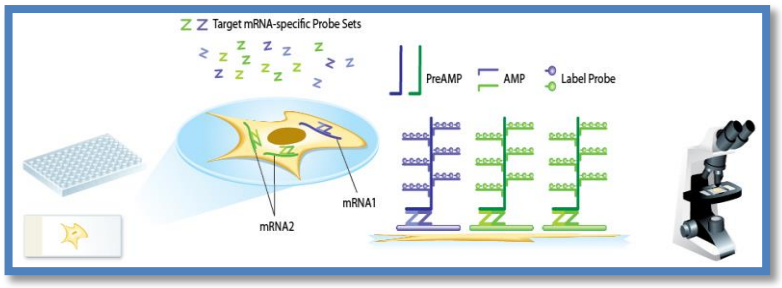

Figure 3. The principle of FISH (Wang et al. J Molec. Diag. 2012; 14:22)

4. qRT-PCR

Reverse transcription polymerase chain reaction (RT-PCR) is commonly used in molecular biology to detect RNA expression levels [6]. RT-PCR is used to clone expressed genes by reverse transcribing the RNA of interest into its DNA complement through the use of reverse transcriptase. Further RT-PCR can be utilized for quantification of RNA by incorporating real-time polymerase chain reaction (qPCR) into the technique [7]. The combined technique is described as quantitative RT-PCR (qRT-PCR). In the RT-PCR technique, the RNA template is first converted into a complementary DNA (cDNA) using reverse transcriptase. The cDNA is then used as a template for exponential amplification using PCR (figure 4.).

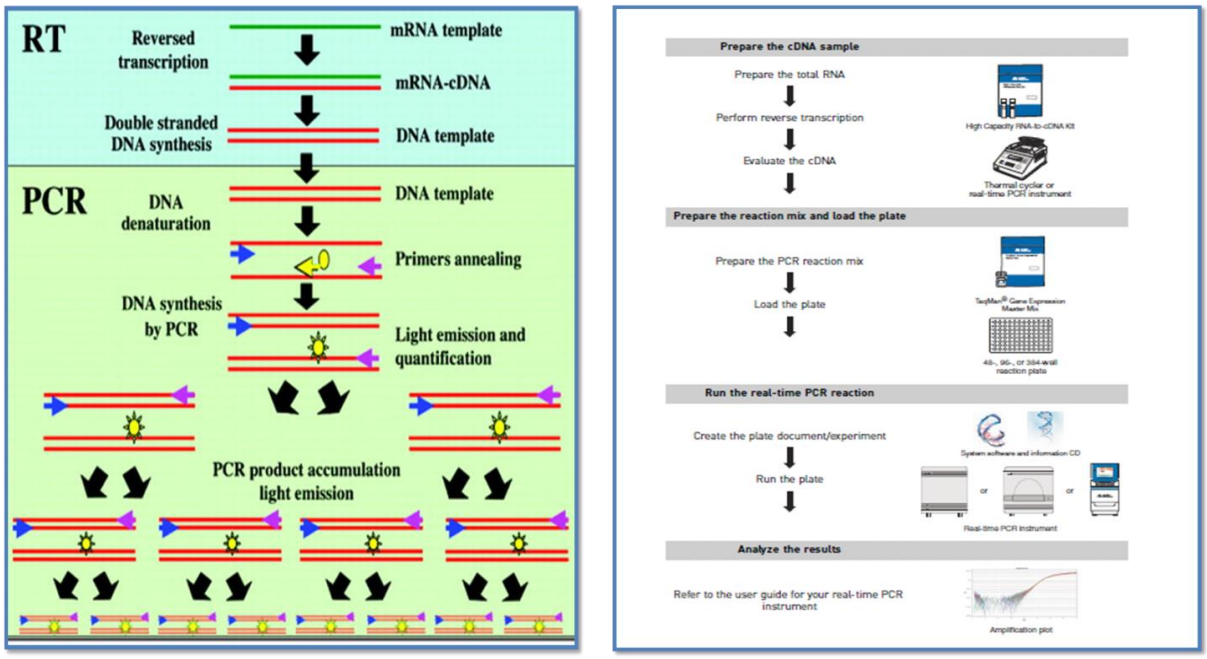

Figure 4. Steps in qRT-PCR

The use of RT-PCR for the detection of RNA transcript has revolutionized the study of gene expression in the following way – it made theoretically possible to detect the transcripts of any particular gene. It enabled sample amplification and eliminates the need of abundant starting material as in the case of NB. RT-PCR provides tolerance for RNA degradation as long as the RNA spanning the primer is intact and a reference gene is as affected by degradation as the target gene [8, 9, 10].

The emergence of novel fluorescent DNA labeling techniques have enable the analysis and detection of PCR products in real-time and has consequently led to the widespread adaptions of qRT-PCR for the analysis of gene expression. Currently, four different fluorescent DNA probes are available for real-time detection of PCR products – SYBR green, TaqMan, Molecular beacons, and Scorpions. All of them allow detection by generation of fluorescent signal. Generation of the fluorescent signal in TaqMan, MB, and Scorpions depend on Förster Resonance Energy Transfer (FRET) coupling of the dye molecule and quencher moiety to the oligonucleotide substrate [11].

SYBR green dye emits its fluorescent signal by binding to the double-stranded DNA (dsDNA) in solution. SYBR Green I exhibits little fluorescence when it is free, but its fluorescence increases up to 1000-fold when it binds dsDNA. Therefore, the intensity of the signal is proportional to the accumulated amount of the PCR product and will increase as the target is amplified (figure 5 A.). The advantages of using dsDNA-binding dyes include simple assay design – only two primers are needed. Design of the probes are not necessary due to unspecific binding of the dye to the ds DNA, which makes this technique simple to use. Ability to test multiple genes quickly without designing multiple probes (e.g., for validation of gene expression data from many genes in microarray experiment), lower initial cost, and the ability to perform a melt-curve analysis to check the specificity of the amplification reaction are other benefits of the technique.

Melt-curve analysis can be used to identify different reaction products, including nonspecific products. After completion of the amplification reaction, melt curve are generated by increasing the temperature in small increments and monitoring the fluorescent signal at each step. As the ds DNA in the reaction denature (DNA “melts”), the fluorescence decreases. The negative first derivative of the change in fluorescence is plotted as a function of temperature. A characteristic peak at the amplicon's melting temperature (T_m, the temperature at which 50% of the base pairs of a DNA duplex are separated) distinguishes it from other products such as primer-dimers, which melt at different temperatures. An example of this is shown in figure 5 B. The melt peak with a T_m of 89ºC represents the specific product. The peak with a T_m of 78ºC represents the nonspecific product.

The major drawback of DNA-binding dyes is their lack of specificity, that is, DNA-binding dyes bind to any dsDNA. As a result, the presence of nonspecific products (primer dimers) in a RT-PCR reaction may contribute to the overall fluorescence and affect the accuracy of quantification. Another consequence is that DNA-binding dyes cannot be used for multiplex reactions because fluorescent signals from different amplicons cannot be distinguished. Instead, parallel reactions can be set up to examine multiple genes, such as a gene of interest and reference gene, in a RT-PCR assay with SYBR Green I. [12].

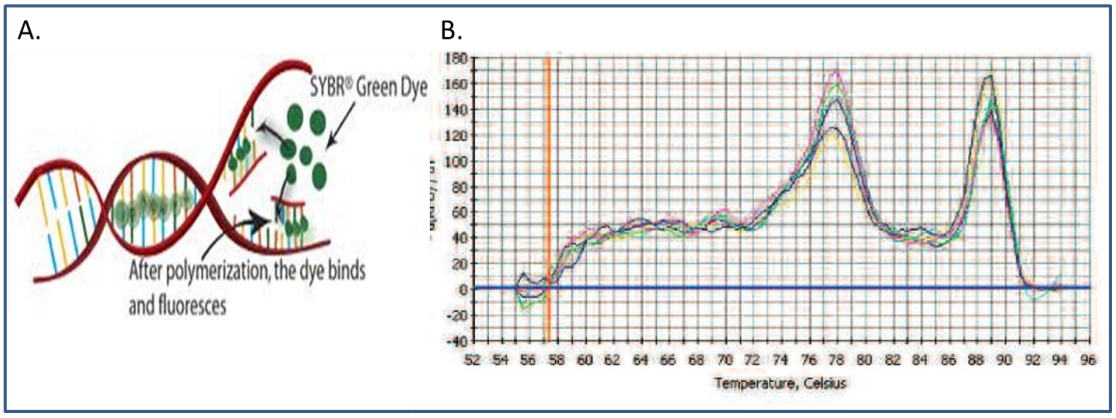

Figure 5. A. SYBR green binding to the double-stranded DNA. B. Melt-curve analysis of reaction product from a SYBR Green I assay. Melt-curve analysis can be used to distinguish specific products from nonspecific products. The negative first derivative of the change in the fluorescence is plotted as a function temperature. The two peaks indicate the T_m values of two PCR products. (BIO-RAD).

TaqMan probes (figure 6) are oligonucleotides with fluorescent dye attached to the 5'-end and a quencher to the 3'- end. During PCR amplification, the probes will hybridized to the target sequences located in the amplicon and as polymerase replicates the template with TaqMan bound, it also cleaved the fluorescent probe due to polymerase 5'-nuclease activity. The close proximity between florochrome and quencher normally prevents fluorescence from being detected through FRET. The decoupling of fluorechrome and the quencher results in the increase of intensity of fluorescence proportional to the number of the probe cleavage cycle [8, 13].

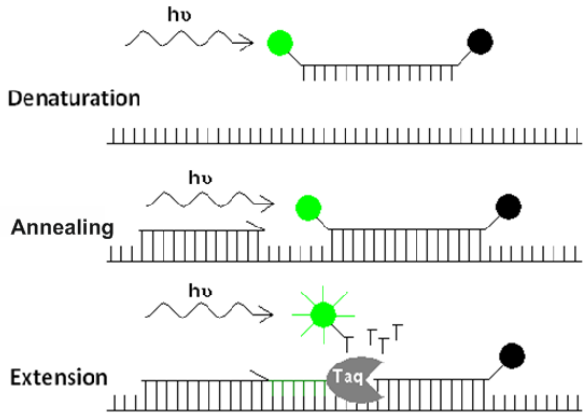

Figure 6. The TaqMan probe hybridizes between the primers in annealing step and during elongation step probe is cleaved by exonuclease activity of Taq Polymerase.

Scorpion probes (figure 7) do not fluorescent in the unhybridized state, due to the fluorescent dye on the 5'- end being quenched by the moiety on the 3' end of the probe. The 3'- end also contain a sequence that is complementary to the extension product of the primer on the 5'- end. When the Scorpion extension binds to its complement on the amplicon, the Scorpion structure opens, prevents FRET, and enables the fluorescent signal detection [14].

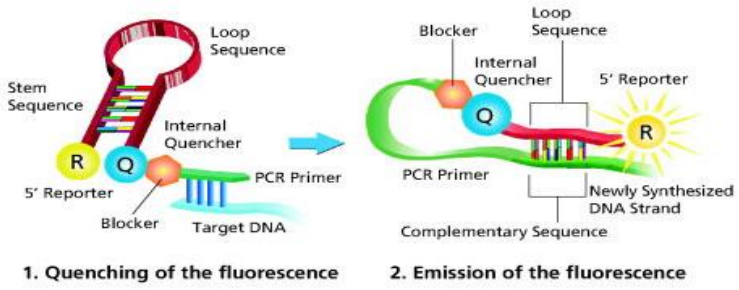

Figure 7. Scorpion probes (Sigma Aldrich)

Amplification of DNA by the polymerase chain reaction is a much more sensitive technique for detecting cellular DNA or RNA sequences than NB and FISH. Approximately 100 000 copies of a DNA or RNA sequence are required for detection by blot hybridization. In contrast, PCR can amplify single copies of DNA or RNA after reverse transcription to readily detectable levels. PCR amplification can be used to detect specific DNA or RNA molecules in very small amounts of starting material, such as extracts of single cells. This sensitivity has made PCR an important method for a

variety of applications, including the analysis of gene expression in cells available in only limited quantities.

5. Reporter gene vectors and assays

Reporter genes are the most frequently used as indicators of transcriptional activity within cells [15]. Typically, the reporter gene or cDNA is joined to a promoter sequence in an expression vector that is transferred into cells. Afterwards the cells are assayed for presence of the reporter by directly measuring the amount of reporter mRNA, the reporter protein itself, or the enzymatic activity of the reporter protein.

Reporter systems are used for both in vitro and in vivo application for study promoter and enhancer sequences, transcription factors, mRNA processing, and translation. Reporters are also used to monitor transfection efficiency, protein-protein interactions, proteins sub-cellular localization [16].

Ideally reporter is not endogenously expressed in the cell of interest, and reporter assay system is high sensitive, quantitative, rapid, easy, reproducible, and safe. Principle of reporter genes for gene expression is present on figure 8.

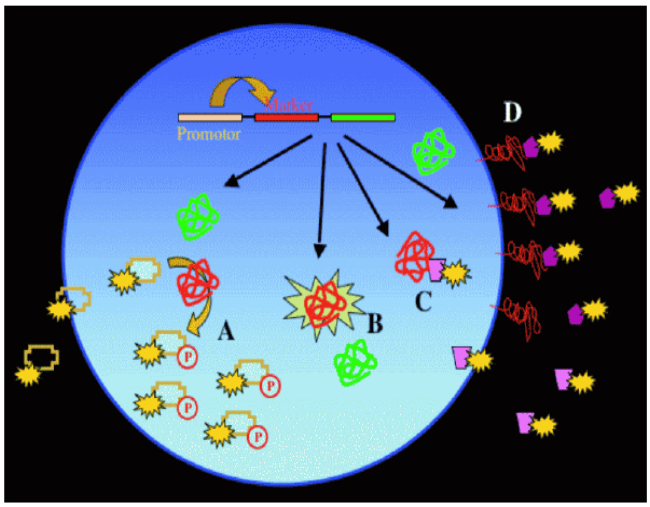

Figure 8. Principle of reporter genes for gene expression. The reporter gene (red) is co-expressed with the gene of interest (green), often by using the same promoter for both genes. The reporter gene can be the HSV thymidine kinase (phosphorylating radioactive-labeled nucleoside-analog, which get trapped in the cell (A), a fluorescent protein like GFP (B), an intracellular target for a marker (C) or a cell membrane receptor as the transferin-receptor (D). (Biomed Imaging Interv J 2006; 2(2): e8).

The reporter genes can be inserted into host cells by viral infection, carrier-mediated transfection, or directed DNA uptake. Following transfection of the DNA, detection of the reporter is accomplished by measuring the reporter m RNA or protein. Detection of the mRNA is a more direct measure of reporter gene expression than protein detection since the effects of transcription are observed directly, avoiding possible artifacts that may be the result of down-stream processing events such as translation or protein instability.

Reporter proteins can be assayed by detecting endogenous characteristics such as enzymatic activity or spectrophotometric characteristics, or indirectly with antibody-based assay [17].

Several reporter genes and assays have been developed and include Chloramphenicol acetyltransferase (CAT), β-galactosidase, luciferase, human growth hormone (hGH), β-glucuronidase, alkaline phosphatase (AP), green fluorescent protein (GFP), and β-lactamase.

5.1 Chloramphenicol acetyltransferase CAT enzyme catalyzes the transfer of the acetyl group from acetyl-CoA to the substrate, chloramphenicol [18]. The enzyme reaction can be quantified by incubating cell lysates with ^{14}C-chloramphenicol and following product formation by physical separation with thin layer chromatography. Alternative isotopic CAT assay have been developed [19] as well as fluorescent chloramphenicol [20]. CAT has been the most frequently used reporter enzyme, and thus a major advantage of this system is that is an extensively validated and widely accepted measure of promoter activity. Another advantage is that the enzyme assays are relatively easy and quite reliable but can be time consuming. A disadvantage of this system is that CAT mRNA accumulates to only very low levels. This can make it difficult to demonstrate that the promoter of interest is initiating transcription at the appropriate position [21].

5.2 Human growth hormone (hGH) reporter assay is immunologically based, employing commercially available radioimmunoassay kits that are relatively quick and convenient to use. hGH is assayed in the medium, rather than in cell extracts. This makes it possible to monitor expression directed by a single population of transfected

cells over time and also makes hGH useful as an internal control for any of the enzymatic assays [22].

5.3 The luciferase enzyme is used most frequently for reporter gene technology. It is derived from the coding sequence of the *luc* gene cloned from the firefly *Photinus pyralis*. The firefly luciferase enzyme catalyzes a reaction using D-luciferin and ATP, in the presence of oxygen and Mg^{2+}, resulting in light emission. The luciferase assay is much faster and more sensitive than the CAT assay and does not use radioactivity. The increased sensitivity is particularly useful if the cell line of interest is hard to transfect, or if the promoter of interest is very weak. A disadvantage of the luciferase assay is that is requires a rather expensive piece of equipment, the luminometer, to measure enzyme activity [23].

5.4 The use of *β-galactosidase* coupled with a chemiluminiscent detection system provides a quick and sensitive alternative nonisotopic reporter system. β- Galactosidase catalyzes the hydrolysis of β-galactoside sugars such as lactose. The enzymatic activity in cell extracts can be assayed with various specialized substrates that allow enzyme activity quantification with a spectrophotometer, fluorometer, or luminometer. A major strength of this reporter gene is the ability to easily assay *in situ* expression with histochemical staining [24, 25]. The β-galactosidase reporter gene is frequently used as a control vector for normalizing transfection efficiency when co-transfected with chimeric DNAs linked to other reported genes [26]. One potential limitation of this reporter gene is that certain mammalian cells have endogenous lysosomal β-galactosidase activity.

5.5 β-Glucuronidase (GUS) is an exoglycosidase which removes terminal β-glucorunic acid residues from the nonreducing end of glycosaminoglycans and other glycoconjugates [27]. β-Glucuronidase is used as a genetic reporter in both plant and animal cells. Like the β-galactosidase reporter, one of the principal advantages of GUS is the wide range of available assays for the enzyme. GUS is most commonly used in higher plants because most plants lack endogenous GUS activity, whereas virtually all mammalian tissues contain glucuronidases that aid in metabolism.

5.6 Alkaline phosphatase (AP) – the enzyme dephosphorylates a broad range of substrates at alkaline pH. A standard spectrophotometric assay is based on the hydrolysis of p-nitrophenyl phosphate (PNPP) by AP. This assay is rapid and simple,

but lacks the sensitivity obtained with other methods. More sensitive colorimetric assay has been developed using flavin-adenine dinucleotide phosphate as a substrate for AP [28, 29].

5.7 Green fluorescent protein (GFP) is cloned from the jellyfish *Aequorea victoria*, serves as an easily detected fluorescent tag requiring no substrates or associated cofactors [30]. GFP from *A. victoria* is a 238 amino acid, 27000 Dalton monomer that emits green light at 508 nm when excited with UV (395 nm) or blue (475 nm) light [31]. Under conditions of high concentrations, the protein may form dimmers and aggregate (figure 9). The active chromophore in GFP required for fluorescence is a hexa-peptide that contains a cyclized Ser-dehydroTyr-Gly trimer. This chromophore is located in the center of protein [32].

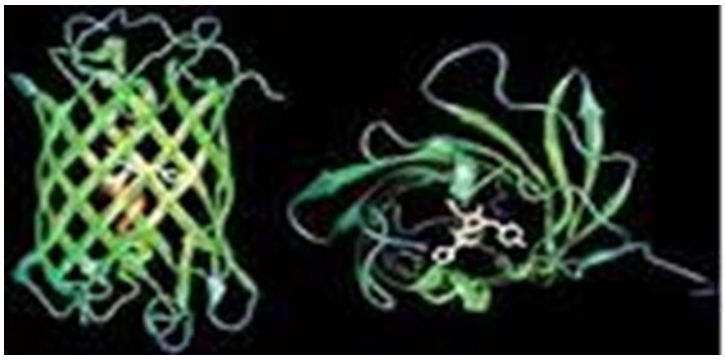

Figure 9. Structure of GFP

The protein requires accurate folding for activity, and mutants that improve the solubility and ability of the protein to fold at 37°C following translation have proved to be especially beneficial for *E. coli* and mammalian cell culture utilization [33]. For mammalian cells expression, the gene codons were engineered to favor more commonly used codons in mammalian cells [34].

GFP-along with its variously engineered versions – has increasingly become widely used as a reporter of gene expression and for studies of protein localization in vivo. Several classes of GFP mutants have been characterized. For example, the red-shifted mutant has an excitation peak that is shifted from 475 to 490 nm, so that is more closely resembles fluorescein excitation. This was accomplished by replacing serine at 65 with threonine [35]. Other amino acid changes in GFP provide proteins that emit light at

different wavelengths. Changing histidine for tyrosine at 66 results in a protein that adsorbs light predominantly at 383 nm, and emits blue light at 477 nm [36]. This mutant is referred as blue fluorescent protein (BFP). The color of light emitted by BFP can be distinguished from that of GFP, whit the use of appropriate fluorescent filters, allowing visualization of both GFP and BFP within the same cell [37]. BFP has a relatively high degree of photo bleaching. However, in the studies of time depending effects when the bleaching of the signal before next measurement is required it could be an advantage. Other mutants of GFP are pH-sensitive, providing indicators of organelle localization in lysosomes and endosomes [38].

Light-stimulated GFP fluoresces in the absence of any other proteins, substrates, or cofactors. GFP gene expression and localization can be directly monitored in living organisms and in live or fixed cells using only UV or blue light illumination [39]. Other advantages of GFP are that it is very stable to heat, extreme pH, and chemical denaturants. GFP fusion proteins can be constructed to study protein transport and localization [40]. Mutants of GFP that are pH sensitive can be function as biosensors. A novel assay for protein-protein interactions using the fluorescent protein employs the phenomenon of fluorescence resonance energy transfer (FRET) [41]. In one example of FRET, excitation of BFP results in emission of blue light of the appropriate wave length to excite a fluorophore of GFP. It is only when GFP is in close proximity to the BFP that a signal of green light will be produced.

Studies using the nematode *Caenorabditis elegans* have demonstrated the utility of GFP as a reporter of gene expression in vivo. The researchers expressed GFP in *C. elegans* under the control of a neuron-specific promoter and used GFP fluorescence to monitor the formation of neuronal processes in real time as the worms developed [39]. Further GFP constructs have been introduced in other animals including mammals.

Scientists reported the first transgenic monkeys— a model of Huntington's disease — but in these animals, the gene did not fully integrate into the monkey's own DNA and was not passed down to their offspring [42]. In other report, scientists used viral DNA as a delivery vehicle to introduce the gene for GFP into the DNA of the common marmoset *Callithrix jacchus*. They show that the gene integrated into the monkey's DNA and was successfully passed down to their offspring, which were healthy and all expressed the new gene [43]. Transgenic mice have contributed immensely to biomedical research, but for many diseases they are too dissimilar from humans for the

results to be meaningful [44]. Non-human primates hold great promise for the study of several human diseases, particularly neurological disorders, for which there are currently no appropriate experimental models. This study marks an important milestone on the road to developing the means to investigate these diseases. Fluorescent proteins have been used to track the development of adult stem cells in pigs [45].

Figure 10. Examples of GFP transgenic mammals

“Brainbow" technology (figure 11) when three different colors of fluorescent protein-cyan, red, and yellow-were introduced into a mouse embryo, and the individual neurons of the mouse's brain became one of 90 different colors lends insight into how brains work [46]. Scientists present a strategy to visualize synaptic circuits by genetically labeling neurons with multiple, distinct colors. In Brainbow transgenes, Cre/lox recombination is used to create a stochastic choice of expression between three or more fluorescent proteins (XFPs). They have been able to reconstruct hundreds of neighboring axons and multiple synaptic contacts in a small volume of a cerebellar lobe. The expression in some lines also allowed mapping glial territories and follow glial cell and neurons over time *in vivo*.

The principle of the method is as follow: the protein Cre recombinase drives inversion or excision of DNA between loxP sites. The original Brainbow method includes both Brainbow-1 and Brainbow-2, which utilize different forms of cre/lox recombination. Brainbow-1 uses DNA constructs with different fluorescent protein genes (XFPs) separated by mutant and canonical forms of loxP. This creates a set of mutually exclusive excision possibilities, since cre

mediated recombination occurs only between identical loxP sites. After recombination occurs, the fluorescent protein that is left directly after the promoter is uniquely expressed. Thus, a construct with four XFPs separated by three different loxP sites, three excision events, and the original construct can produce four different fluorescent proteins.

Brainbow-2 uses Cre excision and inversion to allow multiple expression possibilities in a given construct. In one DNA segment with two oppositely oriented XFPs, Cre will induce a random inversion event that leaves one fluorescent protein in the proper orientation for expression. If two of these invertible sequences are aligned, three different inversion events are possible. When excision events are also considered, one of four fluorescent proteins will be expressed for a given combination of Cre excisions and inversions. For both Brainbow-1 and-2, the expression of a given XFP is a stochastic, or random, event. Brainbow is implemented in vivo by crossing two transgenic organism strains: one that expresses the Cre protein and another that has been transfected with several versions of a loxP/XFP construct. In order to elucidate differential XFP expression patterns into a visible form, brain slices are imaged with confocal microscopy. When exposed to a photon with its particular excitation wavelength, each fluorophore emits a signal that is collected into a red, green, or blue channel, and the resultant light combination is analysed with data analysis software.

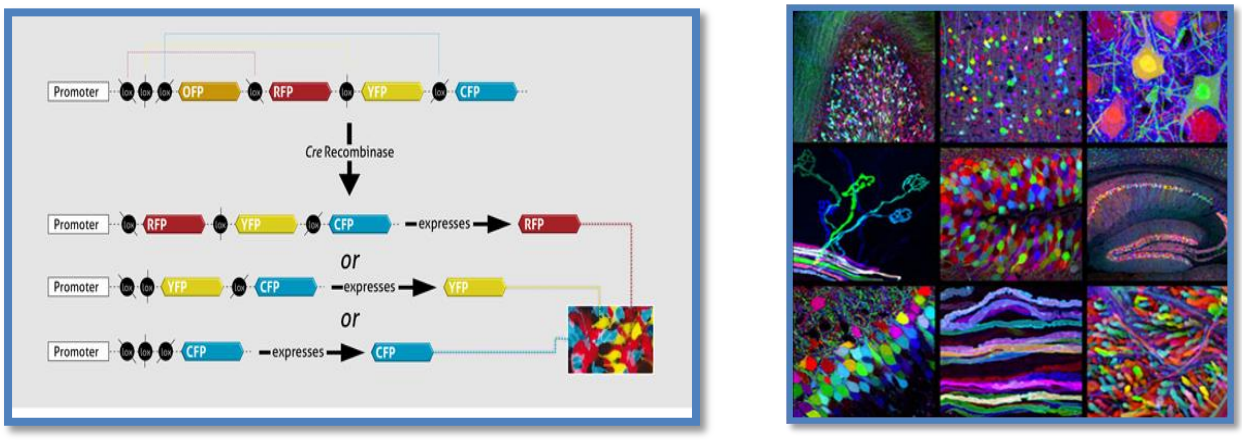

Figure 11. “Brainbow” technology

The limitations of the method consist in complex and time consuming breeding process of transgenic animals from embryonic stem cells. Moreover due to the random nature in

the expression of the fluorescent proteins, it is difficult to precisely control the labeling of neural circuitry, which may result in the poor identification of specific neurons.

Due to high diversity of neuronal populations in mammalian brain Brainbow is most useful when examining single cell resolution against the background of a complex multicellular environment. Resolution limits of optical microscopy makes difficult identification of sinaptic conections between neurons. This limitation can be avoided by the use of synaptic markers to supplement the use of optical microscopy in viewing synaptic connections.

A disadvantage of the GFP protein family is that the protein acts stoichiometrically, not catalytically, and therefore the reporter signal is not naturally amplified. Another drawback is the stability of GFPs and their delayed degradation within the cell. It leads to accumulation of the protein in the cell compartments and false positive results even if the gene is no longer expressed. This is of great important in the case of the study down regulation of the gene expression. Powerful fluorescent microscopes and fluorometers are required for detection, particularly with gene expression driven by low activity promoters [37].

The ability to detect RNAs in individual live cells allows for exact pinpoint when a gene is turn on and off in response to a stimuli or biological development. Detecting gene expression has traditionally been limited to technologies such as RT-PCR, Northern blotting, and fluorescent *in situ* hybridizations that examine expression in lysed or fixed cell populations. In contrast to these destructive methods, green fluorescent proteins (GFP) can be used to follow gene expression in living cells. However, GFP and similar reporter systems cannot measure endogenous mRNA expression in living cells as the GFP gene must be fused to the promoter region of interest in order to function. GFP/promoter constructs can be integrated into the host genome or be located in plasmids. GFP gene product is not necessarily processed as the native gene in terms of transcription, mRNA maturation transport and translation, which can provide errors in the measurements [47, 48]. On more practical terms GFP, require genetically modifications of the cell and are time, labor consuming and sometimes impossible to realize.

References

1. Alwine JC, Kemp DJ, Stark GR. Methods for detection of specific RNAs in agarose gels by transfer to diazobenzyloxymethyl-paper and hybridization with DNA probes. Proc. Natl. Acad. Sci. USA 1977; 74 (12): 5350-4. DOI: 10.1073/pnas.74.12.5350

2. Schlamp K, Weinmann A, Krupp M, Maas T, Galle PR, Teufel A. BlotBase: A northern blot database. Gene 2008; 427 (1-2): 47-50. DOI:10.1016/j.gene.2008.08.026

3. Langer-Safer PR, Levine M, Ward DC. Immunological method for mapping genes on Drosophila polytene chromosomes. Proc. Natl. Acad. Sci. USA 1982; 79 (14): 4381-5

4. Zhang B, Arun G, Mao YS, Lazar Z, Hung G, Bhattacharjee G, Xiao X, Booth CJ, Wu J, Zhang Ch, Spector DL. The lncRNA Malat1 is dispensable for mouse development but its transcription plays a cis-regulatory role in the adult. Cell Rep 2012 July 26; 2 (1): 111-123

5. Lee K, Kunkeaw N, Jeon SH, Lee I, Johnson BH, Kang G-Y, Bang JY, Park H S, Leelayuwat Ch, Lee YS. Precursor miR-886, a novel noncoding RNA repressed in cancer, associates with PKR and modulates its activity. RNA 2011; 17(6): 1076-1089. DOI: 10.126/rna.2701111

6. Freeman WM, Walker SJ, Vrana KE. Quantitative RT-PCR: pitfalls and potential. BioTechiques 1999; 26(1): 112-22, 124-5

7. Joyce C. Quantitative RT-PCR. A review of current methodologies. Methods Mol. Biol. 2002; 193: 83-92

8. Deepak S, Kottapalli K, Rakwal R, Oros G, Rangappa KS, Iwahashi H, Masuo Y, Agrawal GK. Real-Time PCR: Revolutionizing detection and expression analysis of genes. Curr. Genomics 2007; 8(4): 234-251

9. Bustin SA. Quantification of mRNA using real-time reverse transcription PCR (RT-PCR): trends and problems. J. Mol. Endocrinol. 2002; 29(1): 23-39

10. Souazé F, Ntodou-Thomé A, Tran CY, Rostène W, Forgez P. Quantitative RT-PCR: limits and accuracy. BioTechniques 1996; 21(2): 280-5

11. Holden MJ, Wang L. Quantitative Real-Time PCR: Fluorescent probe options and and issues. Standardization and quality assurance in fluorescence measurments II. Springer Series on Fluorescence 2008; 6. Pp. 489

12. Rajeevan MS, Vernon SD, Taysavang N, Unger ER. Validation of array-based gene expression profiles by real-time (kinetic) RT-PCR. J. Mol. Diagn. 2001; 3(1): 26-31. DOI: 10.1016/S1525-1578(10)60646-0

13. Yang DK, Kweon CH, Kim SH, Kwon JH, Han HR. TaqMan reverse transcription polymerase chain reaction for the detection of Japanese encephalitis virus. J. Vet. Sci. 2004; 5(4): 345-51

14. Sharkey FH, Banat IM, Marchant R. Detection and quantification of gene expression in environmental bacteriology. Appl. Environ. Microbiol. 2004; 70 (7): 3795-806. DOI: 10.1128/AEM.70.7.3795-3806.2004

15. Rosenthal N. Identification of regulatory elements of cloned genes with functional assays. Meth. Enzym. 1987; 152, 704-720

16. Alam J, Cook JL. Reporter genes: application to the study of mammalian gene transcription. Anal. Biochem. 1990; 188, 245-254

17. Schenborn E, Groskreutz D. Reporter Gene vectors and assays. Molecular Biotechnology 1999; 13: 29-44. DOI: 1073-6085/1999/13:1/29-44

18. Shaw WV. Chloramphenicol acetyltransferase from chloramphenicol –resistant bacteria. Meth. Enzymol. 1975; 43, 737-755

19. Seed B, Sheen J-Y. A simple phase-extraction assay for chloramphenicol acyltransferase activity. Gene 1988; 67: 271-277

20. Hruby DE., Brinkley JM, Kang HC, Haugland RP, Young SL, Melnor MH. Use of a fluorescent chloramphenicol derivative as a substrate for CAT assays. BioTechniques 1990; 8:170-171

21. Kain SR, Ganguly S. Uses of fusion genes in mammalian transfection. Curr. Prot. Mol. Biol. 1996; 9.6.1-9.6.12

22. Selden RF, Howie KB, Rowe ME, Goodman HM, Moore DD. Human growth hormone as a reporter gene in regulation studies employing transient gene expression. Mol. Cell. Biol. 1986; 6: 3173-3179

23. Bronstein I, Fortin J, Stanley PE, Stewart GSAB, Kricka L. Chemiluminescent and bioluminescent reporter gene assays. Anal. Biochem. 1994; 219: 169-181

24. Sanes JR, Rubenstein JLR, Nicolas J-F. Use of recombinant retrovirus to study post-implantation cell linage in mouse embryos. EMBO J. 1986; 5: 3133-3142

25. Lim K, Chae CB. A simple assay for DNA transfection by incubation of the cells in culture dishes with substrates for beta-galactosidase. BioTechniques 1989; 7: 576-579

26. Hollon T, Yoshimura FK, Variation in enzymatic transient gene expression assay. Anal. Biochem. 1989; 182: 411-418

27. Gallagher SR. GUS Protocols: Using the GUS gene as a reporter of gene expression. Academic Press, San Diego, CA. 1992

28. Henthorn P, Zervos P, Raducha M, Harris H, Kadesch T. Expression of a human placental alkaline phosphatase gene in transfected cells: Use as a reporter for studies of gene expression. Proc. Natl. Acad. Sci. USA. 1988; 85:6342-6346

29. Yoon K, Thiede MA, Rodan GA, Alkaline phosphatase as a reporter enzyme. Gene 1988; 66: 11-17

30. Tsien RY. The green fluorescent protein. Annu. Rev. Biochem. 1989; 67: 509-544

31. Praser DC, Eckenrode VK, Ward WW, Prendergast FG, Mormier MJ. Primary structure of the Aequorea Victoria green fluorescent protein. Gene 1992; 111: 229-233

32. Yang Rl, Moss LG, Phillips GN. The molecular structure of green fluorescent protein. Nature Biotechnology 1996; 14: 1246-1251

33. Crameri A, Whitehorn EA, Tate E, Stemmer WPC. Improved green fluorescent protein by molecular evolution using DNA shuffling. Nature Biotechnology 1996; 14: 315-319

34. Zolotukhin S, Potter M, Hauswirth WW, Guy J, Muzyczka N. A ”humanized” greenfluorescent protein cDNA adapted for high-level expression in mammalian cells. J. Virology 1996; 70:4646-4654

35. Ormo M, Cubitt AB, Kallio K, Gross LA, Tsien RY, Remington SJ. Crystal structure of the Aequorea Victoria green fluorescent protein. Science 1996; 273:1392-1395

36. Patterson GH, Knobel SM, Sharif WD, Kain SR, Piston DW. Use of the green fluorescent protein and its mutants in quantitative fluorescent microscopy. Biophys. J. 1997; 73, 2782-2790

37. Rizutto R, Brini M, DeGiorgi F, Rossi R, Heim R, Tsien RY, Pozzan T. Double labelling of subcellular structures with organelle-targeted GFP mutants in vivo. Current Biology 1996; 6: 183-188

38. Llopis J, McCaffery JM, Miyawaki A, Farquhar MG, Tsien RY. Measurement of cytosolic, mitochondrial, and Golgi pH in single living cells with green fluorescent proteins. Proc. Natl. Acad. Sci. USA 1998; 95: 6803-6808

39. Chalfie M, Tu Y, Euskirchen G, Ward WW, Prasher DC. Green fluorescent protein as a marker for gene expression. Science 1994; 263: 802-805

40. Wang S, Hazelrigg T. Implications for bcd mRNA localization from spatial distribution of exu protein in Drosophila oogenesis. Nature 1994; 369:400-403

41. Cubitt AB, Heim R, Adams SR, Boyd AE, Gross LA, Tsien RY. Understanding, improving and using green fluorescent proteins. Trends Biochem. Sci. 1995; 20: 448-455

42. Yang SH, Cheng PH, Banta H, Piotrowska-Nitsche K, Yang JJ, Cheng EC, Snyder B, Larkin K, Liu J, Orkin J, Fang ZH, Smith Y, Bachevalier J, Zola SM, Li SH, Li XJ, Chan AW. Towards a transgenic model of Huntigton's disease in a non-human primate. Nature 2008; 453 (7197): 921-924. DOI: 10.1038/nature06975

43. Sasaki E, Suemizu H, Shimada A, Hanazawa K, Oiwa R, Kamioka M, Tomioka I, Sotomaru Y. et al. Generation of transgenic non-human primates with germline transmission. Nature 2009; 459: 523-527

44. Oliva Jr. AA, Jiang M, Lam T, Smith KL, Swann JW. Novel hippocampal interneuronal subtypes identified using transgenic mice that express green fluorescent protein in GABAergic interneurons. J. Neuroscience 2000; 20(9): 3354-3368

45. Klassen H, Warfvinge K, Schwartz PH, Kiilgaard JF, Shamie N, Jiang C, Samuel M, Scherfig E, Prather RS, Young MJ. Isolation of progenitor cells from GFP-transgenic pigs and transplantation to the retina of allorecipients. Cloning Stem Cells 2008; 10(3): 391-402. DOI: 10.1089/clo.2008.0010

46. Livet J, Weissman TA, Kang H, Draft RW, Lu J, Bennis R, Sanes JR, Lichtman JW. Transgenic strategies for combinatorial expression of fluorescent proteins in the nervous system. Nature 2007; 450: 56-63. DOI: 10.1038/nature06293

47. Dobek GL, Zhang X, Balazs DA, Godbey WT. Analysis of promoters and expression-targeted gene therapy optimization based on doubling time and transfectability. The FASEB Journal 2011; doi: 10.1096/fj.11-185421

48. Lee J-Y, Colinas J, Wang JY, Mace D, Ohler U, Benfey P. Transcriptional and posttranscriptional regulation of transcription factor expression in Arabidopsis roots. PNAS 2006; vol. 103, no. 15, pp. 6055–6060

Chapter II. Molecular beacons

1. Introduction

Molecular beacons were described in 1996 by Tyagi & Kramer (1996) [1] as oligonucleotide probes that recognized and reported the presence of specific nucleic acids in homogeneous solution. The design probes are single-stranded oligonucleotides with stem-loop structure. The loop is a probe sequence complementary to a predetermined sequence in the target nucleic acid. The stem portion is formed by 5-7 complementary bp and it is not related to the target sequence. A fluorescent dye is attached to the end of one arm and a quenching moiety is attached to the end of another arm. When the target is not present in the solution the both arms hybridized and keep close the fluorochrome and quencher. In this "close state" the fluorescence of fluorochrome is quenched by fluorescence resonance energy transfer (FRET). When the probe recognized the target it forms a longer hybrid which is more stable than the hybrid formed by the arms of the stem. Thus, the quencher and fluorochrome separate and the molecular beacon undergo in "open state" and a fluorescent signal can be detected (figure 12). Only completely complementary targets elicit this response and thus a single mismatch or deletion can be recognized. This makes Molecular beacons highly sensitive and specific probes for detection nucleic acids with broad range of application not only in vitro but also inside living cells.

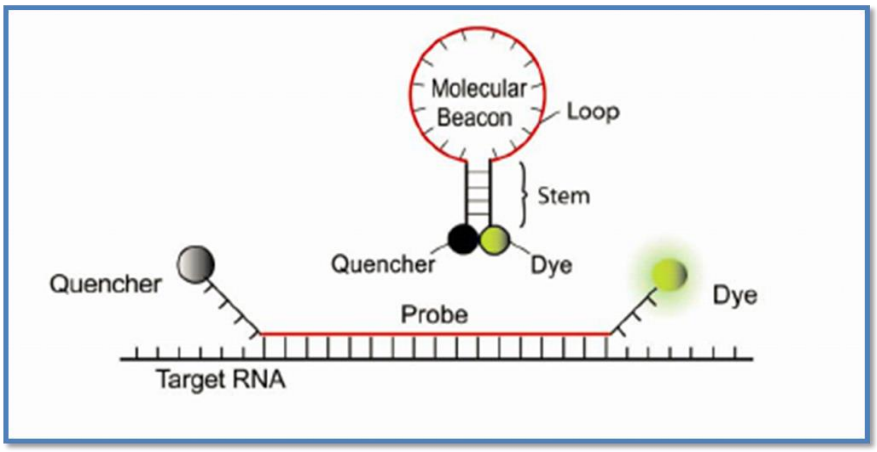

Figure 12. Structure and working principle of molecular beacon (Rhee&Bao 2009)

2. MBs application

2.1 MBs as recognition elements in biosensor development

MB array demonstrated many advantages over conventional arrays [2, 3, 4]. First, no target labeling was needed. Labeling is an important step in most microarray-based target preparation protocols. However, it is time – and labor consuming and expensive. In addition, it can affect the levels of targets originally present in the sample. Secondly, no washing step is required with MBs. Due to the unique on-off signaling process, only MBs hybridized to their target will produce fluorescence. Unbound MBs stay with quenched fluorescence. Third, the hybridization process can easily be monitored in real time and more reliable results can be obtained from the hybridization dynamics curves. Fourth, the high specificity of MBs always ensures that mismatches can be easily discriminated. The presence of a hairpin structure maximizes the specificity of MB probes. Furthermore, unlike linear probes, MBs are insensitive to mismatch type and position, which simplifies probe design (figure 13).

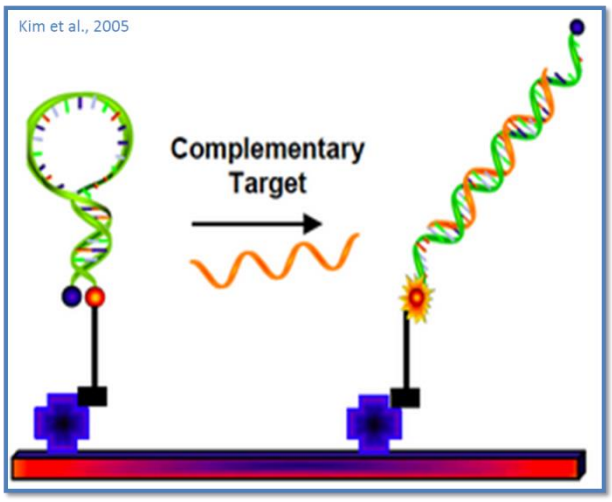

Figure 13. Schematic illustration of MB array. MBs are immobilized using specific biomolecular interactions, such as streptavidin/biotin or covalent cross-linking.

2.2 MBs in clinical diagnostic

The properties of MBs have led to their applications in clinical diagnosis. The combination of MBs and PCR amplifications provides rapid and accurate identification of pathogens and detection of gene mutations in human diseases [5, 6, 7]. The working principle is as follow – during the annealing step of PCR, MBs hybridize to the complementary targets and the

fluorescent signals increased. Meanwhile, excess MBs remain in the closed conformation with quenched fluorescence. The intensity of the fluorescence is proportional to the concentration of the targets. During the extension stage, the MBs hybridized to targets melt and thus do not interfere with polymerization. Multiple targets can be simultaneously detected using a mixture of MBs, and the relative difference of the targets can be determined. Site-products, such as primer dimers and false amplicons, are unlikely detected because MBs can only be fluorescent in the presence of the complementary target.

Due to the high selectivity in distinguishing single-base mismatched target, MBs have been applied in the detection of point mutations and allele discrimination. Variation in DNA sequence plays a critical role in disease development. Since single nucleotide polymorphism (SNP) or a group of SNPs has been identified as a disease-associated marker, selective detection of SNPs can be useful in disease diagnosis, genetic counseling, prognosis and treatment [8].

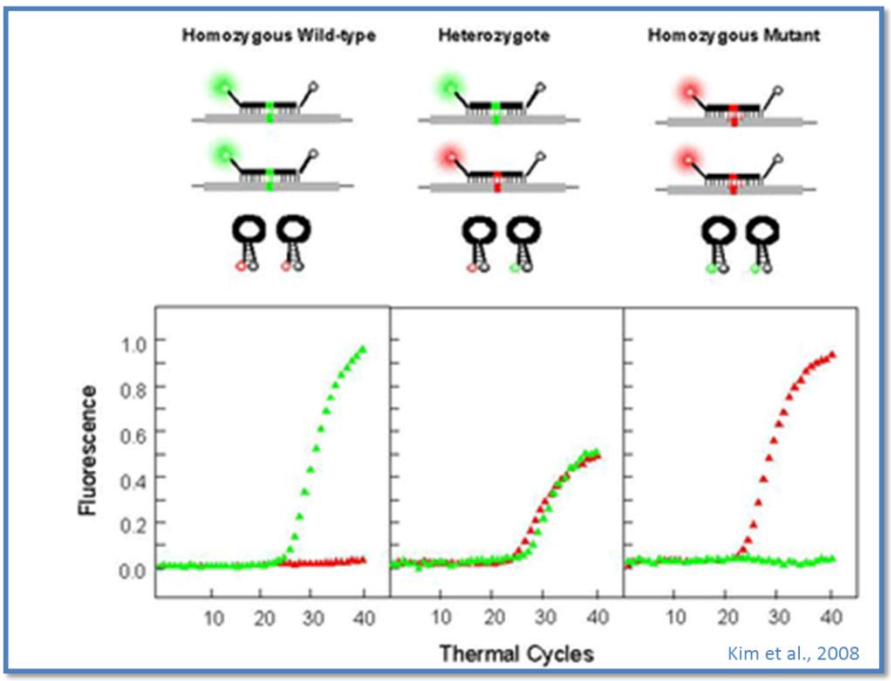

Figure 14. Principle of spectral genotyping using MBs

In figure 14 is present the principle of spectral genotyping using MBs by detection of a SNP in codon 325 of the estrogen receptor gene. In individuals homozygous for the major allele, only the FAM-labeled MB hybridizes to the amplicons and thus is fluorescent, whereas the TET-labeled MB remains closed. In individuals homozygous for the minor allele, only the TET-labeled MB is fluorescent. In heterozygote individuals, both MBs hybridize to the amplicons, but since the total amounts of target available are theoretically the same, the levels

of fluorescence from both fluorophores are decreased, compared with the fluorescence levels in the presence of a homozygous sample [5].

2.3 MBs for live-cell RNA detection

Wang et al. [9.] developed a method to determine the expression levels of a specific RNA using MBs. They applied a system with two MBs and a reference probe as an internal standard for ratiometric analysis. The reference probe was used to avoid the variations due to different MB concentrations in the cell. One MB was used to detect the desired mRNA whereas the other MB was used to hybridize a house keeping mRNA, serving as reference. It offers a good approach for the quantification of gene expression, enabling a more accurate estimation of mRNA levels. In this particular study two different MBs were used, one can envision an extension of this method to study several RNA molecules simultaneously using spectrally different fluorescent dyes for each MB.

Further, the number of studies employing MBs for visualization and tracking mRNA inside living cells is increased. Bratu et al. [10] used MBs for visualization the distribution and transport of oskar mRNA in Drosophila oocytes. Further MBs were used for analyzing the distribution and transport of the mRNA with respect of organels [11] and showed that both mRNA for GAPDH and K-ras are localization in mitochondria.

Combination of protein markers and mRNA target MBs allowed for detection and isolation of cancer stem cells among normal cells using fluorescent activated cell sorting (FACS) [12]. MBs for Oct4 mRNA – transcription factor that are highly expressed in embryonic and cancer stem cells was introduced in mouse carcinoma cell line without affecting cell functionality. In this case, the fluorescent signal from Oct4 mRNA targeting MB provided a clear discrimination between undifferentiated and retinoic acid differentiated cells.

King et al. [13] demonstrated the MBs potential for high-throughput isolation of hESC. They developed a dual FRET MB system using FACS with Oct4 as a target. This system can be applied for identification and isolation of Oct4 expressing hESC by FACS. FRET-positive cells demonstrated pluripotency in culture and *in vivo.* Moreover, hESC transfected with MBs demonstrated normal growth rates and oligonucleotide extinction over time.

Recently, MBs for Sox2 mRNA was used as sole discriminator for cell sorting of mouse embryonic and neural stem cells [14] The Sox2 mRNA positive cells had a higher efficiency to form neurospheres than Sox2 mRNA negative cells. Diagnostic utility of molecular beacon

in bladder cancer was investigated by Zhao et al [15]. They used MBs to detect survivin mRNA, which is specifically expressed in bladder cancer cell lines and demonstrated feasibility of MBs in clinical diagnosis of bladder cancer. However the MB based assay gave false positive results, which compromised its usage in the diagnosis.

MB was also used to follow expression of two microRNAs during myogenesis – miR-26a and miR-206 [16]. The approach included two MBs with different dyes and quenchers which allowed simultaneous visualization of both miRNAs during myogenesis. Real-time changes in β1-integrin expression in osteoblasts in response to surface modification over short periods of time were tracked with MBs [17]. Moreover, the approach allowed the study of changes in mRNA localization in the same live cells. MBs were applied for monitoring temporal gene expression of osteogenic markers such as alkaline phosphatase, type I collagen, and osteocalcin during differentiation of adipose-derived stem cells [18].

3. Design issues for RNA-targeted probes

3.1 Target accessibility

A critical step in designing MBs for live-cell RNA imaging is target accessibility. It is well known that RNA molecules within living cells are commonly associated with RNA-binding proteins, e.g. ribonucleoproteins (RNP). Further, RNA molecules form complex secondary (folded) structures. Therefore, when designing an oligonucleotide probes, it is preferable to avoid targeting RNA sequences that are double stranded, or occupied by RNA-binding proteins; otherwise, the probe has to compete off the RNA strand or the RNA-binding protein in order to hybridize to the target [19]. Indeed, MBs designed for targeting a specific RNA often show no signal when delivered to living cells. [20]. One difficulty in designing oligonucleotide probes is that, although predictions of mRNA secondary structures can be made using software such as Beacon Designer (PremierBiosoft) and mfold (), they are often inaccurate due to limitations of the biophysical models used and the limited understanding of protein-RNA interactions [21]. Therefore, for each gene to target, it may be necessary to select multiple unique sequences along the target RNA and to have corresponding oligonucleotide probes designed, synthesized, and tested in living cells to select the best target sequence.

To identify possible oligonucleotide probe design rules, one study looked at the accessibility of BMP-4 mRNA using different beacon designs [20] MBs were designed to target the start codon and termination codon regions, the siRNA and antisence oligonucleotide probe sites identified previously, and sites that were randomly chosen. All the target sequences were determined to be unique to BMP-4 mRNA. Of the eight MBs designed to target BMP-4 mRNA, it was found that only two beacons gave strong signals, one that targeted the start codon region and one that targeted the termination codon region. It was also founded, that even for a MB that works well, shifting its targeting sequence by just a few bases toward the 3' or 5' ends could significantly reduce the fluorescent signal, further confirming that target accessibility is extremely sensitive to the location of the targeting sequence. Although target accessibility will likely need to be tested on a case-by-case basis, these finding suggest that the start and termination codon regions may be more accessible than other locations on target RNA.

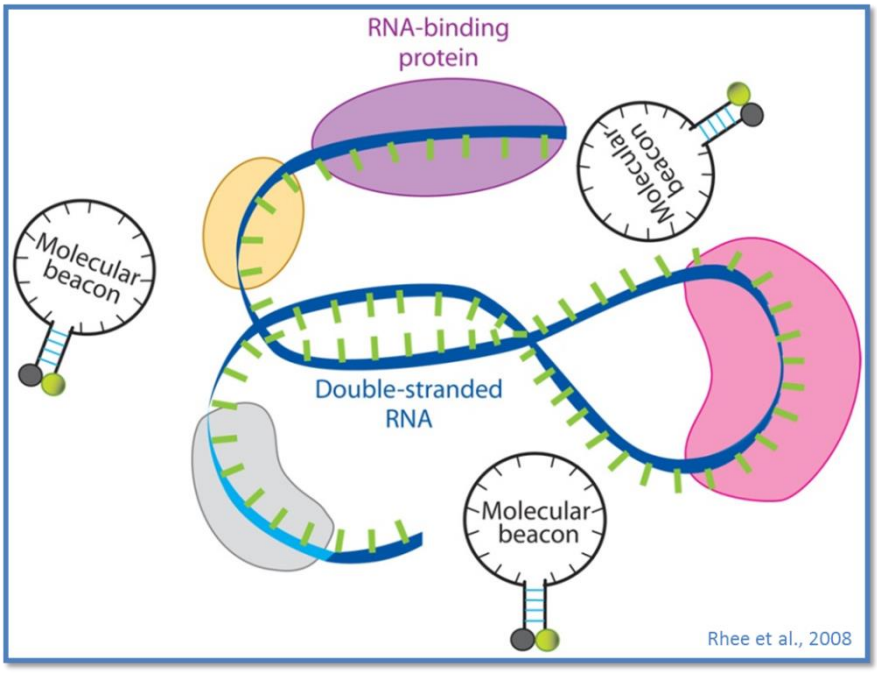

Figure 15. A schematic illustration of a segment of the target mRNA with a double-stranded portion and RNA-binding proteins. A MB has to compete off a mRNA strand or RNA-binding protein in order to hybridize to the target.

3.2 Fluorophores and quenchers

The quenching that takes place when the MB is in its "closed" stem-loop structure conformation occurs by two mechanisms.

The first mechanism is called dynamic quenching and includes Föster's resonance energy transfer (FRET) and Dexter transfer, also named electron transfer quenching. In this quenching mechanism, the photon from the fluorophore is not released to the environment because a long-range dipole-dipole interaction occurs between fluorophore and quencher. For the dynamic quenching mechanism, the transfer efficiency of the energy depends on the spectral overlap between the emission spectrum of the fluorophore and the absorption spectrum of the quencher, the quantum yield of the donor, the relative orientation(dipolar moment), and the distance between the two groups [22, 23]. For a 50% of FRET efficiency, a distance in the range of 20-70 Å (Föster's distance) is needed between the florophore and quencher, losing all the quenching efficiency at a distance ≥ 100 Å (10 nm).

The second mechanism is called static quenching [24] and it requires the formation of ground-state complexes and the mechanism depends on the stem sequence, the linkers, and the fluorophore-quencher pair used in MB design. The most important contributor in the quenching phenomenon is the static or contact quenching; the name describes the nature of the process, which occurs only when reporter and quencher are in close proximity, permitting the physical contact between them. Under these conditions most of the energy transferred is not emitted as light, but emitted in the form of heat through a non-irradiative process [25]. This phenomenon occurs for all the non-fluorescent quenchers and determines basal fluorescence value in the absence of target and the signal-to-noise ratio of the MB. The most frequently used non-fluorescent quenchers in MB synthesis are Dabcyl (4-([4'-(dimethylamino) phenyl] azo) benzoic acid), Black-Hole quenchers BHQ 1 and BHQ 2, and Iowa Black FQ and RQ. Typical static quenching efficiency for these quenchers is in the range of 85-97 % [22, 25]. These quenchers could be paired with various reporters (figure 16).

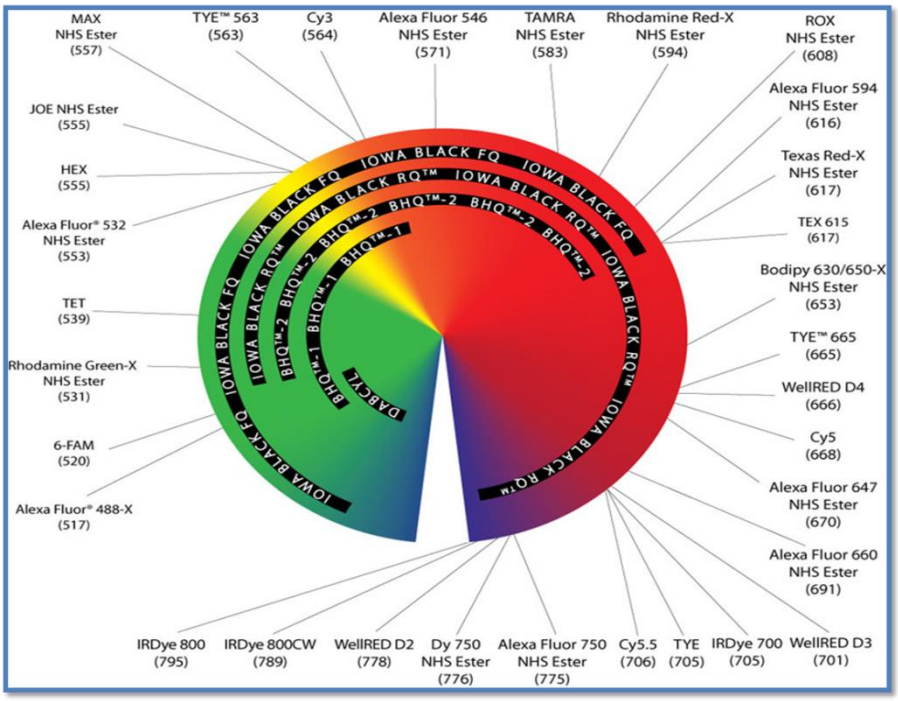

Figure 16. Fluorescent dyes spectrum and quenchers

It has been reported that guanine base (G) can be utilized as quencher in MB design (a method known as G-quenched MB) [26, 27]. Guanine base works as quencher when presents at the opposite end of the florochrome. The base could be placed as overhang or not. MBs without overhanged G show only a 15 % increment in fluorescence intensity moving from "closed" state to the "open" state. When two overhanged G have been used a 2-fold increasing in quenching efficiency was observed [28].

The ability of MBs to sensitively detect specific RNA in living cells is highly contingent upon both the signal –to-background (S: B) ratio and signal-to-noise (S: N) ratio.

$$S{:}B = \frac{\text{maximum fluorescence of the reporter dye in hybridized state (unquenched)}}{\text{maximum fluorescence of the reporter dye in unhybridized state (quenched)}}$$

It is observed that S:B drops off significantly when the MBs are moved from test tube assay to the intracellular environment, where autofluorescence, nonspecific interactions and nuclease degradation can all contribute to background enhancement. The S:N ratio, on the other hand, suffers most from the limited fluorescent intensity of organic fluorophores and a very low enhancement in MB fluorescence due to the presence of a small number of RNA targets in each cell and a low percentage of hybridized MBs. The low S:N ratio of MBs has limited their use to only a handful of highly over-expressed RNAs. It has been estimated that

the lower detection limit may be as high as ~2000 transcripts of RNA per cells [29]. This number is likely to be much lower if the target RNA is concentrated within subcellular domains. Since most of endogenous mRNAs exist in less quantity than can be detected by MBs, they would clearly benefit from further improvement in sensitivity for live-cell applications.

Perhaps the most straightforward way to improve the sensitivity of intracellular RNA detection is to target each RNA with multiple MBs. The total fluorescent signal increases linearly with each additional MB. However the drawback of this approach is the increased likelihood of interfering with translational and normal RNA function. The power of this approach was demonstrated by targeting RNA that was engineered to possess 96 tandem repeats of the same MB binding site in the 3'-untranslated region [30]. It was found that with the combined fluorescence of 96 MBs per RNA, even single molecule sensitivity could be achieved.

Another approach to improve MB sensitivity involves selecting a far to near-infrared (NIR) fluorophore as a reporter dye. In the NIR regime (emission wavelength > 600 nm), cells and media both exhibit lower levels of autofluorescence. At these wavelengths it was observed a reduction in noise, presumably also due to the lower level autofluorescence. Some of the far-red dyes, including Texas red and Alexa 594 [10, 29, 31, 32, 33, 34] have already been incorporated into MB design for live-cell applications. MBs designed with reporter dyes >600 nm generally exhibit significantly higher S:B and S:N ratios compared with MBs designed with blue-shifted dyes. In one related study, the lower detection limit for Cy5 dyes (emission: 668 nm) was determined to be as low ~500 molecules on a conventional inverted fluorescent microscope, compared with ~15000 molecules for TMR (emission: 574 nm) [35].

Proper selection of fluorophore and quencher has a great benefit in regards to signal-to-background ratio, multiplexing, and fluorescent quantification. A systematic study on a wide range of fluorophores-quenchers combinations showed that quenching efficiency may vary between 57% to 98%. Quenching efficiency could be improved using either inorganic quenchers such as gold or by incorporating multiple quenchers into single MB [22]. Other approaches which also could be used to improve signal intensity include the incorporation of quantum dots (QD) or photoluminescent polymers into MB. QDs are brighter and photostable comparing to organic fluorophores. Their broad absorbtion and narrow emission spectra are

highly amenable to multiplexing. However, initial studies have suggested that QD-based MBs exhibit signal-to-background ratio of only 6:1 due to inefficient quenching [36, 37, 38].

3.3 Thermodynamics

The MB-target hybridization is due to Watson-Crick basepairing. Thermal denaturating assays and binary models that simplify the real behavior of the phenomenon considering only the beginning of the hybridization kinetics and the end – steady-state, support the fact that for a given MB perfect matched target pair the melting temperature is 13 ± 3° C higher than for the single-mismatched target [25, 39, 40]. Selectivity potential is the capability of a probe to discriminate single mismatched from perfectly matched target. Its magnitude is determined by the difference of the temperatures at the transition phases.

MBs have three states – free with stem-loop conformation, free as a random coil and bound to its target. In terms of free energy MB is more stable in stem-loop conformation than random coil, therefore such transition is brief. These suggest that when the temperature increases and the dissociation between MB and target occur, MB will acquire the stem-loop conformation preferentially over the random coil state [5, 41, 42]. In this state, fluorophore is quenched and that explains the high signal to background ratio observed with MBs. A more stable stem due to higher C-G content or stem length will produce higher signal to background ratio. This suggests that MBs with more stable stem will obtain more enhanced selectivity because the MB will hybridized to the target only when the interactions MB-target are strong enough to overcome the stem stability, e. g. when the target is perfectly matched. On the other hand MBs with stronger stem may not hybridize in physiological temperature compromising its use for cellular studies. Thus a balance between stability of the hairpin and MB-target selectivity must be reached for successful use of MBs for living cell imaging.

3.4 Selectivity and hybridization rate

The stability of hairpin conformation is ensured by design more stable stem – by increasing its C-G content or stem-length. However increasing stem stability decreases the hybridization rate.

Hybridization rate = complementary nucleotides/MB-length

For an optimal stem design it is necessary to determine the balance between selectivity and hybridization rate for a given assay. Usually MB has a 5-7 nucleotides long stem and a loop of 15-25 nucleotides and hybridized only with loop sequence [39, 40, 43].

For a given MB the rate of hybridization decreases between one and two orders of magnitude when the stem length increased from two to four nucleotides [40]. In order to accelerate the hybridization rate of MB with more stable stem is to increase the loop length. Another option preventing increase of loop length is to include the stem sequence as a part of the complementary region which hybridizes to the target. MB could hybridize the target using partially one arm, partially both arms or totally one arm of the stem. MBs using totally one arm of the stem to hybridize the target are known as shared stem. A shared stem MB offers a higher hybridization rate comparing with a MB with the equal complementary nucleotides using only loop as a hybridization region [25].

For living cell assay it is important that MB discriminate among perfect matched and the single mismatched target at 37°C. It means that the melting temperature of the MB-single-mismatched target pair should be less than 37°C, while the melting temperature of the MB-perfect matched target pair must be above 37°C [44]. This requirement should be consider during design of the stem stability, loop length, and or regions that will participate in the hybridization. If the MB is designed with too high MB-target melting temperature, it will be impossible to differentiate between the perfect match and the single mismatch target. On the other hand, if the MB-target melting temperature is reduced too much, just a little fraction of the perfectly matched target would be bound to the MB at physiological temperature.

3.5 Nuclease resistant MBs

Cells use nucleases for nucleic acid catabolism and reuse the nucleotides for nucleic acids synthesis. Nucleases are used for cellular defense against foreign nucleic acids and for degradation of damaged DNA. Unfortunately nucleases also depredate MB, which constitute a problem for RNA imaging in living cells [45]. It was found that when nonsense MBs (not complementary to any known endogenous RNA) were microinjected into the cytoplasm of cells, they were not only rapidly sequestered into the nucleus, but they also elicited a bright false-positive signal once they passed through the nuclear pores [31]. It was found to be true for a wide range of cell lines including HeLa, MCF-7, NIH3T3, and MDA-MB-231 cells regardless of delivery method (Lipofectamine 2000 or microporation) [32, 46]. The presence

of false positive signals in the nucleus has significant implications when trying to use MBs to measure gene expression. For example, nonspecific opening of MBs can easily be confused with MB hybridization and lead to ambiguous results. Further, nonspecific opening results in a significant loss in the sensitivity and dynamic range of MBs in living cells.

In general, there are two approaches that offer hope of eliminating the nonspecific opening and/or degradation of MBs in living cells: they can be confined to the cytoplasm, or their backbone can be chemically modified. When MBs are confined to the cytoplasm they do not elicit any detectable false-positive signal, even when nuclease-sensitive DNA backbones are utilized. Two strategies for keeping MBs out of the nucleus have been reported in the literature. The first one involves attaching MBs to a macromolecules or nanoparticles, which prevents passage of the MBs through the nuclear pores due to size exclusion [31]. The second approach that can be used to retain MBs in the cytoplasm involves attaching MBs to tRNAs, which can drive nuclear export. However, one concern with using tRNAs is that MBs must at least transiently enter the nucleus prior to export [33].

Although it has been widely reported that MBs with phosphodiester backbones (DNA-MBs) can be used to image RNA in living cells, DNA-MBs are highly susceptible to nuclease degradation and nonspecific interactions, both of which can lead to the generation of false-positive signals. To produce nuclease resistant MB with improved stability at the cytoplasm, modified nucleotides have been incorporated in MB synthesis. These modified nucleotides include 2’-O-methylated, phosphorothioate derivatives, peptide nucleic acids (PNA), and locked nucleic acids (LNA).

The most popular modification involves the use of 2'-O-methyl RNA, which exhibits improved nuclease resistance, higher specificity, faster hybridization kinetics, and a superior affinity for the targets [47]. However 2'-OMe-modified MBs are vulnerable to single strand binding proteins (SSBs) and they open none specifically inside living cells. Thus they generate false-positive signals.

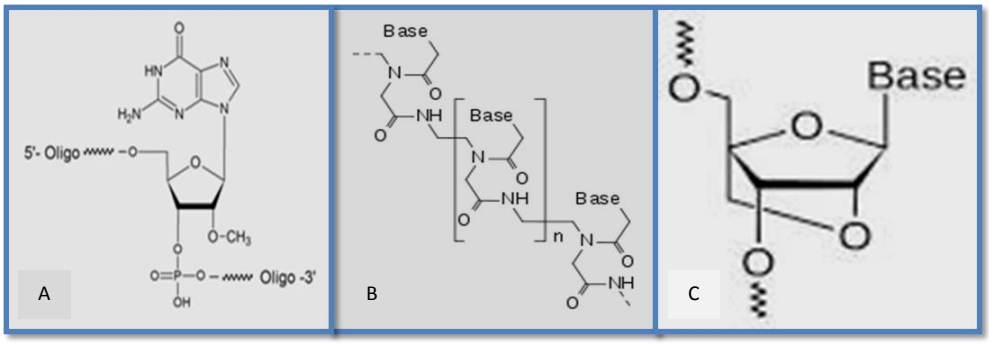

Figure 17. Modified nucleotide bases. A. 2'-O-methyl. B. PNA. C. LNA

Peptide Nucleic acids (PNA) have peptide backbones [48]. PNAs are not degraded by nucleases but have neutral charge, and therefore, are thought to have a lower tendency to interact with intracellular biomolecules [49]. PNAs have not been widely used mainly because PNAs have drawbacks, such as limited solubility causing aggregation in biological environment [50].

Locked Nucleic Acids (LNA) have a bicyclic furanose unit locked in an RNA-mimicking sugar conformation. The incorporation of LNA into the MB backbone presumably eliminated false-positive signals resulting from nuclease degradation and nonspecific interactions; however, hybridization kinetics were significantly slowed due to the high energy barrier of opening the LNA-LNA stem. To resolve this problem, MBs have been designed with a mixture of both LNA and DNA nucleotides in the stem and loop domains (LNA/DNA MB) [51, 52].

Another suitable backbone modification involves preparing MBs with an L-DNA stem [53] L-DNAs are unnatural bases that do not hybridize with natural nucleic acids. It has been reported that L-DNA MBs exhibit reduced intra and inter-molecular stem invasions, enhanced selectivity for the target, and improved biostability.

3.6 Cell-to-cell variations in MB delivery

It is not currently possible to obtain accurate information on cell-to-cell variations in gene expression with conventional MBs. This deficiency stems from the inability to accurately account for the large variations in cellular fluorescence those results from heterogeneous delivery. Thus, cells that have no or low amount of internalized MBs could easily be

mistaken for cells with low gene expression, and resulting in false-negative. Conversely, cells that have high level of internalized MBs generally exhibit a measurable background that can easily be mistaken for probe hybridization, e.g. false-positive. Heterogeneous delivery across a population of cells is a common feature of most (likely all) nucleic acid delivery methods. The inability to measure the efficiency of MB delivery with current MB designs limits their use to studying highly expressed RNA, i.e., studies where fluorescence enhancement upon MB hybridization is significantly greater than the cell-to-cell variability in fluorescence that results from heterogeneous delivery.

Several groups have tried to account for variations in MB delivery by simultaneously introducing both MBs and optically distinct fluorescently labeled oligonucleotides (i.e., a reference probe) into living cells [10, 54, 55]. However, unless microinjection is utilized, it is unlikely that an equal amount of both probes will be delivered into every cell. Further, even if equal quantities are delivered into every cell, there is a very low probability that both probes would exhibit the same intracellular localization pattern and lifetime. This is problematic since any variation in the ratio of MBs to the reference probe, that is not a consequence of MB hybridization, negates the benefits of performing ratiometric measurements. In theory, these problems can be resolved by attaching a reference dye directly to MBs (figure 18), but unfortunately, these results in unwanted interactions between the reference fluorophore, reporter dye, and quencher (FRET and quenching). This problem may be overcome by using quantum dots (QD) as the reference emitter, since QDs are not easily quenched and are photostable [31]. It should be notice that the attachment of a macromolecule/nanoparticle to the MB might complicate and limit the number of viable options for efficiently delivering MBs into the cytoplasm of living cells. Therefore, live cell imaging applications could still benefit from a novel MB design, with an attached reference fluorophore that does not significantly increase the size of the probe.

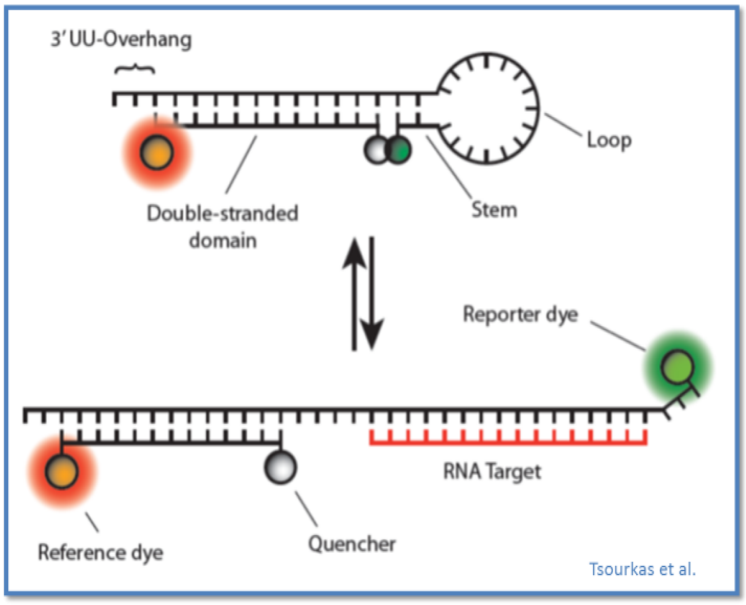

Figure 18. Structure of MB with reference dye

3.7 Sensitivity of the MB fluorescence to the environment

In order to use MBs to accurately measure gene expression in living cells, it is important that the fluorophores that are used not be sensitive to intracellular environment. Unfortunately, many commercially available fluorophores are highly sensitive to their environment. Factors including pH and nonspecific protein interactions have been found to influence fluorescent properties of some fluorophores, either by enhancing or quenching their fluorescence [56]. A strategy capable of assessing the extent to which the emission of commercially available fluorophores is altered within the cytoplasm of single living cells has been developed [35]. Changes in fluorescent emission were detected by comparing the fluorescent signal intensity of each fluorophore to that of a fluorescent reference probe that is insensitive to pH and shielded from the cytoplasmic environment. Comparing the fluorescence ratio F_{DYE}/F_{REF} in living cells and aqueous buffer it is able to identify a number of environment-insensitive fluorophores that may be incorporated into the design of MBs for RNA quantification in living cells [35].

4. Methods for Molecular beacon delivery inside living cells

One of the critical steps required for the accurate detection of RNA molecules in living cells is the efficient delivery of MBs into the cytoplasm. Oligonucleotide probes are generally prevented from access to the cytoplasm due to the barrier imposed by the cell membrane. Further, even if the probe enter the cell successfully, the efficiency of delivery in an imaging assay should be defined not only by how many probes enter the cell or how many cells have probes internalized, but also by what fraction of probes are free to hybridize intracellular RNA. This is in contrast to antisense and gene delivery applications where the reduction/increase in the level of protein expression is the final metric used to define efficiency or success.

Many transfection agents produce punctate fluorescent patterns due to the passage of the MB by the endocytic pathway. Experimental evidence shows that linear fluorescently labeled probes enter in the endosomal/lysosomal pathway with concomitant nuclease-mediated degradation. Reduced amounts of the probe may escape from the endocytic pathway (0.01-10%) after several hours [57]. For these reasons a delivery method in which the MB could enter the cell cytoplasm avoiding endosomal pathway is highly desirable.

Common techniques used for delivery MBs into live cells include microinjection, electroporation, cell-penetrating peptides, and toxin-mediated membrane permeabilization.

4.1 Microinjection

Microinjection is a direct method to deliver oligonucleotide probe into the cytoplasm of a live cell [55]. A limitation of this method is the low number of cells that can be processed at any given time. Moreover, microinjection can affect cell leading to interruption of normal cell function. This led to the use of alternative methods that are thought to be more efficient and less invasive than microinjection. Such methods include cationic transfection agents such as liposomes and dendrimers. However, using of this agents results in punctuate fluorescent patterns that appear to be indicative of endosomal/lysosomal entrapment [58]. MBs entrapped into endocytosis pathway are rapidly degraded by nucleases. Consequently, even when

transfection method allows for endocytosis escape, only low percentage of the probes is active due to not efficient dissociation of MB-transfection agent complexes.

4.2 Electroporation

Electroporation is another method for direct introduction of MBs into cytoplasm of living cells. Traditionally, this method is associated with low cell viability. However, recent advances in electroporation technique like performance in microliter volume, e. g. microporation have led to a reduction in the harmful events such as heat generation, pH variations, and oxide formation. Microporation leads to the uniform cytosolic distribution of MBs probes in live cells with a transfection efficiency of 93 % and average viability of 86 %. [32]. A great advantage of microporation is that delivery of the probes only takes few seconds. This method involves trypsinization, therefore it is several hours before the cells re-adhere to cell-culture plate surface and RNA can be assessed.

4.3 Cell-penetrating peptides

Cell-penetrating peptides (CPPs) have been used to introduce protein, nucleic acids, and other biomolecules into living cells [59, 60, 61]. Among the peptides with membrane translocating activity are antennapedia, HSV-1 VP22, and HIV-1 Tat peptide. The most widely used peptides are HIV-1 Tat peptide and its derivatives, due to their small size and high delivery efficiency. The Tat peptide is rich in cationic amino acids; however the exact mechanism of CPP-induced membrane translocation remains unclear.

Tat peptides were conjugated to molecular beacons using different linkages. Peptide-linked MBs were delivered into living cells to target GAPDH and surviving mRNAs [58]. It was demonstrated that, at relatively low concentrations, peptide-linked MBs were internalized into living cells within 30 min with nearly 100 % efficiency. Moreover, peptide-based delivery did not interfere with either specific targeting or hybridization-induced fluorescence of the probes, and the peptide-linked MBs could have self-delivery, targeting, and reprogramming functions.

Peptide-linked MBs can also be used to target RNA molecules in the cell nucleus by attaching a nuclear localization signal (NLS) peptide to MB. Combining the NLS-linked beacon with the SLO-based reversed membrane permeabilization, MBs designed to target snRNAs U1 and U2 as well as small nucleolar RNA (snoRNA) U3 were delivered into the nuclei of live HeLa cells, and the localization and colocalization (U1 and U2) of these nuclear

RNAs was imaged [62]. This delivery method can be used to image transcriptional and posttranscriptional processing of RNAs in the nucleus of living cells.

4.4 Bio-ballistic

In the bio-ballistics technique, heavy metal particles are coated with molecules, e.g. MBs and propelled into the cells via a gas gun. The first application of this technique was in 1987 on plant cells [63]. In 1990 the technique was used for nucleic acids delivery into mammalian cells [64]. The bio bullets are made with biocompatible metals, for example, gold, having diameters from 1 to 5 micrometers. Bullets are coated with nucleic acid of interest and are propelled by the discharge of a gas into the gun chamber at very high pressure, usually helium or water vapor. The particles enter into the cytoplasm independently of the endosomal pathway, thus avoiding degradation. A disadvantage of the method is that cell membrane can be altered. Bio-ballistic technique is less invasive than microinjection and membrane alterations associated with the shot are usually short lasting. The major disadvantage of the method is that there is no control over the amount of MB delivery into the cell. The amount of MB entering each cell is variable. This method is most suited for cell population studies, but may hamper the interpretation of single cell imaging studies.

4.5 Cell membrane permeabilization

Streptolysin O (SLO) is a pore-forming bacterial toxin and has been used as a simple and rapid means of introducing oligonucleotides into eukaryotic cells [65]. SLO binds as a monomer to cholesterol and oligomerizes into a ring-shaped structure to form pores of approximately 25-30 nm in diameter, allowing the influx of both ions and macromolecules. An essential feature of this technique is that the toxin-based permeabilization is reversible. This can be achieved by introducing oligonucleotides with SLO under serum-free conditions and then removing the mixture and adding normal media with serum [66]. Since cholesterol composition varies with cell types, the permeabilization protocol need to be optimized for each cell type by varying temperature, incubation time, cell number, and SLO concentration. Typically, RNA localization can be assessed 30 min to 2 hours following the introduction of MB probes into cells using SLO-based delivery.

Temporal ability to accurately monitoring the spatio-temporal RNA expression could have a tremendous benefit on understanding gene regulation and control in physiological and pathological conditions. MBs properties make them promising tool for intracellular

monitoring of gene expression and biosensor development. mRNA detection under the native conditions is able to perform due to the unique signaling mechanism of MB action. The remarkable selectivity shows that they specifically detect the desired target among enormous number of unspecific sequences. Sensitivity due to the high quenching efficiency is a great advantage. Thus it can be dynamically trace the cellular responses to external stimuli, such as drug or toxin treatment, as well as differential gene expressions between normal and abnormal cells.

References

1. Tyagi S, Kramer FR. Molecular beacons: probes that fluoresce upon hybridization. Nat. Biotechnol 1996; 14:303-8
2. Fang XH, Liu XJ, Schuster S, Tan WH. Designing a novel molecular beacon for surface-immobilized DNA hybridization studies. J. Am. Chem. Soc. 1999; 121:2921-2922
3. Epstein JR, Leung AP, Lee KH, Walt DR. High-density, microsphere based fiber optic DNA microarrays. Biosens. Bioelectron. 2003; 18:541-546
4. Steemers FG., Ferguson JA, Walt DR. Screening unlabeled DNA targets with randomly ordered fibre-optic gene arrays. Nat. Biotechnol. 2000; 18: 91-94
5. Tyagi S, Bratu DP, Kramer FR. Multicolor molecular beacons for allele discrimination. Nat. Biotechnol. 1998; 16:49-53
6. Tsourkas A, Bao G. Shedding light on health and disease using molecular beacons. Brief. Funct. Genomic Proteomic 2003; 1:372-384
7. Marras SAE, Kramer FR, Tyagi S. Multiplex detection of single-nucleotide variations using molecular beacons. Genet. Anal. 1999; 14: 151-156
8. Brookes AJ. The essence of SNPs. Gene 1999; 234: 177-186
9. Wang K, Tang Z, Yang CJ. et al. Molecular engineering of DNA:molecular beacons. Angewandte Chemie 2009; 48(5): 856-870
10. Bratu DP, Cha BJ, Mhlanga MM, Kramer FR, Tyagi S. Visualizing the distribution and transport of mRNAs in living cells. PNAS 2003; vol. 100, no. 23, pp 13308-13313
11. Santangelo PJ, Nix B, Tsourkas A, Bao G. Dual FRET molecular beacons for mRNA detection in living cells. Nucleic Acids Research 2004; vol. 32, no.6, article e57
12. Rhee WJ, Bao G. Simultaneous detection of mRNA and protein stem cell markers in live cells. BMC Biotechnology 2009; 9:30, DOI: 10.1186/1472-6750-9-30

13. King FW, Liszewski W, Ritner C, Bernstein HS. High-troughput tracking of pluripotent human embryonic stem cells with dual fluorescence resonance energy transfer molecular beacons. Stem cells and Development 2011; 20(3): 475-484. DOI: 10.1089/scd.2010.0219
14. Larsson HM, Lee ST, Roccio M, Velluto D, Lutolf MP, Frey P, Hubbell JA. Sorting live stem cells based on Sox 2 mRNA expression. PLOS ONE 2012, vol. 7, issue 11, e49874
15. Zhao J, Wang Z-Q, Wang X-Y, Yang X-J, He D. Preliminary Study of diagnostic utility of molecular beacons in bladder cancer. Urology 2010, 76 (2) 512.e8-512.e13
16. Kang WJ, Cho YL, Chae JR, Lee JD, Choi K-J, Kim S. Molecular beacon – based bio-imaging of multiple microRNAs during myogenesis. Biomaterials 2011; 32, 1915-1922
17. Lennon FE, Hermann CD, Olivares-Navarrete R, Rhee WJ, Schwartz Z, Bao G, Boyan BD. Use of molecular beacons to image effects of titanium surface microstructure on β1 integrin expression in live osteoblast-like cells. Biomaterials 2010; 31 7640-7647
18. Desai HV, Voruganti IS, Jayasuriya C, Chen Q, Darling EM. Live-cell, Temporal gene expression analysis of osteogenic differentiation in adipose-derived stem cells. Tissue Engineering 2012; DOI: 10.1089/ten.tea.2012.0127
19. Runick SI, Swaminathan J, Sumaroka M, Liebhaber S, Gewirtz AM. Effects of local mRNA structure on posttranscriptional gene silencing. Proc. Natl. Acad. Sci. USA 2008; 105: 13787-92
20. Rhee WJ, Santangelo PJ, Jo H, Bao G. Target accessibility and signal specificity in live-cell detection of BMP-4 mRNA using molecular beacons. Nucleic Acids Res. 2008; 36:e30
21. Pattanayak V, Gifford LK, Lu P, Gewirtz AM. Observed vs predicted structure of fluorescent self-quenching reporter molecules (SQRM): caveats with respect to the use of "stem-loop" oligonucleotides as probes for mRNA folding. RNA 2008; 14:657-65
22. Marras SA, Kramer FR, Tyagi S. Efficiency of fluorescence resonance energy transfer and contact mediated quenching in oligonucleotide probes. Nucleic Acid Res. 2002; 30(21): e122
23. Parkhurst KM, Parkhurst LJ. Donor-acceptor distance distributions in a double-labeled fluorescent oligonucleotide both as a single strand and in duplexes. Biochemistry 1995; 34(1): 293-300
24. Bernacchi S, Mély Y. Exciton interaction in molecular beacons: a sensitive sensor for short range modifications of the nucleic acid structure. Nucleic Acid Res. 2001; 29(13): e62

25. Tsourkas A, Behlke MA, Bao G. Structure-function relationships of shared-stem and conventional molecular beacons. Nucleic Acid Res. 2002; 30(19): 4208-4215
26. Seidel CAM, Schulz A, Sauer MHM. Nucleobase-specific quenching of fluorescent dyes. 1. Nucleobase one-electron redox potentials and their correlation with static and dynamic quenching efficiency. Journal of Physical Chemistry 1996; 100(13): 5541-5553
27. Heinlein T, Knemeyer JP, Piestert O, Wolfrum J, Sauer M. Nucleobase-specific quenching of fluorescent dyes in DNA-hairpins. The Journal of Physical Chemistry 2003; 107(31): 7957-7964
28. Oladepo SA, Loppnow GR. Self-quenching smart probes as a platform for the detection of sequence-specific UV-induced DNA photodamage. Analytical and Bioanalytical Chemistry 2010; 397(7): 2949-2957
29. Tyagi S, Alsmadi O. Imaging native beta-actin mRNA in motile fibroblasts. Biophys. J. 2004; 87:4153-4162
30. Vargas DY, Raj A, Marras SA, Kramer FR, Tyagi S. Mechanism of mRNA transport in the nucleus. Proc. Natl. Acad. Sci. USA 2005; 102: 17008-17013
31. Chen AK, Behlke MA, Tsourkas A. Avoiding false-positive signals with nuclease-vulnerable molecular beacons n single living cells. Nucleic Acids Res. 2007; 35: e105
32. Chen AK, Behlke MA, Tsourkas A. Efficient cytosolic delivery of molecular beacon conjugates and flow cytometric analysis of target RNA. Nucleic Acids Res. 2008; 36: e69
33. Mhalanga MM, Vargas DY, Fung CW, Kramer FR, Tyagi S. tRNA-linked molecular beacons for imaging mRNAs in the cytoplasm of living cells. Nucleic Acids Res. 2005; 33: 1902-1912
34. Peng XH, Cao ZH, Xia JT, Carlson GW, Lewis MM, Wood WC, Yang L. Real-time detection of gene expression in cancer cells using molecular beacon imaging: New strategies for cancer research. Cancer Res. 2005; 65: 1909-1917
35. Chen AK, Cheng Z, Behlke MA, Tsourkas A. Assessing the sensitivity of commercially available fluorophores to the intracellular environment. Anal. Chem. 2008; 80: 7437-7444
36. Kim JH, Morikis D, Ozkan M. Adaptation of inorganic quantum dots for stable molecular beacons. Sensors Actuators B-Chem. 2004; 102: 315-19
37. Kim Y, Soh D, Tan W. Molecular beacons in biomedical detection and clinical diagnosis. Int. J. Clin. Exp. Pathol. 2008; 1: 105-16
38. Kushon SA, Ley KD, Bradford K, Jones RM, McBranch D, Whitten D. Detection of DNA hybridization via fluorescent polymer superquenching. Langmuir 2002; 18: 7245-49

39. Bonnet G, Tyagi S, Libchaber A, Kramer FR. Thermodynamic basis of the enhanced specificity of structured DNA probes. Proc. Natl. Acad. Sci. USA 1999; 96(11): 6171-6176
40. Tsourkas A, Behlke A, Rose SD, Bao D. Hybridization kinetics and thermodynamics of molecular beacons. Nucleic Acid Res. 2003; 31(4): 1319-1330
41. Tyagi S, Marras SAE, Kramer FR.Wevelenght-shifting molecular beacons. Nature Biotechnology 2000; 18(11):1191-1196
42. Tan L, Li Y, Drake TJ, et al. Molecular beacons for bioanalytical applications. Analyst 2005; 130(7): 1002-1005
43. Zuker M. Mfold web server for nucleic cid folding and hybridization prediction. Nucleic Acid Res. 2003; 31(13): 3406-3415
44. Perlette J, Tan W. Real-time monitoring of intracellular mRNA hybridization inside single living cells. Analytical Chemistry 2001; 73(22): 5544-5550
45. Yang CJ, Li JJ, Tan W. Using molecular beacons for sensitive fluorescence assays of the enzymatic cleavage of nucleic acids. Methods inMolecular Biology 2006; 335: 71-81
46. Chen AK, Behlke MA, Tsourkas A. Subcellular trafficking and functionality of 2'-O-methyl and 2'-O-methyl-phosphorothioate molecular beacons. Nucleic Acids Res. 2009
47. Tsourkas A, Behlke MA, Bao G. Hybridization of 2'-O-methyl and 2'-deoxy molecular beacons to RNA and DNA targets. Nucleic Acids Res. 2002; 30:5168-5174
48. Good L, Nielsen PE, Progress in developing PNA as a gene-targeted drug. Antisence Nucleic Acid Drug Dev. 1997; 7: 431-437
49. Leiros I, Timmins J, Hall DR, McSweeney S. Crystal structure and DNA-binding analysis of RecO from Deinococcus radiodurans. EMBO J. 2005; 24: 906-918
50. Dueholm KL, Egholm M, Behrens C, Chistensen L, et al. Synthesis of peptide nucleic-acid monomers containing the 4 natural nucleobases – thymine, cytosine, adenine, and guanie and their oligomerization. J. Org. Chem. 1994; 59: 5767-5773
51. Wu Y, Yang J, Moroz LL, Tan W. Nucleic acid beacons for long-term real-time intracellular monitoring. Anal. Chem. 2008; 80: 3025-3028
52. Yang CJ, Wang L, Wu Y, Kim Y, Medley CD, Lin H, Tan W. Synthesis and investigation of deoxyribonucleic acid/locked nucleic acid chimeric molecular beacons. Nucleic Acids Res. 2007; 35: 4030-4041
53. Kim Y, Yang J, Tan W. Superior structure stability and selectivity of hairpin nucleic acid probes with an L-DNA stem. Nucleic Acids Res. 2007; 35: 7279-7287

54. Drake TJ, Medley CD, Sen A, Rogers RJ, Tan W. Stochasticity of manganese superoxide dismutase mRNA expression in breast carcinoma cells by molecular beacon imaging. Chembiochem 2005; 6: 2041-2047
55. Medley CD, Drake TJ, Tomasini JM, Rogers RJ, Tan W. Simultaneous monitoring of the expression of multiple genes inside of single breast carcinoma cells. Anal. Chem. 2005; 77: 4713-4718
56. Graber ML, DiLillo DC, Friedman BL, Pastoriza-Munoz E. Characteristics of fluoroprobes for measuring intracellular pH. Anal. Biochem. 1986; 156:202-212
57. Dokka S, Rojanasakul Y. Novel nonendocytic delivery of antisence oligonucleotides. Adv. Drug Deliv. Rev. 2000; 44:35-49
58. Nitin N, Santangelo PJ, Kim G, Nie S, Bao G. Peptide-linked molecular beacons for efficient delivery and rapid mRNA detection in living cells. Nucleic Acids Res. 2004; 32:e58
59. Becker-Hapak M, McAllister SS, Dowdy SF. TAT-mediated protein transduction into mammalian cells. Methods 2001; 24:247-56
60. Snyder EL, Dowdy SF. Protein/peptide transduction domains: potential to deliver large DNA molecules into cells. Curr. Opin. Mol. Ther. 2001; 3:147-52
61. Wadia JS, Dowdy SF. Protein transduction technology. Curr. Opin. Biotechnol. 2002; 13: 52-56
62. Nitin N, Bao G. NLS peptide conjugated molecular beacons for visualizing nuclear RNA in living cells. Bioconj. Chem. 2008; 19(11): 2205-11
63. Klein TM, Wolf ED, Wu R, Sanford J. C. High-velocity microprojectiles for delivering nucleic acids into living cells. Nature 1987; 327(6117): 70-73
64. Yang NS, Burkholder J, Roberts B, Martinell B, McCabe D. In vivo and in vitro gene transfer to mammalian somatic cells by particle bombardment. Proc. Natl. Acad. Sci. USA 1990; 87(24): 9568-9572
65. Giles RV, Spiller DG, Grzybowski J, Clark RE, Nicklin P, Tidd DM. Selecting optimal oligonucleotide composition for maximal antisense effect following Streptolysin O-mediated delivery into human leukemia cells. Nucleic Acids Res. 1998; 26(7): 1567-1575
66. Walev I, Bhakdi SC, Hofmann F, et al. Delivery of proteins into living cells by reversible membrane permeabilization with Streptolysin-O. Proc. Natl. Acad. Sci. USA 2001; 98(6): 3185-3190

Chapter III. Molecular beacons - design, synthesis, targets library

The main goal of this study was design and synthesized a broad range of molecular beacons targeting genes up-regulated or down-regulated during differentiation, genes with fluctuating expression within cell cycle as well as housekeeping genes with relatively constant expression. Thus dynamic changes like gain-of-expression or loss-of-expression can be detected and followed as a response to different stimuli.

1. Molecular beacons design

mRNA - targeting molecular beacons were designed using Beacon Designer 7.9 (Premier Biosoft). The target sequence for each MB was analyzed by Human Genome BLAST (http://blast.ncbi.nlm.nih.gov/Blast.cgi) to minimize risks of unspecific binding to unrelated mRNA. The program was used to avoid cross homologies, repeats, and low complexity regions based on expect (E)-value and percentage identity. The E-value is the number of hits expected with similar or better score and it depicts the significance of match (an E-value of 0 indicates complete homology). Regions with E-value greater than the target value were avoided. Percentage identity is the percentage of identical bases between query and subject sequence in an alignment. A percentage identity of 100 indicates complete homology. The regions with percentage identity greater than the percentage identity criterion (default = 98 for the human genome) were avoided. Regions not satisfying both E-value and the percentage identity criteria were avoided.

It is important to design the molecular beacon in an area of the target with minimal secondary structure formation. This helps to prevent the template from preferentially annealing to itself faster than to the molecular beacon. The program identified and avoided template sequence predicted to give rise to significant secondary structures.

The parameters for MBs design was set to ensure that the search succeeded in finding the best possible sequence. The length of MBs was between 18 and 30 bp. The melting temperature (T_m) values of the probes are calculated using nearest neighbor thermodynamic calculation

using Santa Lucia values [1]. The parameters were set as follow: hairpin maximum dG (the free energy of the most stable alternate hairpin that is acceptable) 4 -kcal/mol; self-dimer maximum dG (the free energy of the most stable self-dimer that is acceptable) 7 -kcal/mol; cross dimer maximum dG (the free energy of the most stable cross-dimer that is acceptable in a multiplex reaction) 7 -kcal/mol; run/repeat maximum – 5 bp/dinucleotide probes with single (e.g. AAAAA) runs or dinucleotide (ATATATATAT) repeats of length greater than the specified value were discarded. After selecting a probe sequence, two complementary arm sequences were added, one on each side of the probe sequence. The stem region of MB was five bp long, with a CG content of 80 %.

All calculations performed with this program used the following conditions: Temperature for beacon free energy calculation 55°C, monovalent ion concentration 100 mM, free Mg^{2+} concentration 3 mM, target concentration 250 nM.

In Beacon Designer the search algoritm calculates all properties of every possible probe within the allowed length and positional boundaries, and rates them. The rating determines how well the designed oligonucleotide meets the search parameters relative to tolerance limits specified for each parameter. The parameters used the rating are maximum hairpin dG, maximum self-dimer dG, maximum run/repeat length, maximum cross-dimer dG and T_m; if all parameters are exactly on target, the rating is 100. The rating of the probe depends on two factors: how close the probe is to the target value of each parameter, and how tightly the tolerances (permissible value of variation acceptable by the program from a pre-set standard value) are specified. Highly rated probes have most or all parameters near their ideal values and are very likely to work well. For the MB probe search the quality of the designed probe is displayed as “best” (rating greater or equal to 75), “good” (rating between 74 and 50), “poor” (rating bellow 50), or “not found”. Only MBs with a “best” rating were chosen for synthesis and further evaluation.

2. Molecular beacons synthesis

Molecular beacons were synthesized as DNA or with 2’-O-methyl RNA backbone, fluorochrome molecule (Cy3 or Texas red) attached to the 5’-end and black hole quencher 2 (BHQ2) attached to the 3’-end (Eurofins MWG Operon). The exact composition of MBs is described further in the corresponding chapter. Sequences of designed and used molecular

beacons (in red font color) are listed in table 1. Molecular beacons were diluted in RNAse/DNAse free dH_2O to yield stock concentration of 100 µM and stored at -20° C.

3. Molecular beacons targets

Molecular beacon targets were divided into groups. The first group covered the markers for pluripotency – the most common markers such as Oct4, Sox2 and Nanog, as well as markers for completely reprogrammed induced pluripotent stem cells (iPSC) – like REX1 and DNMT3B.

The second group included markers for cells differentiated in neuronal linage – neuronal stem cell markers (Musashi 1), ectoderm marker (nestin), markers for mature neurons (NeuN, MAP2, Tuj1), neurite outgrowth (GAP43, Neuropilin), synapsis formation (synaptophisin), markers for highly specialized dopamine neurons (Nurr1, TH) as well as glial marker (GFAP).

Further a set of MBs targeting marker of the other two primary germ cell layers – endo- and mesoderm were designed as well as markers for adipogenic differentiation.

Table 1.

Pluripotent stem cell markers	
Oct 4 (645) var 1	CATGTTCTTGAAGCTAAGCTGCA
Oct 4 (620) var 2	TCATTCACCCATTCCCTGTT
Oct 4 (734) var 3	TTAGAGAAATAGATAAGCTGCTAAGTT
Sox 2	CGCCGCCGATGATTGTTATTAT
Nanog var 1	TGGAAGATGTTAGAGAAATAGGAC
Nanog var 2	GAGAAATAGGACCTCCAGA
REX 1 (ZFP42)	AAGTGAGTCCTCTTCCAGG
DNMT3B	AGGTCTTGCCAGCTCGCA
TDGF1	AAGAAGTAAGAAGTAGTTCTGTAAGGAA
GDF 3	ACATCCAGCAGGTTGAAGTG
v-Myc	CCGCTTCTCCACAGTGACC
CD 133	GCTTTATGGGAGTCTTGGG

Neuronal markers	
Nestin (ectoderm)	TCTCACTACCTCCACATCCT
GAP-43	ATGTGTCCACGGAAGCTAG
NeuN	TCCCATTCAGCTTCTCCCG
MAP 2	GTTGTCTCTGGCTGAGAAACTAA
TH	ACACCTTCACAGCTCGGGA
Tuj 1	CGAATCCACCAGCTCCGC
Nurr 1	GCCTGTGCTGTAGTTGTCCATA
GFAP	GGTGGCTTCATCTGCTTCCTG
Musashi 1 (NSC)	CTCCACGATGTCCTCACTCT
Synaptophisin	GGGTCTCCTGGCTTGAGG
Neuropilin	AAAGAAAGCAGCGAGGCAATG
NG2	CTGGAAGGCCAAGGGTGC
Neurogenin	CGCTTGCATTCAATCATTACAA
Endo-/mesoderm markers	
primitive	
GATA 4	TTAAATCCAGCATTGAGCAAAG
GATA 5	CAGGTTTCTGGCATTGCT
GATA 6	TTCCAGCACATATTCCACAG
Sox17	CCCAGGACAACATTTCTTTGAT
AFP	TTGGAAGCATTCAACTGCATT
B-catenin	GTTGAGCAAGGCAACCATT
Gsc (Goosecoid)	GTGTGCAAGAAAGTAGCATCGT
Hnf1b	TTTGTCTGTCATATTTCCAGAACTCT
definitive	
FOXA2 (HNF-3β)	GGATGGAGTTCTGCCAGCG
Primitive streak/gastrulation markers	
Mixl 1	AGGCAGTTCACATCTACCTCAAGA
Brachyury	AGGAGTTCAGCATGATCTGGC

House keeping markers	
B-actin	CAGCACTGTGTTGGCGTACA
GAPDH	AGTTGGTGGTGCAGGAGG
Proliferation and cell cycle markers	
Cyclin B1	CCGACCCAGACCAAAGTTT
Cyclin B2	AGTTCGCCTAATAGTCACATGA
Cdk 2	GAGCAGAGGCATCCATGA
PCNA	AGTGTCACCGTTGAAGAGA
Adipogenic markers	
Adiponectin	CGATGAATGAATGAATAAATGAATGAGT
LPL	TACTTTCACAGTCGGGTTCC
PPRA gamma	TTGTGAATGGAATGTCTTCGTAAT
C/EBP alfa	GACTGATCGTGCTTCGTGT
C/EBP beta	TTGCGTCAGTCCCGTGTAC
C/EBP delta	GGTGGTAAGTCCAGGCTG

4. Molecular beacons characterization

Further MBs were characterized in regard to melting temperatures, signal intensity and signal to noise ratio (S/N). In general it was observed that in most cases MBs with 2-O-methyl RNA backbone have higher signal to noise ratio but lower signal (figure A). In contrast DNA probes own higher signal intensity but lower signal-to-noise ratio (figure B).

Melting points of the stem above 40ºC verifies that sponaneous opening of MBs is not occurring inside the cells (figure C and D).

Thake all this into acount we decide to test modified backbone probes into living cells. Moreover they are nuclease resistent and thus fals positive signals can be avoided. However some of the initial experiments were performed with DNA MBs.

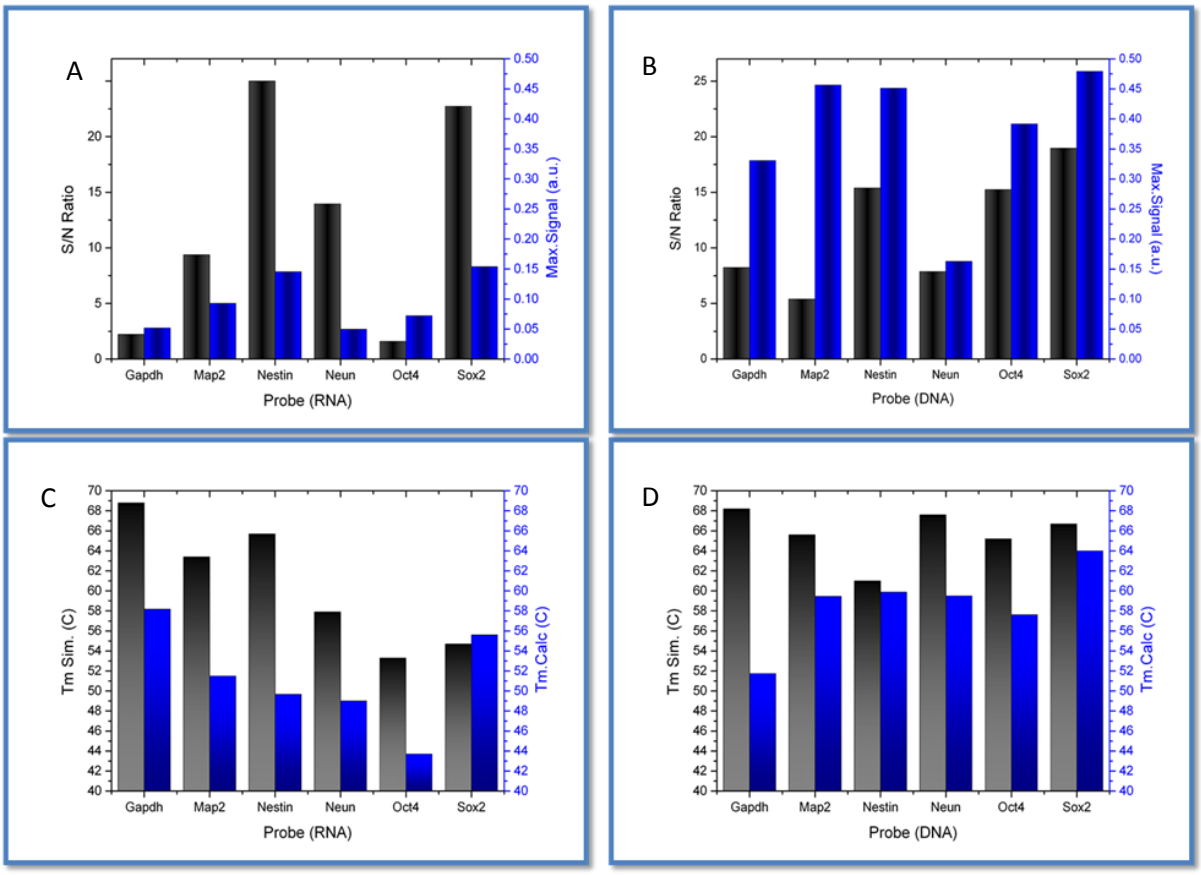

Figure 19. In vitro characterization of MBs. A and B - Signal- to- noise ratio (black bars) and maximum signal (blue bars) of RNA and DNA probes. C ad D – melting temperatures – experimentaly detected (black bars) and calculated (blue bars) of RNA and DNA probes

References

1. SantaLuciaJ., Jr. A unified view of polymer, dumbbell, and oligonucleotide DNA nearest-neighbor thermodynamics. Proc. Natl. Acad. Sci. USA 1998; 95:1460-1465.

Chapter IV. MBs detection and tracking of neuronal markers expression in living human neurons

1. Introduction

Tracking, when a gene is on or off, is crucial to elucidate signaling networks but requires ideally that gene expression can be followed in real time in living cells. The aim of this study was to demonstrate significance of MBs for studying molecular events inside living cells and particularly to detect and trace dynamically changes in gene expression during differentiation of stem cells into neural lineage. To follow gene expression during differentiation of human embryonic mesencephalon derived cells into dopamine neurons, MBs probes targeting markers for different stages in neuronal development were designed and synthesized as 2'-O-methyl RNA backbone oligonucleotides. Here is described the design and usage of MBs towards GAPDH, NeuN, MAP2, Nestin and Tyrosine hydroxylase (TH) mRNA to follow neural stem cell progression from neural progenitors, mature neurons, into highly specialized dopaminergic neurons. Time laps of growing and differentiating cells allowed for determination of differentiation stage of each cell in the population during seven-day experiment.

For a model system human embryonic mesencephalon derived cells were used. LUHMES cell line (ATCC, CRL2927) is a subclone of MESC2.10 cells was derived from first trimester human mesencephalic cells retrovirally infected with a LINX v-myc vector [1]. In this system, a tetracycline-controlled transactivator (tTA) strongly activates transcription from a minimal CMV promoter in the absence of tetracycline. Constitutive expression of v-myc allowed cells to proliferate continuously in culture. Replacement with the culture supplemented with tetracycline abolished transcription activation by tTA and blocked the production of v-myc. In addition to tetracycline medium also contained db-cAMP and GDNF – factors that promoted the differentiation of cells into DA-producing neurons (figure 20).

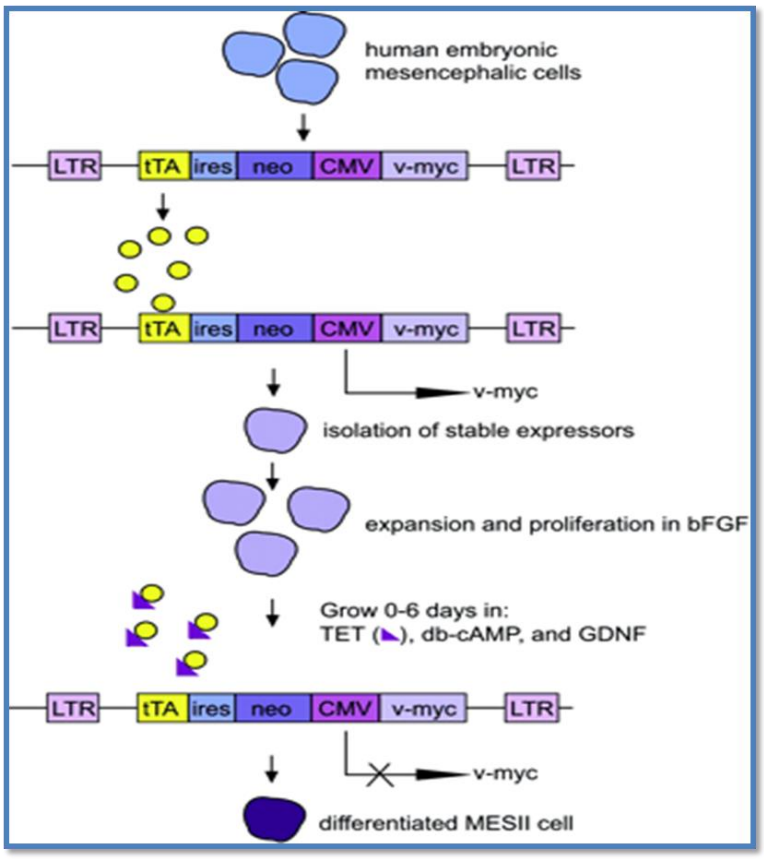

Figure 20. Generation of MESC2.10 cells. Eight weeks old human mesencephalic cells were retrovirally infected with a LINX *v-myc* vector. A tetracycline-controlled transactivator (tTA, yellow circles) strongly activates transcription from a minimal CMV promoter in the absence of tetracycline. Constitutive expression of *v-myc* in the absence of tetracycline allowed cells to proliferate continuously in culture. Replacement with medium containing 1µg/ml tetracycline (purple triangles) abolished transcription activation by tTA and blocked the production of *v-myc* (Lotharius et al., 2002).

The proliferating d0 cells not only expressed markers of neuronal precursors, but also many neuronal markers and several dopaminergic features. Thus, d0 have already a definite neuronal commitment. After 6 days in differentiation medium, additional neuronal and dopaminergic features are up-regulated, including TH, which would typically be found in differentiated dopaminergic neurons [2]. However, some of the features usually associated with immature neurons, such as nestin expression, are not lost in this stage. The mixed maturity status of differentiated LUHMES makes this particular cell line a valuable model for investigation the detection properties of MBs in

terms of dynamics in gene expression on a single cell level and discrimination cell-to-cell variations.

MBs targets used here covered markers for immature progenitors, mature and highly specialized neurons. Nestin is a type VI intermediate filament protein and it is widely employed marker of multipotent neural stem cells. Nestin is highly expressed in dividing progenitor cells during development of nervous system. Upon differentiation, nestin becomes down-regulated. However, it is still expressed in differentiated LUHMES.

NeuN (Fox-3) is a neuronal nuclear antigen and it is commonly used as a biomarker for neurons. It is up-regulated as neurons mature. MAP2 (microtubule-associated protein) is involved in microtubule assembly which is an essential step in neurogenesis. The protein is enriched in dendrites, implicating a role in determining and stabilizing dendritic shape during neuron development. It is shown that MAP2 staining in LUHMES appears to be restricted to the cell single main extension on d5 and d10 of differentiation.

Tyrosine hydroxylase is one of the most important markers of mature dopamine neurons. It is enzyme catalyzing reaction converting L-tyrosine to L-DOPA – a step in the biosynthesis of catecholamines. The activity of the TH is reduced in the patients with neurodegenerative diseases such as Parkinson's and Alzheimer's disease.

Finally, a toxin based membrane permeabilization method for delivery of MBs into neurons was optimized and successfully applied in LUHMES.

2. Material and methods

2.1 Molecular beacons

Sequences of MBs used in this experimental set-up are listed in Table 2. MBs were synthesized with an 2'-O-methyl RNA backbone, Cy3 molecule attached to the 5'-end, and black hole quencher 2 (BHQ-2) attached to the 3'-end (Eurofines MWG Operon).

Table 2. Molecular beacon sequences

MB target	GenBank N	Sequence
GAPDH	NM_002046.3	CGCUC AGUUGGUGGUGCAGGAGG GAGCG
Nestin	NM_006617	CGCUCUCUCACUACCUCCACAUCCUUGAGCG
NeuN	NM_001082575.1	CGCUC UCCCAUUCAGCUUCUCCCG GAGCG
MAP2	NM_002374.3	CGCUCGUUGUCUCUGGCUGAGAAACUAA GAGCG
TH	NM_199292.2	CGCUCACACCUUCACAGCUCGGGA GAGCG

2.2 Propagation of undifferentiated LUHMES cells

Propagation was performed by using cell culture flasks pre-coated with Geltrex™ LDEV-Free hESC-qualified Reduced Growth Factor Basement Membrane Matrix (Invitrogen) diluted 1:100 in PBS. Cultures were maintain in proliferation medium, consisting of Advanced DMEM/F12 (Sigma), 1xN2 supplement (Gibco), 2 mM L-glutamine, and 40 ng/ml recombinant bFGF (Invitrogen).

2.3 Differentiation of LUHMES into dopamine neurons

Cells were grown to a density of 60-70 %; the differentiation process was then initiated by adding differentiation medium consisting of Advanced DMEM/F12, 1xN2 supplement, 2 mM L-glutamine, 1 mM dbcAMP, 1 µg/ml tetracycline, and 2 ng/ml recombinant human GDNF (R&D system). The half of the differentiation medium was changed every second day.

2.4 Toxin based membrane permeabilization

MBs were introduced into the cytoplasm of living cells by toxin-based membrane permeabilization using Streptolysin O (SLO, Sigma). Prior to use, SLO (1 µg/ml) was activated with Tris (2-carboxyethyl) phosphine hydrochloride solution (TCEP, Sigma) at a final concentration 5mM, for at least 30 min at 37°C. Adherent LUHMES cells were washed with Dulbecco's phosphate-buffered saline (DPBS) without Ca^{2+} and Mg^{2+}, and trypsinized for 3 min at 37°C. The cell suspension was centrifuged for 5 min

at 190 x g to collect the cells. The cells were re-suspended in Opti-MEM medium. 1 x 10^5 cells were incubated with activated SLO at a concentrations between 1 ng/ml (0.07 U/ml) and 800 ng/ml (59.7 U/ml) and MBs (2µM) in a final volume 100µl for approximately 15 min. Permeabilized cells were resealed by washing in DPBS containing Ca^{2+} and Mg^{2+}, and plated on Geltrex®-coated dishes in GM. The differentiation process was started 24 h after plating by exchanging the GM with DM. The steps of SLO transfections are schematically present in figure 21.

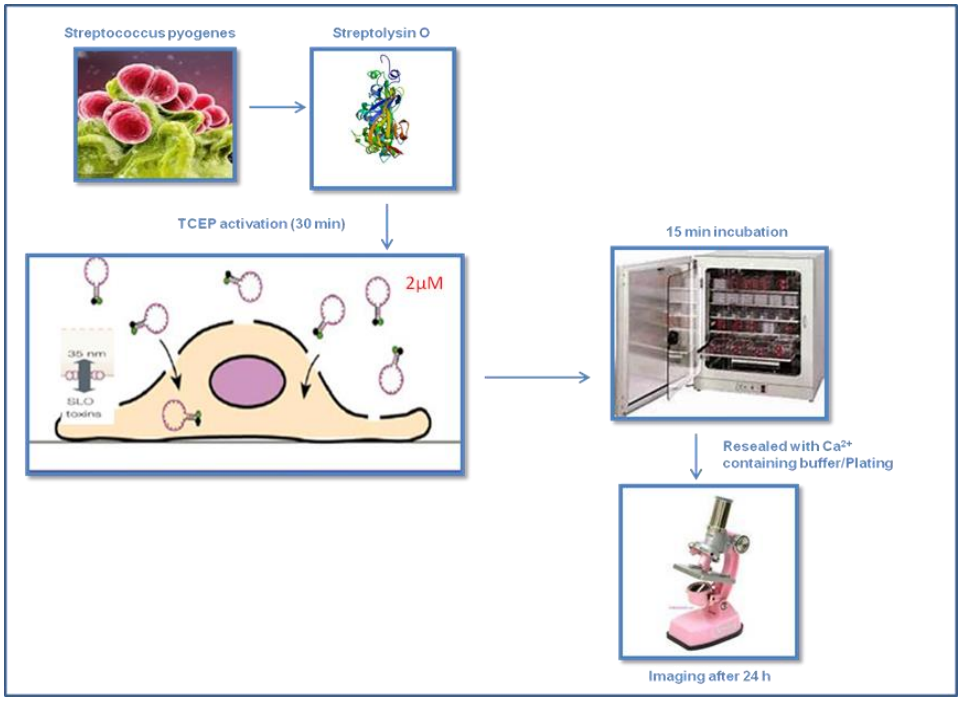

Figure 21. Schematically presentation of SLO transfection steps

2.5 Detection of cellular viability

Cellular viability was detected by calcein-propidium iodide staining. Medium from each well was carefully removed and cells were incubated for 30 min with 3 µM calcein AM (live dye) and 2.5 µM propidium iodide (dead dye) diluted in warm 1x DPBS without Ca^{2+} and Mg^{2+}.

2.6 Imaging and image analysis

Phase contrast and fluorescent images were acquired with Carl Zeiss Axio Vision 4.8.2 equipped with ApoTome Imaging system, 40x/0.75 Plan-Neofluar objective, HBO lamp, and a Zeiss Axiocam MRm B/W camera. The same exposure time and filter set – 43 HE Ds Red 538-570 nm were used for all experiments. Single-cell image analysis

was done using ImageJ software. A region of interest (ROI) was draw around the cell and the total fluorescent intensity was measured. The background fluorescence was detected by drawing a ROI in an area outside the cell of interest and measured the total fluorescent intensity. In ImageJ, the total fluorescent intensity is reported as Integrated density – the sum of the values of the pixels in the selection. The background measurement of fluorescent intensity was subtracted from the cellular measurement [3]. Cells expressing gene of interest were determinate as number of cells with positive fluorescent signal from targeting MB per 100 counted cells.

2.7 Quantitative real-time polymerase chain reaction (qRT-PCR)

The total RNA was isolated using commercially available RNeasy Mini kit (Quiagen). Adherent cells were lysed directly on the dish by the addition of lysis buffer. The lysates were collected and purified according manufacturer's instructions. Single-stranded cDNA was prepared from total RNA using RT random primers under standard conditions with MultiScribe Reverse Transcriptase (Applied Byosystem). The cDNA from each sample was diluted and used for real-time PCR analysis for quantification of neuronal marker expressions. TaqMan assays (Invitrogen) for target genes were used are listed in the table 3.

Table 3.

Assay	ID
GAPDH	ID Hs03929097_g1
Nestin	Hs00707120_s1
MAP 2	Hs00258900_m1
NeuN (RBFOX3)	Hs01370653_m1
TH	ID Hs00165941_m1

PCR amplifications were performed in duplicates with Chromo4 Real-Time Detection system (BioRad) at 95°C for 10 s followed by 40 cycles of 95°C for 5 s and 60°C for 30 s. To quantify the relative expression of each gene, the C_t (threshold cycle) values were normalized to the C_t value of GAPDH (e.g ΔC_t = C_t(target) - C_t(GAPDH). All experiments included negative controls consisting of no cDNA for any assay.

2.8 Statistical analysis

Results are expressed as mean ± standard error of the mean (SEM). qPCR were analyzed using a Student's t test (n=5). Analyses were performed using Graph Pad Prism v.6 (GraphPad Software Inc., CA, USA).

3. Results

3.1 Introduction of MB into cells.

Cell viability and transfection efficiency was investigated as a function of SLO concentration ranging from 1 ng/ml (corresponding to 0.07 U/ml) to 800 ng/ml (corresponding to 59.7 U/ml). Transfection efficiency was evaluated using a molecular beacon towards GAPDH mRNA. Cell viability was evaluated using calcein/propidium iodide staining. An SLO concentration of 17 U/ml (230 ng/ml) was determined to be the optimal concentration with 75% of the cells showing signal from MB-GAPDH 24h post-transfection and with >95% cell showing viability. (Figure 22 A). Moreover, cells showed no growth or differentiation defects and they exhibited the same morphology as non-transfected cells (Fig 22 B shows untransfected cells and white light images in Figure 24 show transfected cells). SLO concentration of 17 U/ml (230 ng/ml) was used in further experiments.

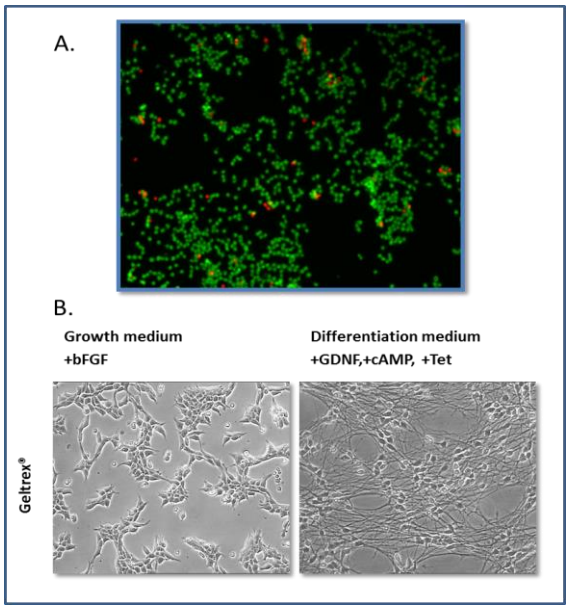

Figure 22. Cell viability after SLO treatment and morphology of LUHMES. (A) Cells treated with 17 U/ml SLO and stained with calcein/PI for detection of cell viability after toxin-based membrane permeabilization. Live cells are stained in green, dead cells are stained in red. (B) Morphology of non-transfected LUHMES on Geltrex® in GM (left) and DM (right).

The number of molecular beacons effectively transfected inside the cells was deduced through a simple model of diffusion. In this study the molecular beacons were reduced to solid object of fixed radius crossing the cellular membrane because of diffusion. Other interactions, such as electrostatic interaction between RNA, protein and membranes, were ignored.

It was considered that a cell of 10µm diameter immersed in a uniform medium with a concentration of 2 µM molecular beacons (see material and methods). The cellular membrane was considered to be 10 nm thick and spangled with 200 pores (2 pores per μm^2) of 30 nm diameter generated by SLO treatment [4.].

The model showed that the concentration will reach a steady state inside the cell within seconds and it is possible to consider the intracellular MB concentration to be equal to the MB found in the medium. The concentration was uniform and reached a steady state after only 1.5 seconds which is far shorter than the 15 minutes the pores are open during transfection. The precise number of MBs inside the cell was calculated by dividing the volume of the cell by the volume of a single beacon excluding the area of the nucleus in which the beacons are not piercing, that in this case is ~90% of the total cell volume. Assuming a cell with size 10x10x10 micrometer in volume, the result showed that about 56000 beacons are transfected into each cell. Bustin [6.] approximated that there is about 10^8 mRNA copies GAPDH per microgram total RNA. Assuming that there are about 4 pg total RNA per cell, there are about 400 GAPDH mRNA copies per cell indicating that there are about 100-fold more MBs than possible target. For lower expressed genes, the MB to target ratio is far higher.

3.2 Molecular beacons detect increasing neuronal markers gene expression in LUHMES after differentiation into dopamine neurons

Molecular beacons targeted against mRNA specific for neural progenitors (Nestin), mature neurons NeuN and MAP2 and highly specialized dopamine neurons (Tyrosin hydroxylase, TH) were delivered into embryonic midbrain derived cells (LUHMES). Molecular beacon targeting GAPDH was used as a control. Cells were left to attach to the culture plates for 24h after transfection in GM supplemented with bFGF. 24h after

transfection the differentiation process was induced by switching medium to DM containing dbcAMP, tetracycline and GDNF. Fluorescent signal examination started 24h after transfection and images were taken every 24h for 192h. The patterns of fluorescence signal emitted from cells varied (Figure 23.), and included small dotted signals (Figure 22. A1, B1), more compact punctate shape (Figure 23. A2, B2), or cytoplasmic widespread cluster-like fluorescence (Fig. 23. A3, B3). The last pattern was more often observed in differentiated cells due to the compact cell body and tight perinuclear cytoplasm organization. Non-differentiated cells showed signals in the lamelipodia and cell body space (Figure 23. A2), while differentiated cells showed only cell body localized MB signals (Figure 24.). All signals categories were included when calculating percentage of positive cells (see below). Large bright signals were interpreted as false positives, being emitted from morphologically dead cells (Figure 23. C). Those false positive signals were excluded from the analysis.

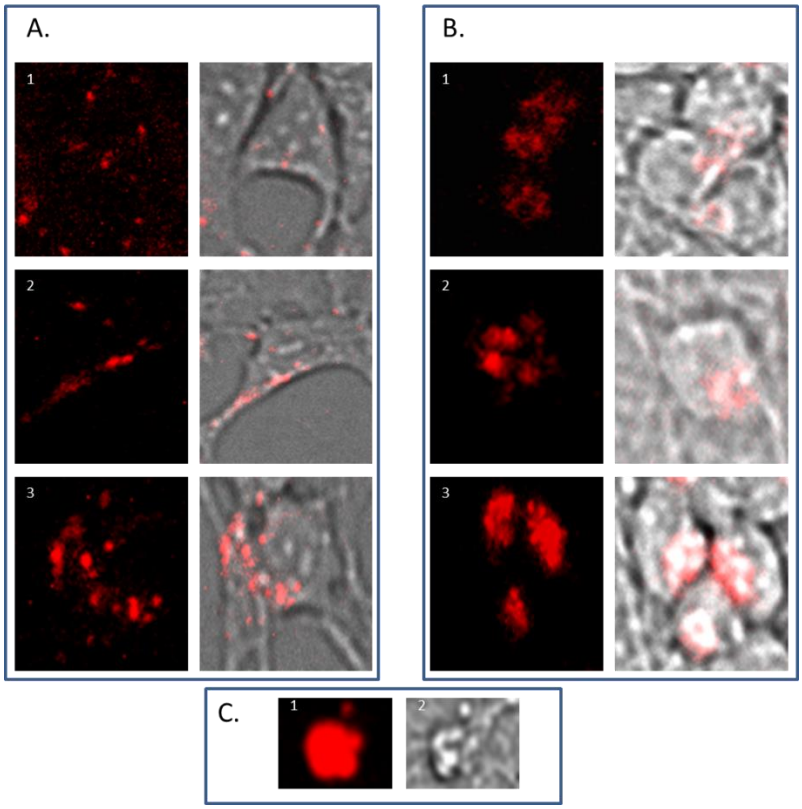

Figure 23. Different MB signal patterns observed in LUHMES cells grown in GM 24 h after transfection (A) and 168 h post differentiation (B). A1, B1 - dotted signals; A2, B2 - compact punctate shape; A3, B3 - cluster-like fluorescence. (C) C1 - Big bright fluorescent clusters originating from apoptotic cells (artifact). This pattern of signal was excluded from calculations of the number of positive cells and signal intensity. C2 - Morphology of apoptotic cell with blebbing. The signal shown is using GAPDH-MBs.

Figure 24 shows images of the signals emitted from MBs signals taken 24h post transfection and 168h after induction of differentiation. GAPDH MB was used as transfection control and approximately 75% of cells showed to be positive 24h post transfection. Nestin, an intermediate filament protein expressed in dividing cells during the early stages of development of CNS and nuclear protein antigen (NeuN) were also detected 24h after transfection but only in about 40 % of the cells (Figure 24 and Figure 25). By contrast, MAP2 and TH were not expressed in cells 24 h post induction of differentiation (Figure 24 and Figure 25).

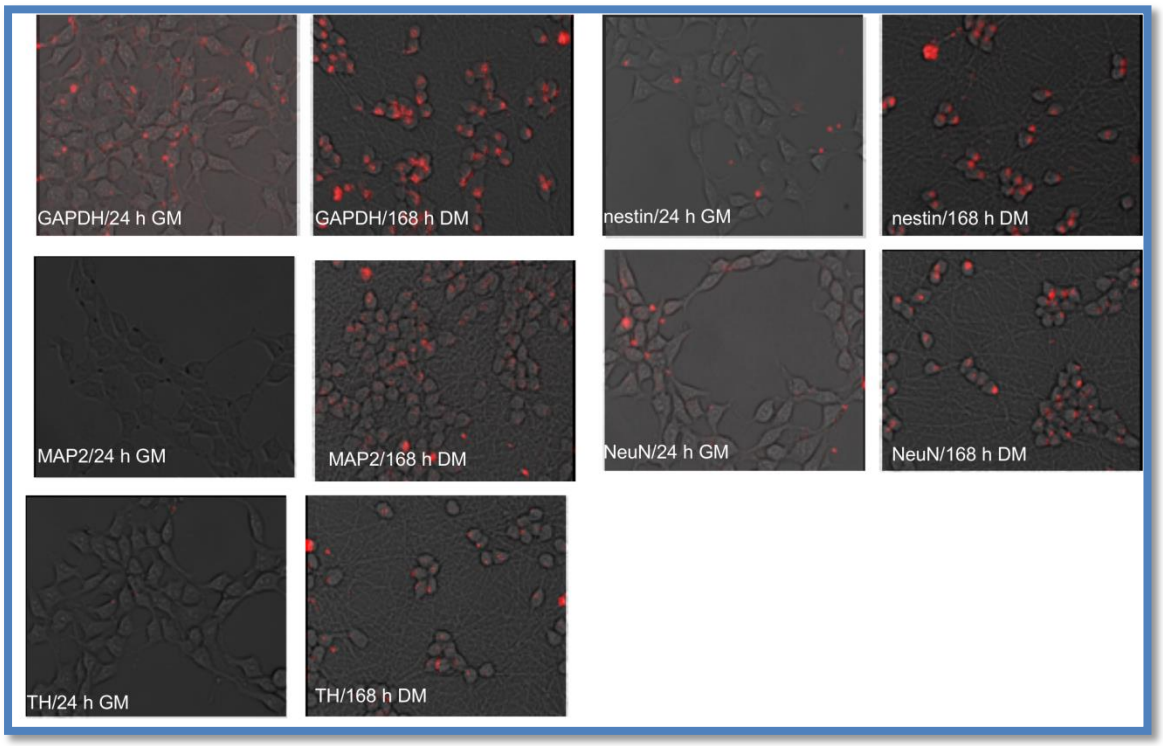

Figure 24. Signals from molecular beacons targeting housekeeping gene expression of GAPDH, intermediate filament protein, and markers for neuronal progenitors (nestin), microtubule-associated protein 2 (MAP2), neuronal nuclear antigen (NeuN), and tyrosine hydroxylase (TH). Cells were SLO transfected and seeded in growth medium (GM), containing 40 ng/ml bFGF. The differentiation process was started 24 h later culturing in differentiation medium (DM) supplemented with dbcAMP, tetracycline, and GDNF.

Expression of MAP2 appeared in 30 % of the cells 48h post induction of differentiation (Figure 25) while the first TH positive cells appeared 72h post induction (Figure 25).

The number of positive cells expressing neuronal markers reached the maximum in a different time points as follows – 85 % nestin and NeuN positive cells 120h post induction, 85 % MAP 2 positive cells 144h post induction and 70 % of cell population was positive for TH 192 h post induction.

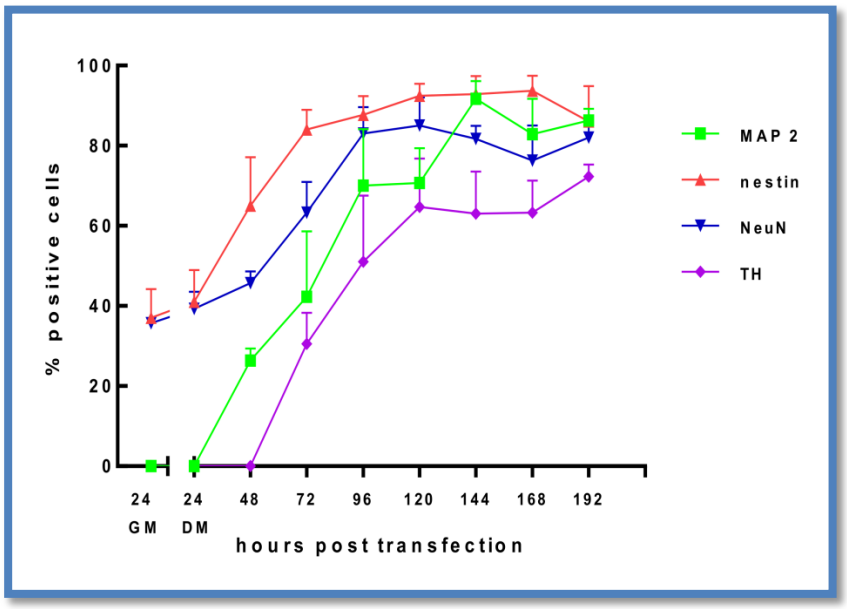

Figure 25. Percentage of cells expressing the neuronal markers nestin, MAP2, NeuN, and TH. Results are presented as mean ± standard error of the mean (SEM).

The intensity in the signal of nestin-MB increased about two-fold compared to point of induction levels. The maximum increase in nestin-MB signals was observed 120 h post induction. A slight decrease in the signal was detected 192h after induction. The signal intensity changes observed for NeuN-MB were similar. However, the maximal signal of NeuN was observed 168h post induction (Figure 26.). In contrast, no signal was recorded from MAP2-MB and TH-MB at 24 h post induction. The MAP2-MB signal plateaued 120 h post induction, while TH-MB signal plateaued 72-96 h post induction. MAP2 signal intensity decreased slightly 192 h post induction, while TH levels remained constant.

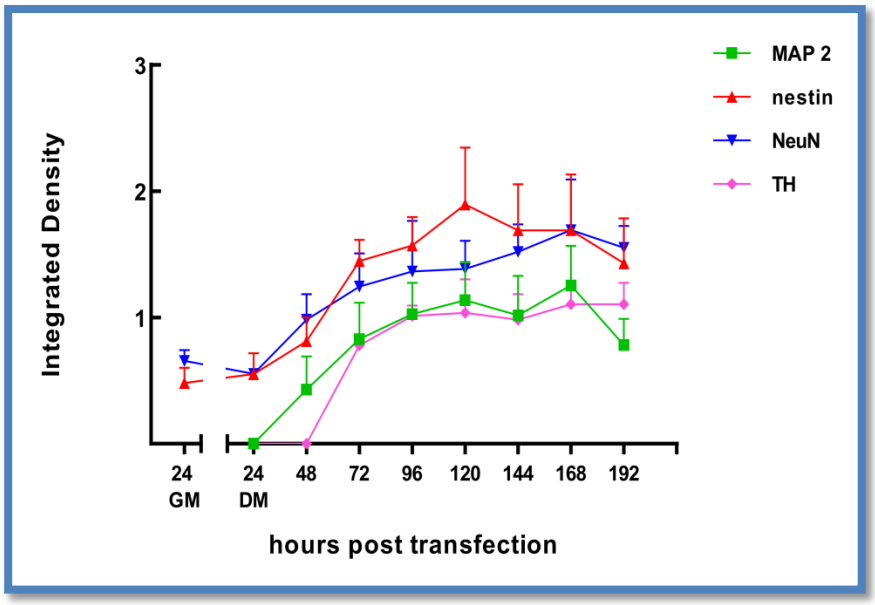

Figure 26. Integrated density of MBs targeting the neuronal markers. Data are displayed as mean ± standard error of the mean.

3.3 qRT-PCR results verified the MBs signal intensity changes.

To corroborate the results using different MB, qRT-PCR was used to measure the respective mRNA expression before and 168 h after differentiation. GAPDH was used as an internal positive control. Expression of nestin and NeuN was detected in non-differentiated cells, and it significantly increased after seven days of differentiation (Figure 27). In contrast, expression of neuronal markers MAP2 and TH was not detected in non-differentiated cells, but was later expressed, corroborating the accuracy of the measurements made using MBs (Figures 24, 25, and 26).

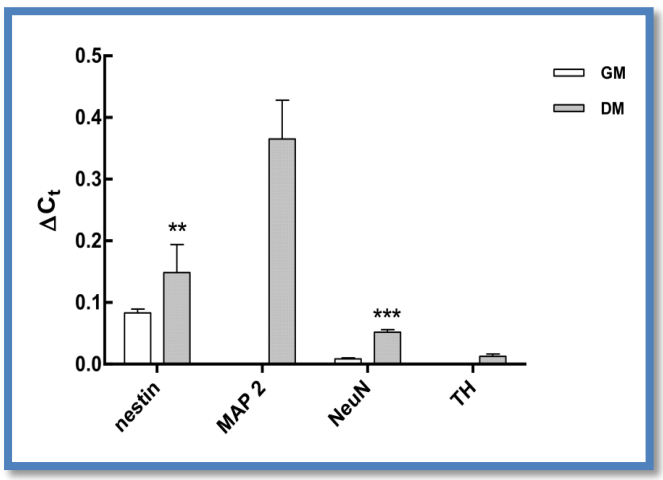

Figure 27. Analysis of mRNA expression levels of neuronal markers using qRT-PCR in non-differentiated and dopamine-like differentiated LUHMES. Expression was normalized to GAPDH mRNA expression. Data are expressed as mean ± SEM. **P<0.01, ***P<0.001.

4. Discussion

Since MBs were first described, their application as sensors for detection gene expression on RNA level inside living cell has been predicted but used only in a limited number of studies. Here we described the use of a panel of MBs targeting molecular markers specific for the progressive stages of neuronal differentiation, and demonstrate that MBs can be used as a routine gene expression assay, as well as reporter gene technology.

The design of MBs requires careful consideration, in particular with regards to target specificity. Our results suggest that the detected signals are specific, since signal from MBs targeting different markers during differentiation following the correct biological sequence. The expression of house-keeping gene GAPDH (constant expression), the progenitor marker nestin (expressed during the early stages of differentiation of neuronal progenitors), and the neuronal nuclear antigen NeuN were all detected. The total number of positive cells for each marker differed, as expected. Thus, the number of GAPDH positive cells was twice the number of cells positive for the neuronal markers. Following differentiation, signal from the mature neuron marker MAP2 was detectable. Finally, TH expression was detected 72 h after differentiation was induced, as described by Scholz et al [2]. All this findings were corroborated by qRT-PCR.

One significant advantage of *in situ* methodologies is the ability to gather spatial data on biological phenomena of interest. In these experiments, each cell appears follow its own course during differentiation; some cells express the genes of interest very early, while the percentage of neuronal marker-expressing cells increases more rapidly during the later stages of neurogenesis. This suggests that there are different expression pattern and population-level heterogeneity during neuronal differentiation. In contrast to PCR-based assays, which collect data from the differentiating population as a whole, MBs accurately measure expression of genes of interest on a single cell level. MBs can be used to repeatedly assess gene expression in the same cell population over time, which is not possible using the destructive methods.

Commonly utilized transfection methods for oligonucleotide delivery, such as lipid and dendrimer-based delivery methods, have often failed to deliver MBs into cells. MB-transfection agent complexes do not always dissociate efficiently once internalized,

leading to brightly fluorescing punctate aggregates that interfere with fluorescent measurements. Furthermore, MB-transfection agent complexes can often lead to entrapment and degradation of the probes within endosome/lysosome compartments, thus increasing background signal. The transfection efficiency of neurons is particularly limited [6], and indeed LUHMES represent a particularly challenging system, since they cannot be transfected using standard methods, such as with lipo- or nucleofection. One routinely used method for direct introduction of MBs into the cytoplasmic compartment of living cells is toxin-based membrane permeabilization using streptolysin-O (SLO), as used in this study. Although it has been successfully used to deliver MBs into a wide variety of cell types, including human dermal fibroblasts, stem cells, and cancer cells [4.], SLO is not a popular method for neuronal transfection. Here we show that the SLO-membrane permeabilization delivery method is a rapid, efficient, and gentle method for the delivery of MBs into neurons. Cells viability was high and the transfection efficiency nearly 100%.

5. Conclusion

We designed MBs targeting multiple factors in order to profile cells during neuronal differentiation, and optimized the method for delivering MBs to living neurons. The simulations show that during transfection the concentration of MBs reach a steady state after few seconds and that we end up with 100-fold more MB than possible target. MBs offer significant advantages over traditional techniques because they allow for real-time imaging of individual cells and preserve spatial information. They overcome the need to lyse cells for qPCR, or fix cells for molecular imaging techniques such FISH. Time-consuming and technically challenging genetic manipulations are not required.

References

1. Lotharius J., Barg S., Wiekop P., Lundberg C., Raymon H. K., Brundin P. Effect of mutant α-synuclein on dopamine homeostasis in a new human mesencephalic cell line. The Journal of Biological Chemistry 2002; vol. 277, no 41, pp. 38884-38894.
2. Scholz D., Pöltl D., Genewsky A., Weng M., Waldmann T., Shildknecht S., Leist M. Rapid, complete and large-scale generation of post-mitotic neurons

from the human LUHMES cell line. Journal of Neurochemistry 2011; vol. 119, issue 5, pp. 957-71.

3. Chen A., Rhee W. J., Bao G., Tsourkas A. Delivery of molecular beacons for live-cell imaging and analysis of RNA. RNA detection and visualization: Methods and Protocols, Methods in Molecular Biology, vol. 714, Jefferey E. Gerst (ed.); DOI: 10.1007/978-1-61779-005-8_10.
4. Keyel P. A., Loultheva L., Roth R., Salter R. D., Watkins S. C., Yokoyama W. M., Heuser J. Streptolysin O clearance through sequestration into blebs that bud passively from the plasma membrane. Journal of Cell Science. 2011, 124, 2414-2423.
5. Bustin S. A. Absolute quantification of mRNA using real-time reverse transcription polymerase chain reaction assays. Journal of Molecular Endocrinology 2000; 25, 169–193.
6. Karra, D., Dahm, R. Transfection techniques for neuronal cells. J Neurosci 2010; 30, 6171-7.

Chapter V. MBs detection of pluripotent stem cell markers in hESC and iPSC

1. Introduction

Owing to a lack of specific and definitive markers, stem cells are usually defined by virtue of their functional characteristics. Well-accepted definition of a stem cell is an undifferentiated cell which retains the capacity to proliferate, self-renew, produce a large family of differentiated functional progeny, regenerate the tissue after injury and retain a flexible use of those options.

Embryonic stem cells (ESCs) are derived from totipotent inner mass cells of the early mammalian embryo and are capable of unlimited, undifferentiated proliferation *in vitro*. They are pluripotent – capable to differentiate to all cell types in the body except extra-embryonic linages - trophoblast and placenta and thus cannot develop into whole organism as totipotent germ cells.

Adult stem cells are found in most tissues and are characterized by their ability to self-renew and undergo differentiation into specialized effector cells. These properties make stem cells crucial for maintaining tissue homeostasis, and for tissue repair after injury; they are therefore of great interest for their potential therapeutic use, and their contribution to pathological processes such carcinogenesis. Stem cells exist in either a quiescent or activated state, and have the ability to switch between these states [1]. The progeny of stem cells have also been shown to have the ability to revert back to stem cells [2]. The stem differentiation potential is present on figure 28.

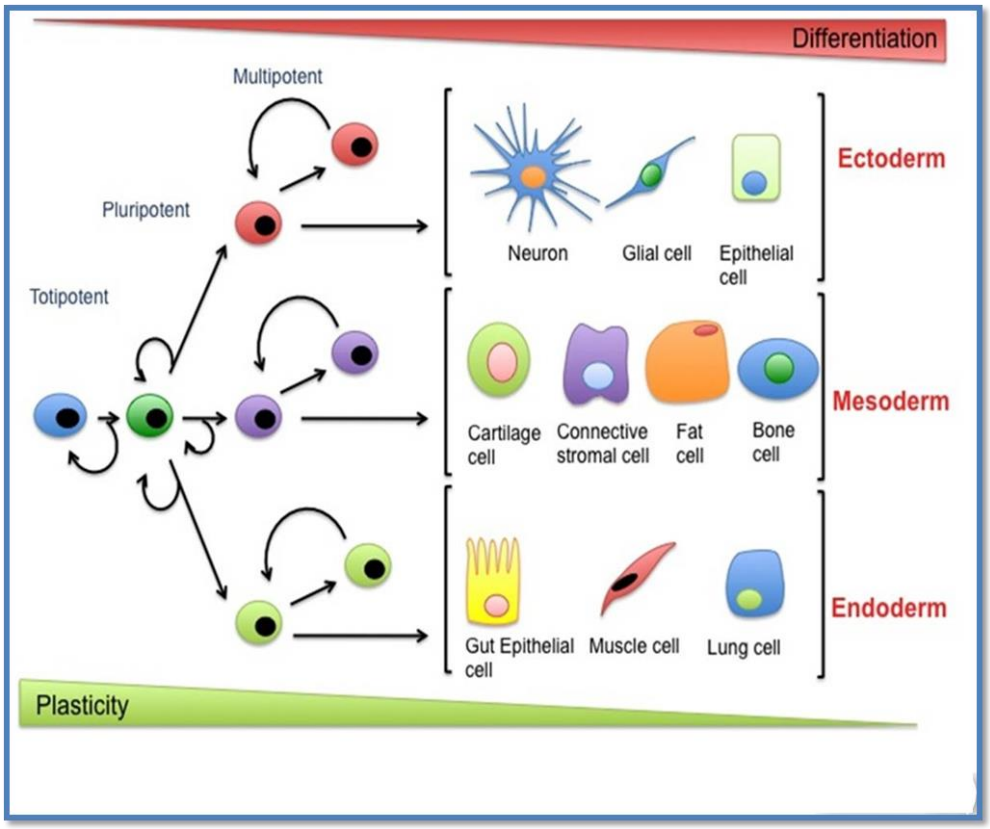

Figure 28. Differentiation of totipotent cells into different cell linages

Induced pluripotent stem cells (iPSC) are derived from animal and human somatic cells via overexpression of a certain set of genes. The first mouse and human iPSC were derived by overexpression of Oct4, Sox2, Klf4, and c-Myc, the cDNA of which was delivered to somatic cells using retroviral vectors [3, 4]. iPSC share a number of characteristics with embryonic stem cells (ESC), such as morphology, type of growth, gene expression pattern, chromatin methylation patterns, embryoid body formation, teratoma formation, viable chimera formation, and potency and differentiability, but the full extent of their relation to natural pluripotent stem cells is still being assess. These properties make iPSC a unique model that can be used to study the molecular bases of pluripotency and to obtain transgenic animals. iPSC circumvent the existing technical and ethical problems associated with ESC isolation. Currently, numerous studies are aimed at generating patient-specific iPSC from humans with inherited or acquired diseases and development of methods of directed differentiation of iPSC cells into various cell types required for cell therapy [5]. Moreover, hiPSC can be useful for a wide range of toxicological and pharmacological studies, including screening of new drugs using iPSC derivatives from individuals with unique genetic backgrounds.

A number of different cellular processes should take place in order adult somatic cells to undergo reprograming into iPSC [6]. Three phases of reprogramming are determined termed

initiation, maturation, and stabilization. Mesenchymal-epithelial transition (MET) – a reversible biological process that involves the transition from motile, multipolar spindle-shaped cells to planar arrays of polarized cells – successfully begin the initiation phase of reprogramming (figure 29).

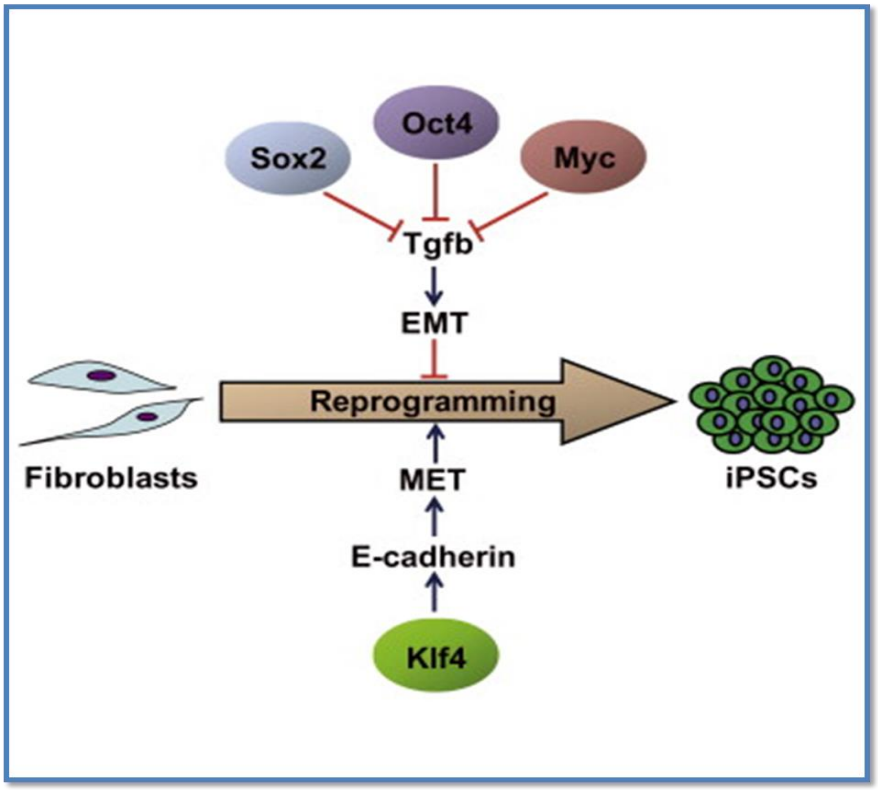

Figure 29. Mesenchymal-epithelial transition (Li R. et al. Cell Stem Cell 2010; 7(1): 51-63)

During cellular reprogramming only a small fraction of cells become bona fide iPSC. Analysis of early stages revealed considerable variation in gene expression between cells in contrast of late stages. Stochastic gene expression early in reprogramming is followed by a late hierarchical phase with Sox2 being the upstream factor in a gene expression hierarchy. Clonal analyses support the stochastic model, demonstrating that activation of pluripotency markers occurs at different time points after transfection in individual daughters of the same initial cell. iPSC colonies that appeared morphologically similar to human ESC by phase contrast microscopy – small, tightly packed cells, with tight colony borders – segregate into different types. Some of them appear to be frozen in states that resemble intermediate stages of reprogramming whereas other represents bona fide iPSC. From a practical point of view analysis of multiple markers is essential to distinguish the fully reprogrammed state from partially reprogrammed intermediates [7].

Multiple criteria have been proposed to evaluate the pluripotent state of generated hiPSC. Key among these criteria includes routine morphological analysis of cells for the presence of high nuclear-cytoplasmic ratio, cell surface and gene expression of pluripotent markers, demonstration of differentiation capabilities into derivatives from the three developmental germ layers – ecto-, endo- and mesoderm, and functional outcomes to demonstrate developmental potency. The functional assays include *in vitro* differentiation, teratoma formation, chimera development, germline transmission, and tetraploid complementation [8]. The most stringent test to screen for pluripotency is the ability to demonstrate germline competency after chimera development. Unfortunately for hiPSC this assay is not possible. Teratoma formation of hiPSC injected into immunocompromised mice and subsequent analysis of tissue formation has been widely used as an important methodology to investigate the developmental ability of the generated hiPSC.

One alternative of teratoma formation assay is an *in vitro* approach involving the generation of embryoid bodies (EBs) from hiPSC. In this approach, the undifferentiated hiPSC are placed in suspension, which promotes stochastic differentiation into cells of all three germ layers [9]. EBs are three-dimensional aggregates of pluripotent stem cells. EBs exhibit heterogeneous patterns of differentiated cell types. Therefore, the 3D structure, including the establishment of complex cell adhesions and paracrine signaling within the EB microenvironment, enables differentiation and morphogenesis which yields micro-tissues that are similar to native tissues structures.

In this chapter the usability of MBs for detecting pluripotent marker Oct4 and Sox2 in hESC and iPSC as well as Oct4 expression in derived EBs is demonstrated. Moreover, a protocol for virus-free deriving iPSC transfected with polycistronic plasmid vector and spontaneous EBs formation is described.

2. Materials and methods

2.1 Molecular beacons

Oct 4 (620) - NM_203289.4 (var. 2)

Texas red (Cy3) CGCUC UCAUUCACCCAUUCCCUGUU GAGCG BHQ2

TR CGCTC TCATTCACCCATTCCCUGTT GAGCG

Transcript Variant 2: This variant (2) differs in the 5' UTR, lacks a portion of the 5' coding region, and uses a downstream non-AUG (CUG) start codon, compared to variant 1. The resulting isoform (2, also known as OCT4B-190) is shorter at the N-terminus, compared to isoform 1. Both variants 2 and 3 encode the same isoform.
Oct4 (645) - NM_002701.4 (var. 1)

BHQ2 CGCUC CAUGUUCUUGAAGCUAAGCUGCA GAGCG Texas red

This transcript variant (1) encodes the longer isoform (1, also known as OCT4A).
Oct4 (620) - MB recognizes the sequence in the short form of Oct 4 and Oct2 (645)- MB targets a sequence which is present in both form of transcription factor.

Sox2 (NM_003106.3)

Cy3 CGCUC CGCCGCCGAUGAUUGUUAUUAU GAGCG BHQ2
TR CGCTC CGCCGCCGATGATTGTTATTAT GAGCG BHQ2

2.2 hESC line

BG01V (ATCC, SCRC-2002) is a human embryonic stem cell line with an abnormal karyotype (49, XXY, +12, +17). It was derived from the wild-type, parental hESC line BG01. Cells were grown on top of Mytomycine C pretreated mouse embryonic fibroblasts (MEF, ATCC, SCRC-1040). Complete growth medium consists of DMEM/F12 supplemented with 2 mM L-glutamine (Sigma), 1x MEM non-essential amino acid solution, 0.1 mM 2-mercaptoethanol (Sigma), 4 ng/ml bFGF (Invitrogen), 5 % knockout serum replacement, 15 % fetal bovine serum, 1% Penicillin/Streptomycin. Further cells were adapted to feeder free growth conditions on Geltrex (Invitrogen).

2.3 Generation of iPSC

2.3.1 Cell lines

Adipose-derived stem cells isolated from liposuction aspirates (ASC) and mesenchymal stem cells (MSC-hTERT) were used to derive iPSC. Cells were maintained in DMEM/F12 medium with GlutaMax, 10 % fetal calf serum and 1% Penicillin/Streptomycin.

2.3.2 Plasmid

pCAG2LMKOSimO, (Addgene 20866) is a polycistronic plasmid vector carrying four mouse reprogramming factors: Oct4, Sox2, Klf4, and c-Myc, constructed and described by Kaji et al. [10]. All iPSC clones that were derived by use of pCAG2LMKOSimO contained a plasmid DNA insert, which could be excised from the genome with Cre recombinase [10]. For transfection, plasmid DNA was isolated using the EndoFree Plasmid Midi Kit (Quiagen) according to the manufacturer's protocol.

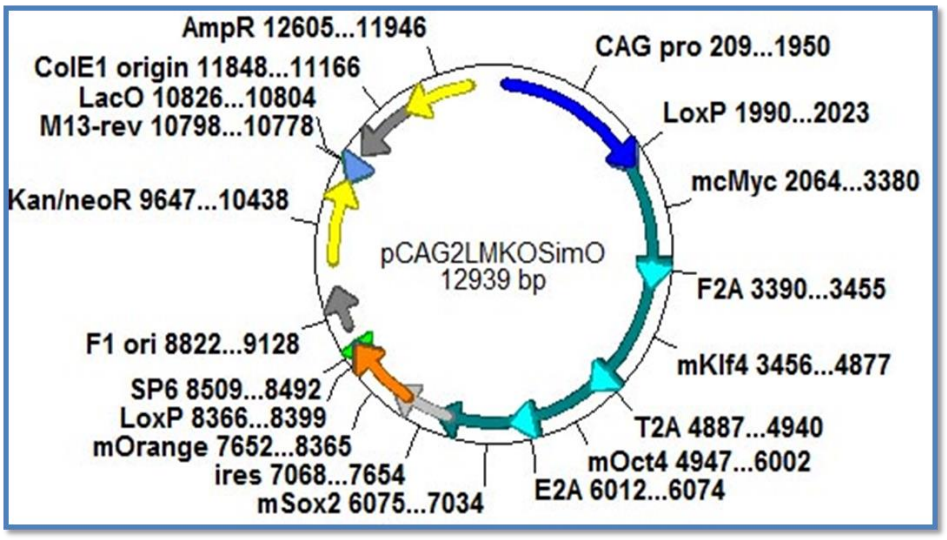

Figure 30. pCAG2LMKOSimO, (Addgene 20866) codding for mouse Oct4, Sox2, Klf4 and c-Myc.

2.3.3 Transfection

Cells were grown on 60 mm Petri dishes precoated with CELLStart™ (Invitrogen) diluted 1:50 in DPBS or uncoated dishes depending on growth condition afterwards until they reached ~ 80% confluence. Cells were washed with warm DPBS and 3ml preheated OptiMem medium was added. The cells were transfected with plasmid (3.3 µg per dish) using FuGENE 6 in a ratio 1:2. Briefly, the plasmid was dissolved in OptiMem and FuGENE reagent was added directly. Mixture was vortexing briefly and incubated for 10 min at room temperature. Mixture volume of 150 µl was added to the cells in medium volume of 3 ml and mixed thoroughly. The medium was replaced with a fresh portion of complete growth medium 6 h after transfection. Transfection was repeated after 24 h.

2.4 Growth conditions for iPSC

The iPSC derived from ASC and MSC were growth in two different conditions – feeder and feeder free.

2.4.1 Feeder free conditions

ASC were seeded on CELLStart™ (Xeno-free cell culture substrate, Invitrogen) before first transfection. 24 h after second transfection ASC medium was switched to STEMPRO® hESC SFM (serum free medium) complete medium containing 1x DMEM/F12/Glutamax™, 1x STEMPRO® hESC SFM growth supplement (Gibco), 1.8 % v/v BSA, 8 ng/ml bFGF (Ivitrogen), 0.1 mM 2-mercaptoethanol, 1% v/v Penicillin/Streptomycin, 1 mM valproic acid. The medium was changed daily.

MSC were seeded on poly-L-ornitine/fibronectin coated dishes (procedure described in Chapter IV) after second transfection in STEMPRO® hESC SFM complete medium.

2.4.2 Growth on feeder layer

Cells were trypsinated 24 h after second transfection and plated on top of mouse embryonic fibroblasts (3T3) Mytomycine C pretreated. iPSC were maintained in DMEM/12 medium supplemented with Glutamax, Penicillin/Streptomycin, 1x Knockout serum replacement, 1x nonessential amino acids, 10 ng/ml bFGF, 0.1 mM 2-mercaptoethanol, 1 mM valproic acid. The medium was changed daily.

2.5 Embryoid bodies formation and neuronal induction

Around two weeks after induction iPSC colonies formed on MEF spontaneously started forming 3D structures morphologically resembling embryoid bodies (fig). Medium was changed to neuronal induction medium (NIM) containing DMEM:F12, Glutamax, 1% Penicillin/Streptomycine, NEAA, 1x N2 supplement, and 20 ng/ml bFGF. Three days later EBs were moved to plates coated with CellStart. On the d8 after neuronal induction NIM was supplemented with 100ng/ml FGF-8b, and 250 ng/ml SHH.

2.6 Transfection with MBs

hESCs growing on MEF were treated with collagenase IV solution in DMEM/F12 at a concentration of 0.5 mg/ml (or ~200U/ml) for 45 min. When the majority of the hESC colonies detached, an appropriate volume of DMEM/F12 was added and the cell suspension was collected. Cells were centrifuged for 5 min at 200 x g at 25°C, the cells re-suspended in Opti-MEM, and the procedure for transfection of adherent LUHMES was followed. Finally, cells were plated on Geltrex®-coated dishes in complete hESC medium.

iPSC and EBs were transfected directly on the dish. The medium was remove, cells were washed three times with pre-warmed DPBS. Opti-Mem containing activated SLO and MB (2µM) were added to the cells. After 15 min incubation transfection medium was removed, cells were washed three times with pre-warmed DPBS and complete growth medium was added.

3. Results

3.1 MBs detect pluripotent markers Oct4 and Sox2 in hESC

MBs targeting Oct4 and Sox2 mRNA were designed and synthesized with a 2'-O-methyl RNA backbone. The utility of MBs targeting Oct4 and Sox2 was first verified by introducing them into a hESC line, which is known to highly express both pluripotent markers, and is therefore a good positive control. Cells were examined 24h after transfection and signal from both beacons was detected (figure 31).

A.

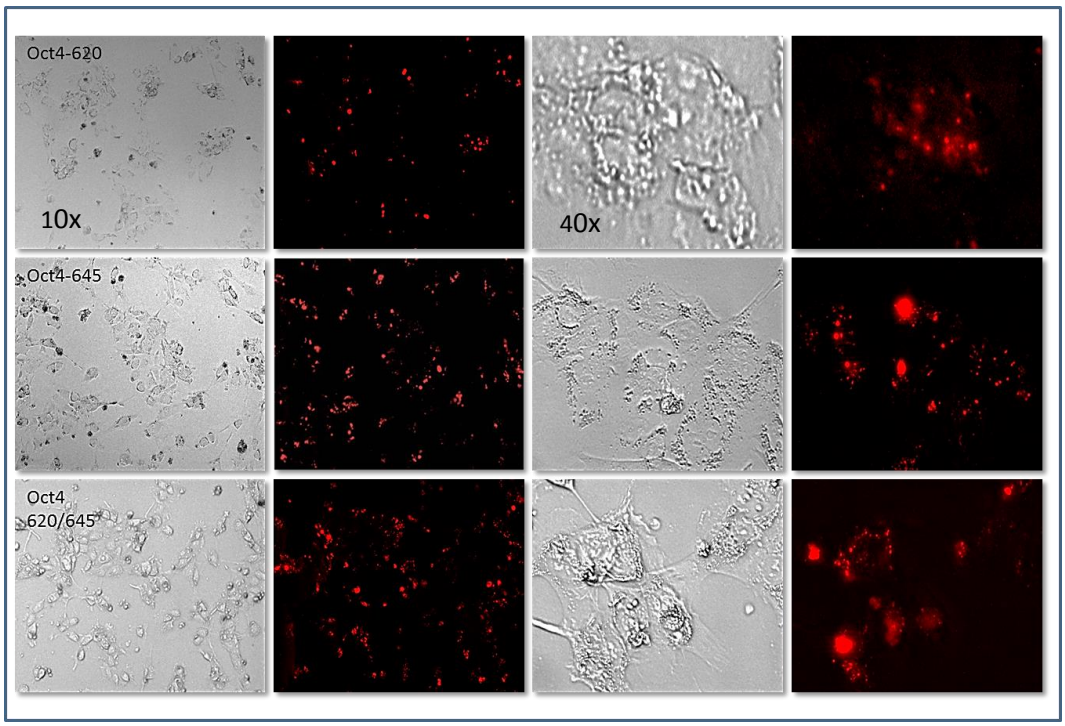

B.

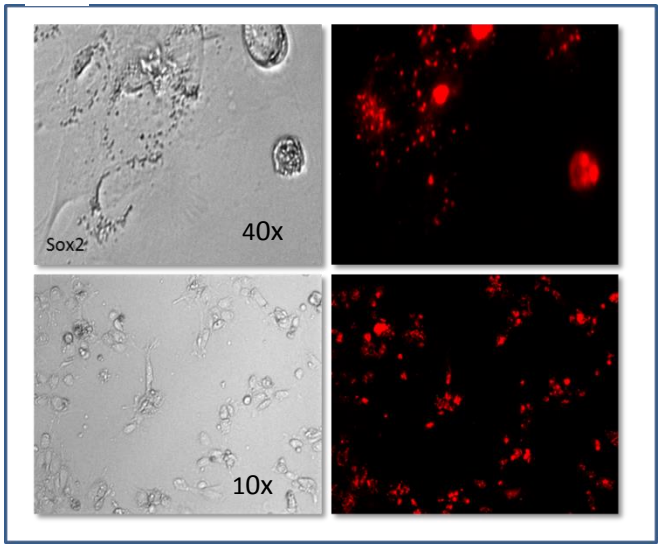

Figure 31. hESC BG 01V transfected with MBs targeting for A. Oct4 MBs short isoform (Oct4 620), long isoform (Oct 645), and double transfection with both MBs. B. Sox2 MB

Two Oct4-MBs targeting different isoforms of the transcription factor were designed and were transfected individually or in mixture into hESC. Oct4 MB (620) targets the shorter isoform 2 (Oct4B) of the transcription factor from position 620 till 640. Oct4-MB (645) targets the longer isoform of Oct4 (Oct4A) from position 645 till 668. To avoid quenching due to the close proximity of both MB after hybridization MBs were designed so that BHQ2 is attached on the 5'-end in Oct4-MB (645)(Figure 32). It was detected a stronger signal coming from Oct4-MB targeting the longer form suggesting that this particular isoform was

expressed higher in hESC comparing to the shorter one which is more spread in non-pluripotent cell types [11].

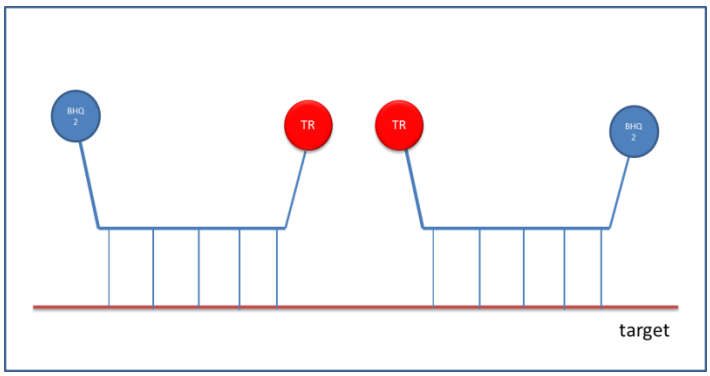

Figure 32. Hybridization of Oct4 MBs to the long isoform of Oct4

Because Oct2 (645) MB targets a sequence which is present in both form of transcription factor, it is not clear whether the increasing in the signal from mixture of both Oct4 targeting MBs is due to multiplying of the signal by simultaneous hybridization of both probes to the same mRNA molecule, or because the simultaneous detection of both isoforms of Oct4 which seems are expressed in pluripotent stem cells.

3.2 Morphology of the iPSC colonies in different growth conditions and their fate

It was observed that iPSC formed colonies differed in their morphology and fate depending on growth conditions. MET was initiated in ASC in Xeno-free conditions and well defined ESC-like colonies started appearing around 2 weeks after transfection. However, the biggest colonies reached diameter of around 300 µm but further growth was not detected. Furthermore, only few colonies per dish was observed suggesting that those growth conditions were not sufficient for complete reprograming of the cells and further maintain.

ESC-like colonies from MSC appeared immediately after moving into p-L-o/fibronectin coated dishes and STEMPRO® hESC SFM complete medium.

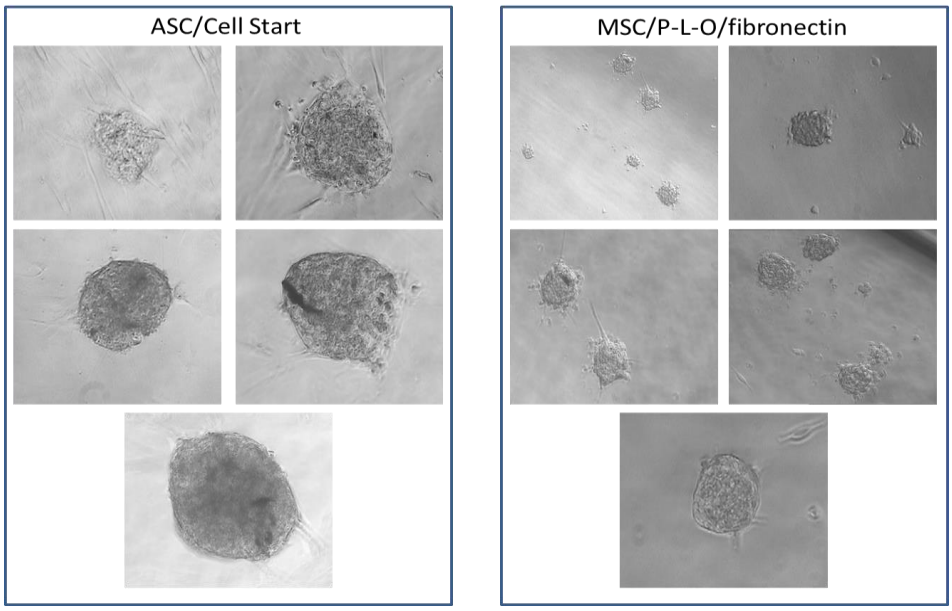

Figure 33. Stages in formation of iPSC colonies from ASC and MSC on feeder-free conditions

In contrast iPSC colonies from ASC and MSC on MytoC treated 3T3 fibroblasts appeared few days after transfection and showed fast growth and proliferation. Significant more number of colonies was observed comparing to xeno-free conditions. However those conditions were not able to maintain undifferentiated stage of the colonies and formation of EBs started three weeks later (figure 35).

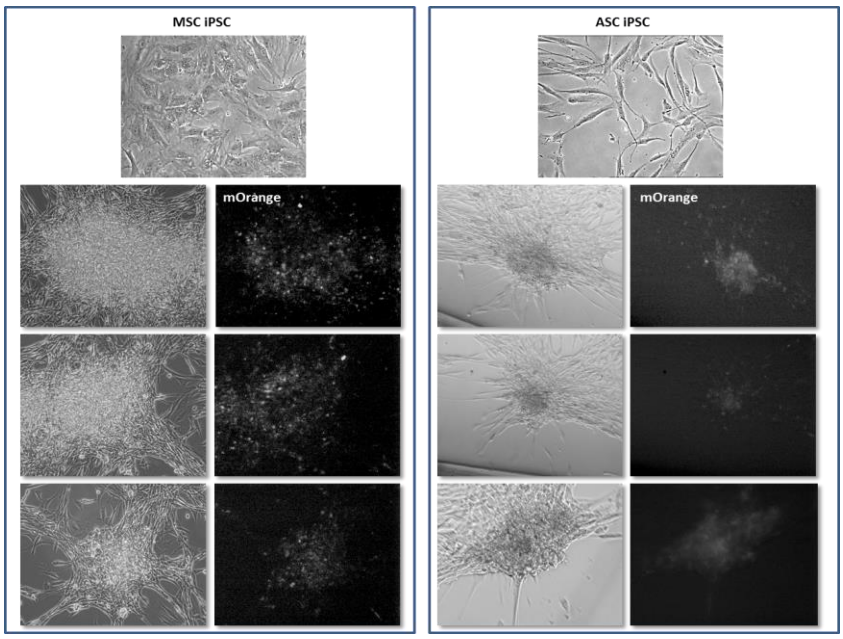

Figure 34. Stages in formation of iPSC colonies from ASC and MSC grown on Mitomycine C treated 3T3 fibroblasts

Further the embryoid bodies were exposed on neural induction conditions. When the medium was switched to NIM EBs detached from the feeder layer and formed free floating spheres. Exposure to FGF8b and SHH trigger to process formation in some cells in the outer layer of the EBs. However, EBs did not attached to the coating substrate CellStart and here the differentiation procedure was terminated.

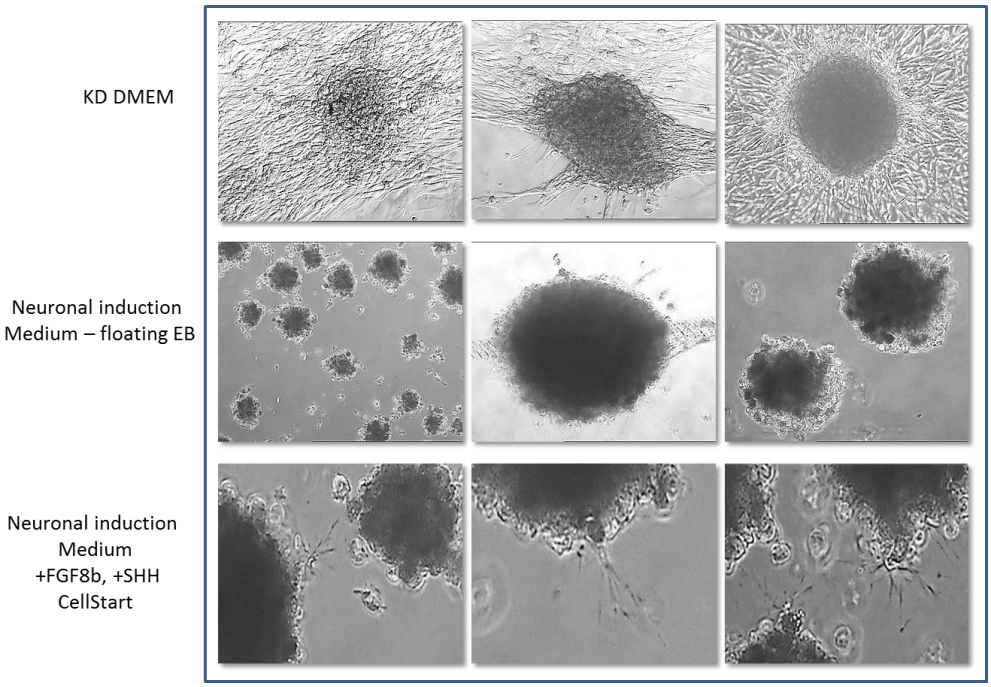

Figure 35. Formation of embryoid bodies from ASC

`

3.3 MBs detection of human Oct4 and Sox2

iPSC were derived by transfection with plasmid carrying mouse genes for Oct4, Klf4, c-Myc and Sox2. However, endogenous expression of Oct4 and Sox2 was detected by transfecting with MBs targeting human Oct4 (620) and Sox2 respectively. Both sequences were analyzed by BLAST and no match with a transcript from mouse genome was detected. Furthermore, plasmid transfected but not transformed cells seen around iPSC colonies (figure 36) did not showed fluorescent signal after transfection with MBs suggesting specificity of the pluripotent markers targeting beacons.

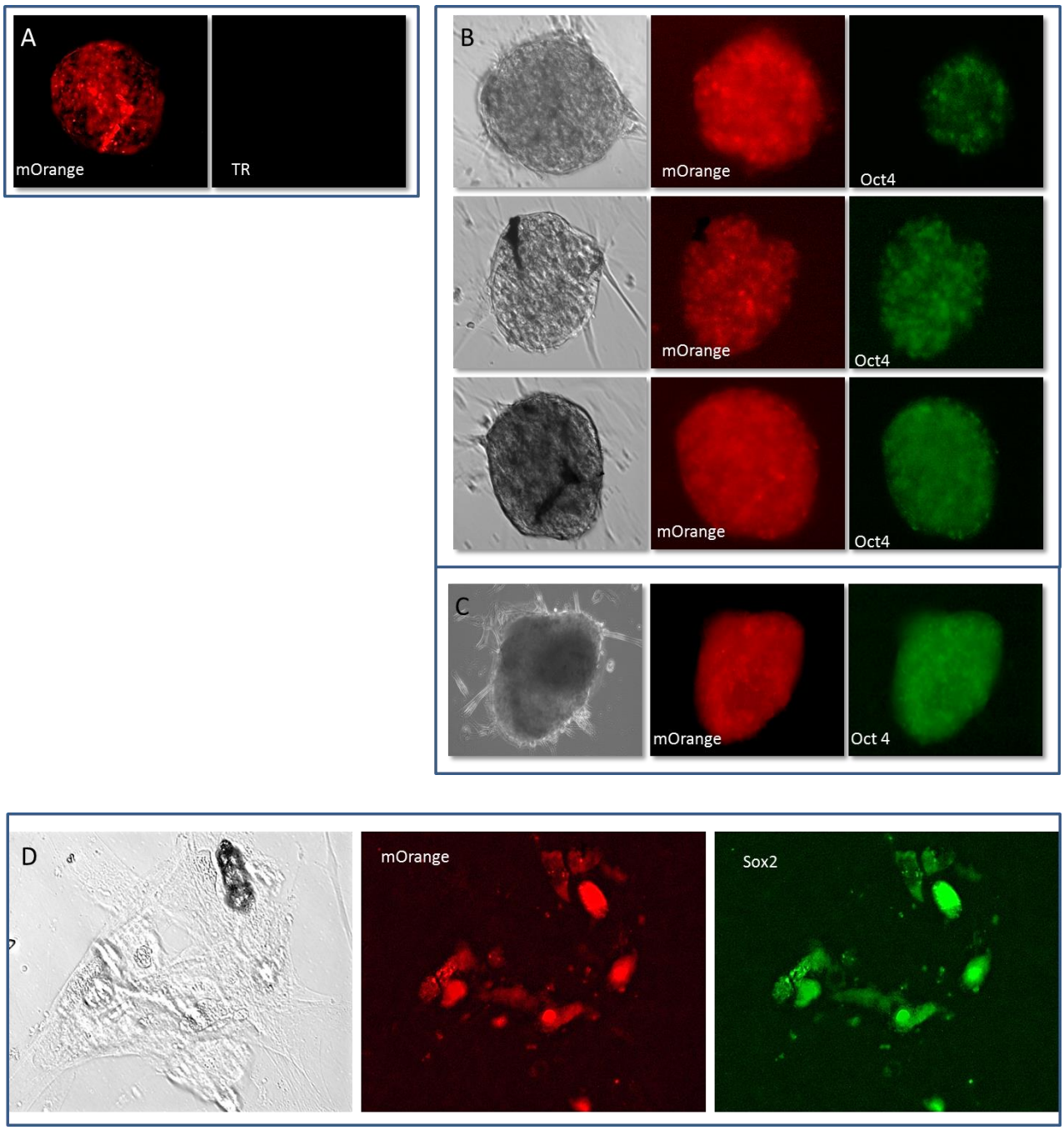

Figure 36. ASC derived iPSC colonies and EBs. A. Control non-transfected wih MB iPSC colony expressing mOrange, shows no background fluorescence. B. iPSC colonies grown on feeder free conditions and transfected with MB targeting Oct4 48 h after transfection (TR/BHQ2/2-O-Me backbone). C. EB/like structure formed from iPSC on 3T3 feeder layer and transfected with same Oct4-MB. D. iPSC transfected with Sox2-MB (40x magnification) – TR/BHQ2/DNA backbone.

4. Discussion

The major obstacle hinder large scale application of iPSC for regenerative purposes in humans is the need to use vectors that integrate into the cell genome, because retro- and lentiviral vectors can cause uncontrollable insertion mutagenesis [12]. Moreover, activation of viral constructs carrying the oncogenic c-Myc and Klf4 genes can increase the rate of tumour genesis. One relevant solution is the use of either non-integrated vectors or vectors that can be excised from the genome [13].

In this chapter was described derivation of iPSC from ASC and MSC trough transfection with a plasmid pCAG2LMKOSimO carrying a set of four mouse genes - Oct4, Sox2, Klf4, and c-Myc, which could be excised from the genome with Cre recombinase. As it was described previously [13] mouse embryonic fibroblasts were reprogrammed by plasmid carrying Oct4, Sox2, Klf4, and c-Myc cDNA and most of derived colonies displayed the properties of pluripotent cells. However they did not contain plasmid inserts in the genome. In contrast, Medvedev et al. [14] did not observe those phenomena in iPSC derived from pCAG2LMKOSimO plasmid transfected human foetal neural stem cells.

Here two different cell types - ASC and MSC were used to obtained iPSC colonies. The colonies showed the morphology of ESC. However, grown on feeder free conditions they did not growth further suggesting that growth conditions are not completely appropriate and further optimisation of the protocol is required. In contrast, iPSC maintained on Mitomycine C treated 3T3 fibroblasts growth faster and spontaneously formed embryoid bodies. However, it was not the optimal growth condition to maintain the pluripotency and the beginning of differentiation process was observed. All those findings collaborate with results describing by Chan et al. [15] who identified distinct colony types that morphologically resemble embryonic stem cells yet differ in molecular phenotype and differentiation potential. Even colonies that appeared morphologically similar to hESC by phase contrast microscopy segregate to three types. Type I and II appeared to be frozen in states that resemble intermediate stage of reprogramming whereas type III represents the bona fide iPSC. Moreover multiple endogenous pluripotency mRNA (Oct4, Sox2, Nanog etc.) showed a gradation of expression in type I, II, and III cells. Markers like REX1, DNMT3B and ABCG2 were validated as markers that distinguished incompletely reprogrammed colonies from bona fide iPSC. It is here the application of MBs as sensors for detection and evaluation the stage of reprograming of somatic cells into iPSC. Design and synthesis of MBs targeting

markers for bona fide iPSC have priceless value for dynamic monitoring and evaluation of reprogramming process, optimization of transfection and growth conditions, especially in the cases of human applications.

We were able to discriminate endogenous expression of human Oct4 and Sox2 genes from the transcripts of mouse genes carried by the plasmid using MBs. The both Oct4 and Sox2 MBs sequences were analysed by BLAST and no match with mouse Oct4 was detected. This suggests that the detected signal is coming from endogenous human Oct4 and Sox2 which expression is induced later in the transforming process.

References

1. Li L, Clevers H. Coexistence of quiescent and active adult stem cells in mammals. Science 2010; 327: 542-545
2. Davies EL, Fuller MT. Regulation of self-renewal and differentiation in adult stem cell linages: lessons from the Drosophila male germ line. Cold Spring Harb. Symp. Quant. Biol. 2008; 73: 137-145
3. Takahashi K, Yamanaka S. Induction of pluripotent stem cells from mouse embryonic and adult fibroblast cultures by defined factors. Cell 2006; 126: 663-676
4. Takahashi K, Tanabe K, Ohnuki M, Narita M, Ichisaka T, Tomoda K, Yamanaka S. Induction of pluripotent stem cells from adult human fibroblasts by defined factors. Cell 2007; 131: 861-872
5. Park I-H, Aurora N, Huo H, Maherali N, Ahfeldt T, Shimamura A, Lensch MW, Cowan C, Hochedlinger K, Daley G.Q. Disease-Specific induced pluripotent stem cells. Cell 2008; 134: 877-886
6. Ronghui L, Liang J, Ni S, Zhou T, Qing X, Li H, He W, Chen J, Li F, et al. A Mesenchymal-to-Epithelial Transition Initiates and Is Required for the Nuclear Reprogramming of Mouse Fibroblasts. Cell Stem Cell 2010; 7(1): 51-63
7. Buganim Y, Faddah DA, Cheng AW, Itskovich E, Markoulaki S, Ganz K, Klemm SL, van Oudenaarden A, Jaenisch R. Single-Cell Expression Analyses during Cellular Reprogramming Reveal an Early Stochastic and a Late Hierarchic Phase. Cell 2012; 150: 1209-1222

8. Sheridan SD, Surampudi V, Rao RR. Analysis of Embryoid Bodies Derived from Human Induced Pluripotent Stem Cells as a Means to Assess Pluripotency. Stem Cells International 2012; doi:10.1155/2012/738910
9. Kurosawa H. Methods for inducing embryoid body formation: in vitro differentiation system of embryonic stem cells. Journal of Bioscience and Bioengineering. 2007; 103(5): 389-398

10. Kaji K, Norrby K, Paca A, Mileikovsky M, Mohseni P, Woltjen K. Virus-free induction of pluripotency and subsequent excision of reprogramming factors. Nature Letters 2009; 458: 771-776. DOI: 10.1038/nature07864
11. Atlasi Y, Mowla SJ, Ziaee SAM, Gokhale PJ, Andrews PW. OCT4 spliced variants are differently expressed in human pluripotent and nonpluripotent cells. Stem Cells 2008; 26: 3068-3074
12. Okita K, Ichisaka T, Yamanaka S. Generation of germline-competent induced pluripotent stem cells. Nature 2007; 448: 313-317
13. Okita K, Nakagawa M, Hyenjong H, Ichisaka T, Yamanaka S. Generation of mouse induced pluripotent stem cells without viral vectors. Science 2008; 322: 949-953
14. Medvedev S P, Grigor´eva EV, Schevchenko AI, Malakhova AA, et al. Human induced pluripotent stem cells derived from fetal neural stem cells successfully undergo directed differentiation into cartilage. Stem cells and development 2011; 20(6): 1099-1112
15. Chan EM., Ratanasirintrawoot S, Park I-H, Manos, et al. Live cell imaging distinguishes bona fide human iPS cells from partially reprogrammed cells. Nature Biotechnology 2009; 27: 1033-1038

Chapter VI. Tracking distribution of cells with stem cell signature inside neurospheres

1. Introduction

Neural stem cells (NSC) are tissue-specific multipotent stem cells that have the capacity to proliferate, self-renew, and the ability to produce a large family of differentiated progeny [1]. NSCs occupy special environment in the adult mammalian brain including humans - so called "niches", and continuously generate new neurons that functionally integrate into neural circuits [2]. *In vitro*, long-term culture systems are based either on cell growth on monolayer, or as free floating clonal cell aggregates called neurospheres. Neurospheres allows for continuous growth and propagation of potentially heterogeneous populations of NSCs and their progenitors, and exhibit intra-clonal neural cell-linage diversity containing in addition to NSCs, neuronal and glial progenitors in different stages of differentiation [3].

Neurosphere forming assay is widely using as a model for neuronal development, and for studying neurogenesis [4]. They have also been used to characterize the factors and molecular mechanisms controlling stem cell properties, and to find the gene expression signatures that characterize different cell populations [5, 6].

However, the following limitations of neurospheres mean that they are insufficient on their own to definitively prove the existence of a stem cell population within the cluster [7, 8]. First, multiple populations of more committed progenitor cells, as well as stem cells, can give rise to neurospheres. Second, most of the stem cells are in the quiescent stage, which is incompatible with neurosphere formation. Third, cells within the neurosphere can shuttle between quiescent and activated states, and even more committed progenitors can revert back to a more primitive state [9]. Furthermore, the neurosphere is a dynamic structure and therefore tracking cellular movements within neurospheres is important for their complete characterization, since cell-cell or cell-environment interactions may have a significant impact on NSCs differentiation, and contribute to the heterogeneity of the neurosphere [10].

It is therefore important to employ time laps microscopy when using the neurosphere forming assay, in order to accurately and confidently detect cells with stem cell characteristics within the clusters, and track their behavior when exposed to different stimuli.

With these limitations in mind, the following questions arise: do neurosperes contain cells with a stem cell signature; what is the distribution of cells within the clusters (i. e. do they formed niches); what is their fate during differentiation; and most importantly from an experimental point of view, how can cells can be tracked in real time without affecting cell viability and differentiation? Although a universal stem cell marker does not exist, one of the most meaningful measures of stemness is the expression of transcription factors such as Oct4, Sox2, and Nanog. However, the detection of expression of these genes in living cells usually requires fusion of gene promoters with a reporter gene, such as green fluorescent protein (GFP). Instead of using genetic manipulation, transcription factor gene expression can also be detected using molecular beacon technology, in which the presence of specific mRNAs can be detected after transfection.

In this particular experimental set up we investigated, as a function of time, the location of Oct4, Sox2 and Nanog mRNA positive cells within LUHMES derived neurospheres grown in either growth medium (GM) or in differentiation medium (DM). For the first time we demonstrate that MBs can be used to determine the exact location of stem cell markers positive cells inside living neurospheres, allowing us to confirm a model of stem cell distribution within differentiating neurospheres.

2. Materials and methods

2.1 Neurosphere formation from LUHMES cell line

Cells were cultured in cell culture flasks coated with 50µg/ml poly-L/ornithine (Sigma) overnight at room temperature, followed by coating with 1µg/ml human fibronectin (Sigma) for at least 3h at 37ºC. Both coating components were diluted in sterile water. Cells were grown in medium (GM) described previously in Chapter IV.

Adherent monolayer cultures maintain is described in Chapter IV.

2.2 Differentiation of LUHMES

Differentiation was initiated by adding DM consisting of advanced DMEM/F12 (Sigma), 1x N2 supplement (Gibco), 2mM L-glutamine, 1mM dbcAMP (Sigma), 1µg/ml tetracycline, and 2ng/ml recombinant human GDNF (R&D system).

2.3 Molecular beacons

Configurations of MBs used in this experiment are listed in table 4

Table 4. Molecular beacon sequences

Target	NM	Sequence	Fluorochrome	Quencher
Oct4	NM_203289	CGCUC UCAUUCACCCAUUCCCUGUU GAGCG	Cy3	BHQ2
Sox2	NM_003106.3	CGCUC UCAUUCACCCAUUCCCUGUU GAGCG	Cy3	BHQ2
Nanog	NM_024865.2	CGCTC TGGAAGATGTTAGAGAAATAGGAC GAGCG	TexasRed	BHQ2

*Stem formation sequences are underlined

2.4 Transfection of MBs into neurospheres

$1x10^5$ cells were seeded on poly-L-ornitin/fibronectin/coated 12 well plates for neurosphere formation. Neurospheres were transfected 72h after neurosphere formation. Free-floating neurospheres were collected by centrifugation for 5 min at 190 x g, and then incubated with the mixture containing 17U/ml TCEP/activated SLO, and 2 µM MBs for 15 min at 37ºC.

Transfection of MBs into LUHMES cells for monolayer growth is described in Chapter IV.

2.5 Cell viability assay

Cellular viability after SLO-mediated transfection was detected by calcein/propidium iodide staining (see Chapter IV).

2.6 Quantitative real-time polymerase chain reaction (qRT-PCR)

Total RNA from neurospheres was isolated using the RNeasy Mini kit (Quiagen). Neurospheres were collected by centrifugation prior to the addition of lysis buffer. The lysates were collected and purified according to the manufacturer's instructions. The detailed procedures for cDNA preparation and Taqman assay are described in Chapter IV. The

Taqman assays used in this experiment were Oct4 (POU5F ID Hs04260367_gH), Sox2 (ID Hs01053049_s1), Nanog (ID Hs0426366_g1), and GAPDH (ID Hs03929097_g1) as an internal control. All experiments included negative controls of no cDNA in the reaction mixture.

2.7 Immunocytochemistry

Neurospheres were grown in 8-well LabTek Permanox chamber slides (Nunc, Roskilde, Denmark), precoated with poly-L-ornitin/fibronectin, while monolayers were cultured on Geltrex®-coated chamber slides. Cells were fixed in 4% (v/v) formaldehyde in PBS containing 0.05M sucrose (v/v) and 0.4mM $CaCl_2$ for 20 min, and blocked with 1% (w/v) bovine serum albumin (BSA) in PBS. Overnight incubation with primary antibody diluted in PBS containing 5% (v/v) fetal calf serum (FCS), 50mM glycine, and 0.025% (v/v) Triton X100, was followed by incubation with secondary antibody for 1 h at RT. The primary and secondary antibodies are listed in table 5. DAPI (0.1µg/ml) was added to the buffer in the last washing step in order to stain the nuclei.

Antibody	Host	Working dilution	Source	Cat No.
Primary antibodies				
Oct4	Rabbit	1:400	Cell Signaling Technology	#2750
Sox2	Goat	1:100	Santa Cruz Biotechnology, Inc.	Sc-17320
Secondary antibodies				
Alexa Fluor 488 anti-rabbit IgG	Goat	1:1000	Life Technologies	A-11008
FITC-conjugated anti-goat IgG	Rabbit	1:40	Dako Cytomation	F025002

Table 5 . The primary and secondary antibodies used within this study

2.8 Imaging and image analysis

Phase contrast and fluorescent images were acquired on the Carl Zeiss Axio Vision 4.8.2 equipped with the ApoTome imaging system, 10x/0.3 and 40x/0.75 Plan-Neofluar objective, HXB lamp, and a Zeiss Axiocam MRm B/W camera. The same exposure time and filter set (43 HE Ds Red 538-570 nm) were used for all experiments.

Single-cell image analysis was performed using ImageJ software. A region of interest (ROI) was draw around the cell and the total fluorescence intensity was measured. The background fluorescence was detected by drawing a ROI in an area outside the cell of interest, and the total fluorescent intensity measured for this ROI. In ImageJ the total fluorescent intensity is reported as integrated density (ID), which is the sum of the values of the pixels in the selection. The background fluorescent intensity was subtracted from the cellular measurement as previously described [11].

2.9 Statistical analysis

Results are expressed as mean ± standard error of the mean (S.E.M.). qRT-PCR results were analyzed using a Student's t-test (n=5). Analyses were performed using GraphPad Prism v6 (GraphPad Software Inc., CA, USA).

3. Results

3.1 LUHMES-derived neurospheres express stem cell markers Oct4, Sox2, and Nanog.

According to the original description by Lotharius et al. (the depositor of the LUHMES cell line in ATCC), LUHMES cells grow as a monolayer on plates pre-coated with poly-L-ornitine/fibronectin [12]. Under these conditions, we observed consistently that the cells detached and formed free-floating neurospheres (Figure 37).

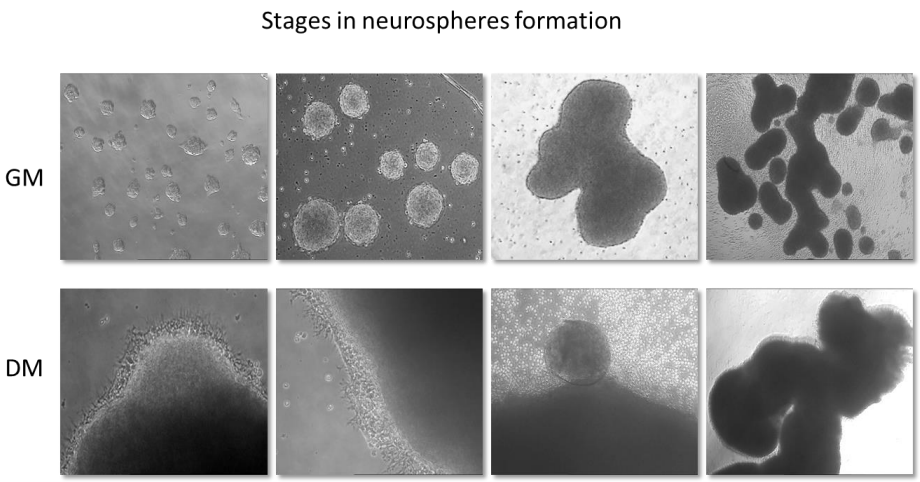

Figure 37. Stages in neurosphere formation from LUHMES.

In contrast, LUHMES cells grown on Geltrex® formed a monolayer. We therefore had the means to study LUHMES cells in monolayers and neurospheres, and compare differences in the biological properties between the two. We hypothesized that embryonic mesencephalic derived cells will differ with respect to the expression of stem cell markers depending on whether they are grown in a monolayer or as neurospheres. We also hypothesized that culture in GM or DM will alter the distribution of cells with stem cell characteristics within neurospheres. In order to find out whether cells expressing stem cell markers are present in neurospheres, and how they reorganize during differentiation, MBs targeting Oct4, Sox2, and Nanog mRNAs were designed.

MBs were introduced into LUHMES cells by SLO-mediated membrane permeabilization. We confirmed that this method did not adversely affect cell viability within neurospheres by measuring cell viability using calcein/propidium iodide staining, which showed that cells maintain viability after SLO transfection (Figure 38) with overall very low numbers of apoptotic cells observed; most of the dead cells were found outside neurospheres, and apoptosis and necrosis was not observed in the inner core of the neurospheres. In addition to demonstrating that MBs do not promote cell death, this also confirmed that fluorescence inside the neurospheres is specific for MBs and is not autofluorescence from dead or dying cells. Monolayers of LUHMES showed >95% viability after the transfection procedure (see Chapter IV).

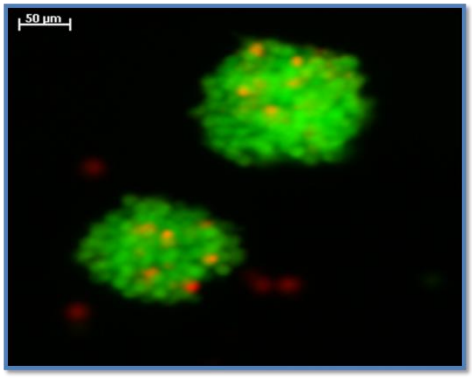

Figure 38. Cell viability within neurospheres. Cells were treated with 17 U/ml SLO and stained with calcein/PI in order to detect cell viability and cell death after transfection (10 x). Live cells (green), dead cells (red).

The signal from the Sox2-targeting MB was detected both in cells growing as neurospheres, and in cells growing as monolayer (Figures 39A and 40A).

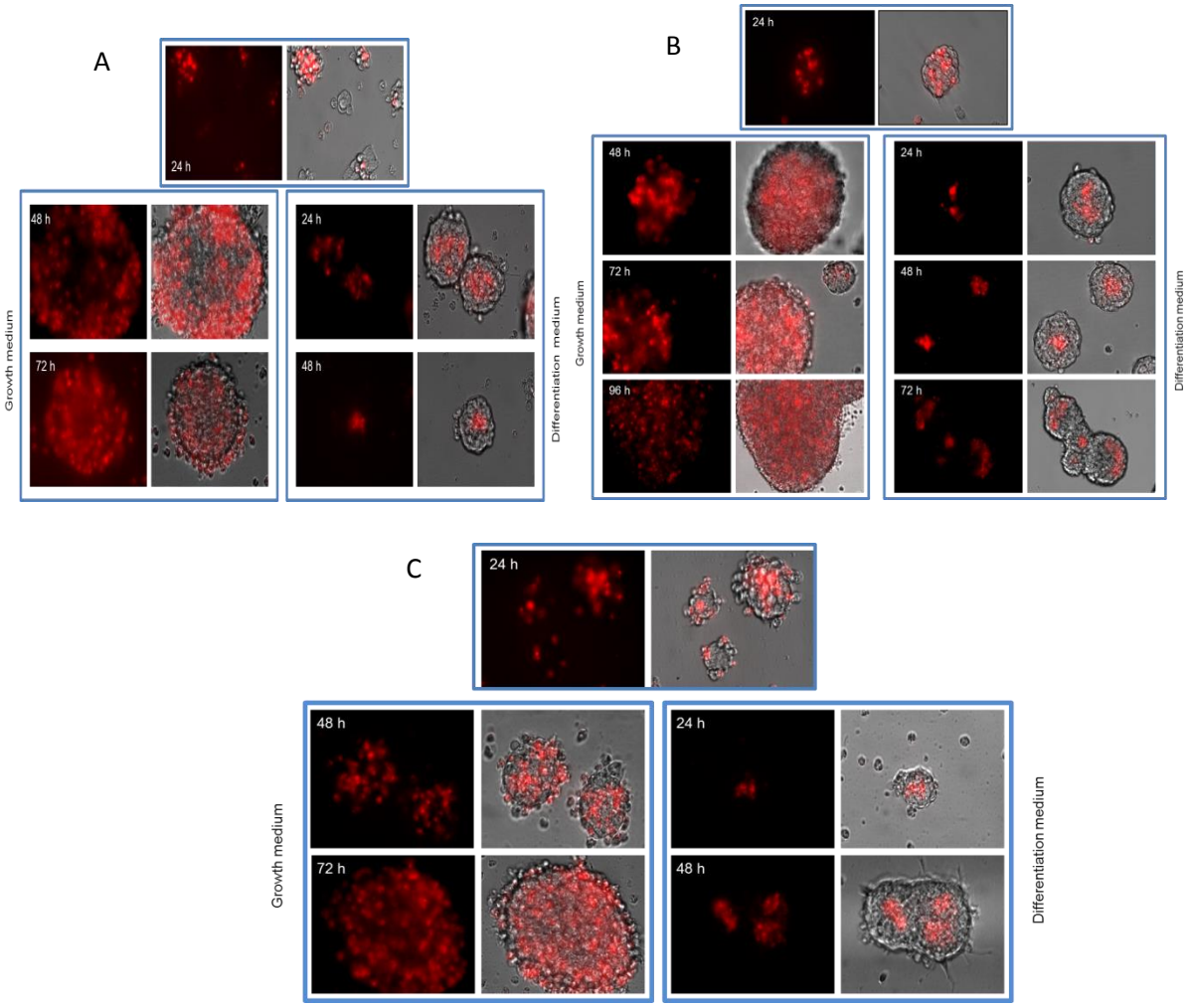

Figure 39. Detection of stem cells markers in neurospheres using MBs targeting **A** Sox2, **B** Oct4 and **C** Nanog. After 72h growth in GM, neurospheres were SLO-transfected with MBs. Cells were kept in GM until 24h post-transfection, at which time the medium was switched to either GM or DM. Gene expression was detected 24, 48, 72, and 96h (i.e. 24, 48, and 72h after differentiation induction) after transfection.

In contrast, Oct4 and Nanog (detected by qRT-PCR) was expressed in cells growing in neurospheres, but not expressed in cells growing as monolayers (Figures 39 B, and 40 B). These results demonstrated that cells growing in neurospheres express the pluripotent state-related genes Oct4 and Nanog in addition to the neuronal stem cell marker Sox2. 24 h after transfection positive for stem cell markers cells were localized mainly on the surface of the neurosperes. It is likely due to more efficient transfection on the surface rather inside neurosphere. After 24h in DM cells positive for Oct4, Sox2, and Nanog were found in the inner core of neurospheres while in GM they are diffusely spread (figures 39). It was observed that both the number of Oct4, Sox2 and Nanog-positive cells, and the absolute number of cells, increased with time in the spheres grown in GM. Neurospheres cultured in

DM either proliferated (figure 39) or showed signs of differentiation of the rim of the neurosphere. It was difficult to determinate the number of the respective Oct4, Sox2 and Nanog positive cells within neurospheres in DM because they formed tight clusters in the center. The Sox2, Oct4, and Nanog-positive cells in DM were localized always in the center of the sphere (Figure 39A, B and C). Significant decrease in signal intensity of Sox2/Oct4 MBs with the time was not detected in GM conditions suggesting stability of the reporter fluorophore to photobleaching or depletion of transfected MB pool.

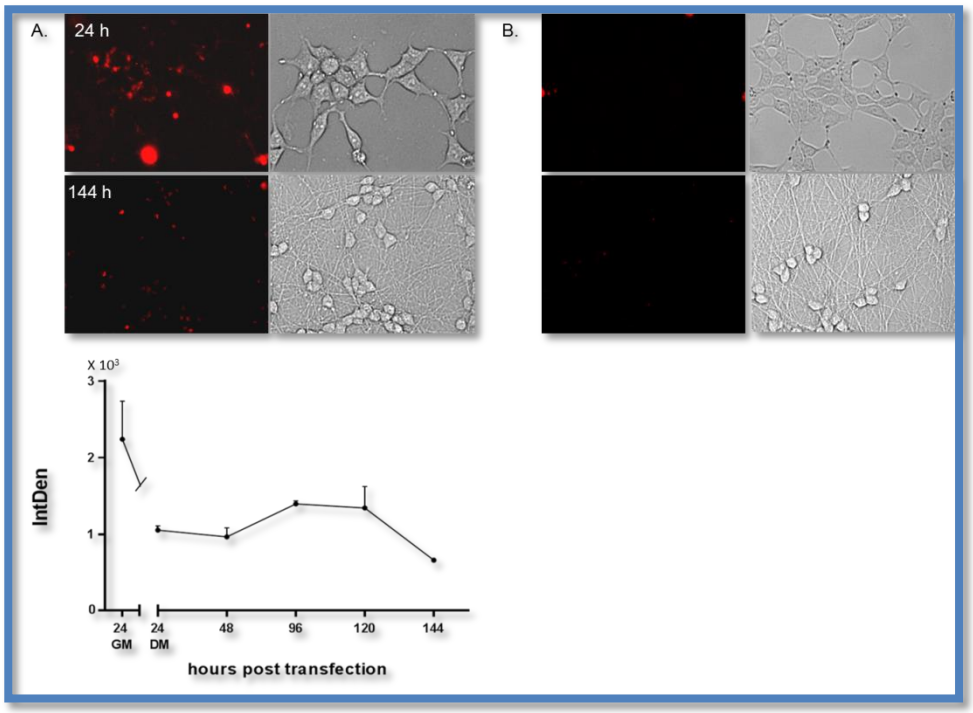

Figure 40. Detection of Sox2 (**A**) and Oct4 (**B**) in adherent LUHMES using MBs. Bright field and fluorescent photomicrographs taken 24h after transfection and 144h after induction of differentiation. **C.** Integrated density of Sox2 targeting MBs as function of time. Data is presented as mean ± S.E.M.

The intensity of Sox2-MB signal in adherent neurons was measured using image analysis (Figure 40 A), and it was found to be high 24h after transfection, and decreased 24h after the start of the differentiation process. The signal intensity fluctuated during culture in DM, and was halved compared to initial values after 144 h (figure 40C). Oct4 was not expressed, precluding an equivalent analysis (figure 40 B).

3.2 MBs detection and tracking of Oct4 positive cells inside neurospheres during differentiation.

Oct4 expression was measured and followed over time in neurospheres during the process of differentiation. Images of neurospheres were captured as z-stacks with Zeiss Apotome and assembled into a 3D representation (Figure 41). Some of the neurospheres attached to the bottom of the plate when exposed to DM. The neurospheres were of varying size from small (50µm in diameter) to large (200µm in diameter). Cells located at the rim of the sphere formed long neurites and differentiated into cells with neuronal morphology (Figures 41B and 41D inset). Other neurospheres grew in size instead of showing features of differentiation (Figure 41C inset). Fusion between growing neurospheres was also seen (Figure 41A inset). In all cases, 24h after switching to DM, Oct4-positive cells were organized in the center of the neurospheres (Figure 41), with no increase in the number of positive cells observed. The cells at the periphery of neurospheres showed clear evidence of neural outgrowths, indicating that these cells differentiate under these conditions.

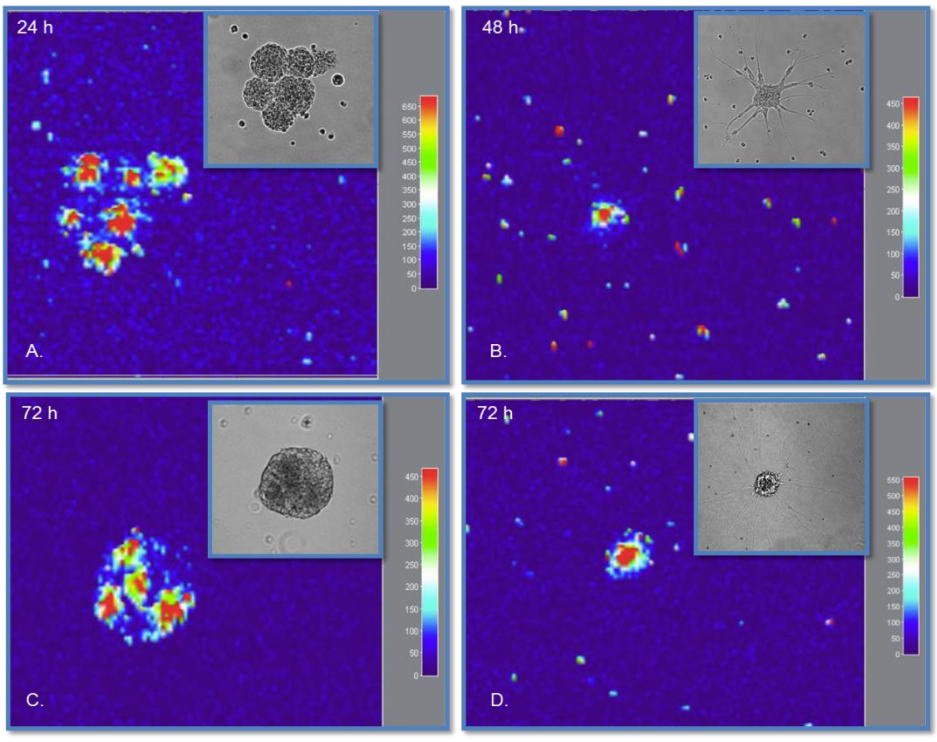

Figure 41. Tracking Oct4-positive cells inside neurospheres during differentiation. **A** 24h after initiation of differentiation, Oct4-positive cells are still diffusely spread in some neurospheres, while in others they start localizing to the inner core. **B** 48h later the neurospheres attach to the matrix and the cells located around the rim start to form neurites. Neurospheres demonstrate varying sizes and differentiation potential. **C** Fusion between neurospheres was seen, together with neurite formation. **D** In both cases, the MB-detected Oct4-

positive cell population was located in the middle of neurospheres. Images were acquired with ApoTome Imaging system, 10x/0.3 Plan Neofluar objective and DsRed filter set.

3.3 qRT-PCR and immunocytochemical analysis of stem cell markers.

qRT-PCR detection of transcript for Oct4, Sox2 and Nanog, and immunofluorescence staining of Sox2 and Oct4 proteins, were used to verify the results observed using MBs to visualize Oct4, Sox2, and Nanog in LUHMES cells. qRT-PCR confirmed that neurospheres expressed all stem cell markers (Figure 42). No significant differences in Oct4 and Nanog expression levels were found between growing and differentiated neurospheres. Oct4 and Nanog expression was barely detectable in either differentiating or growing LUHMES cells grown in monolayers. In contrast, significant Sox2 expression was detected in both neurospheres and adherent cells in GM. Sox2 expression dramatically decreased during differentiation of adherent cells and neurospheres, the latter showing less pronounced decreases in expression. Both Sox2-MB and qPCR were therefore able to detect decreases in Sox2 expression.

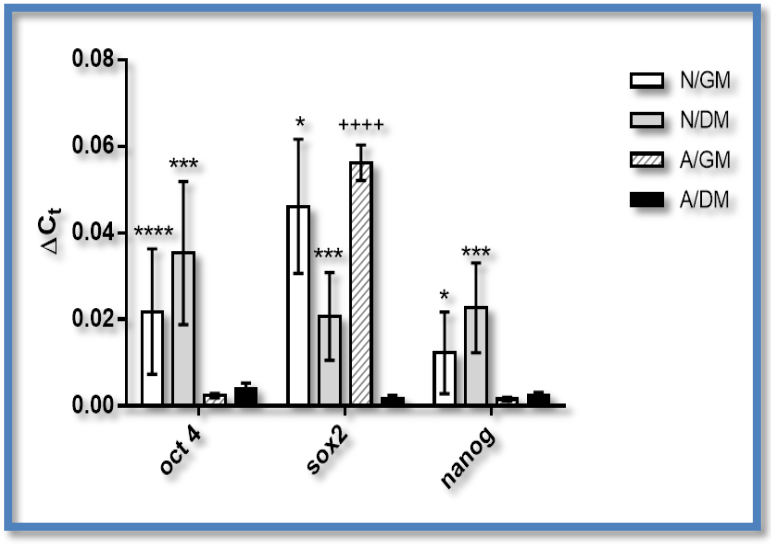

Figure 42. qRT-PCR analysis of mRNA levels of Oct4, Sox2 and Nanog under different growth conditions. Cells grown as neurospheres in GM (white bar), cells grown as neurospheres in DM (gray bar), cells grown as monolayer in GM (hatched bar), and cells grown as monolayer in DM (black bar). Expression was normalized to GAPDH mRNA expression. Data is present as mean ± S.E.M. n = 5 *p<0.05 ***p<0.001, ****p<0.0001 compared to monolayer cell growth, ++++p<0.0001 compared to cells cultured in growth medium. Differentiation process for 5 days.

Staining with antibodies targeted against Oct4 demonstrated protein expression in neurospheres, but not in monolayer cultures (Figures 43), corroborating the qRT-PCR and MB results.

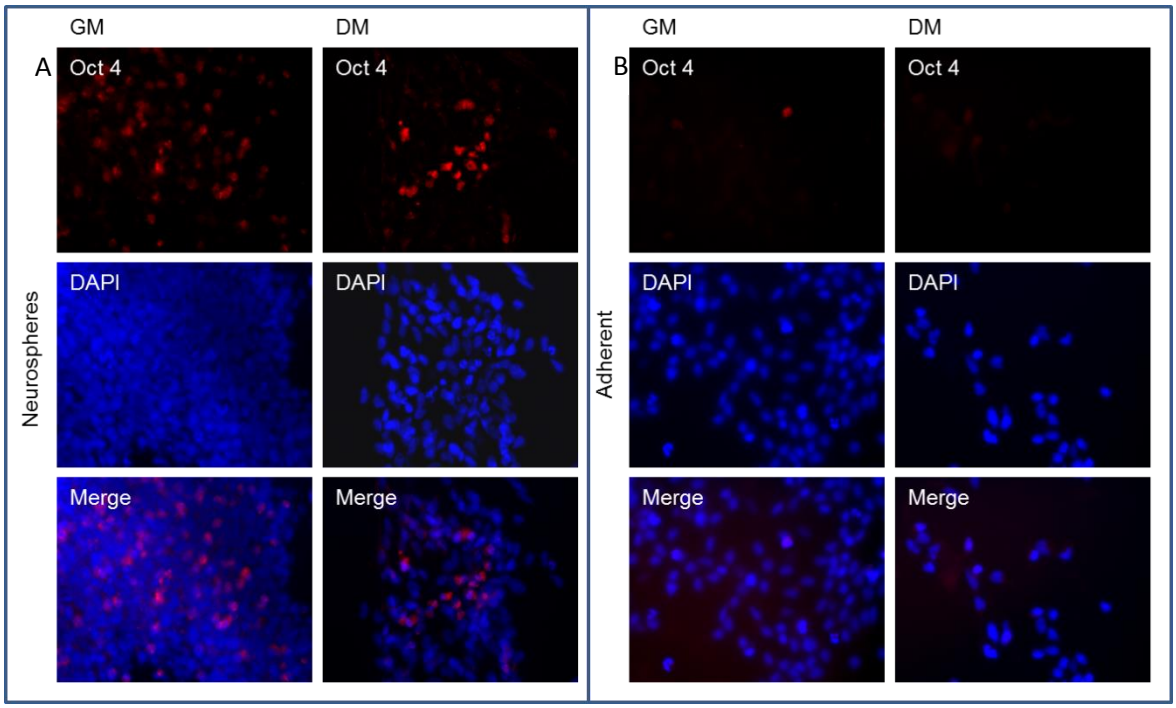

Figure 43. Immunocytochemistry of **A** Neurospheres and **B** adherent LUHMES stained for Oct4. Expression at the protein level was detected in neurospheres under both GM and DM culture conditions. Oct4-positive cells are diffusely spread within neurospheres when cultured in GM, and localized in the center of neurospheres in DM. Oct4 expression at the protein level was not detected in cells growing as a monolayer.

The Oct4 protein was localized in the cytoplasm of the cells within neurospheres grown in DM. Moreover the localization of Oct4 protein positive cells followed the distribution of Oct4 MB positive cells were observed mainly in the center of the sphere. Due to the high cell number and density in neurospheres grown in GM, it was difficult to determine the intracellular localization of the Oct4 protein. It has been described previously [13, 14] that two splice variants of Oct4 exist, Oct4A and Oct4B, with nuclear and cytoplasmic localization domains, respectively. Oct4A is restricted to stem cells, whereas Oct4B can be detected also in various nonpluripotent cell types [15]. Although the antibody used in this study detects both isoforms.

Sox2 protein was detected under all growth conditions with cytoplasmic localization (Figure 44). A decrease in number of Sox2 protein-positive cells was observed in both monolayer

cultures and neurospheres after exposure to DM. These results again corroborate the qRT-PCR and Sox2-MB results. Both Oct4 and Sox2-positive immunostained cells in neurospheres grown in DM showed a distribution of staining similar to the signal detected by MBs, namely being localized mainly in the center of the cluster.

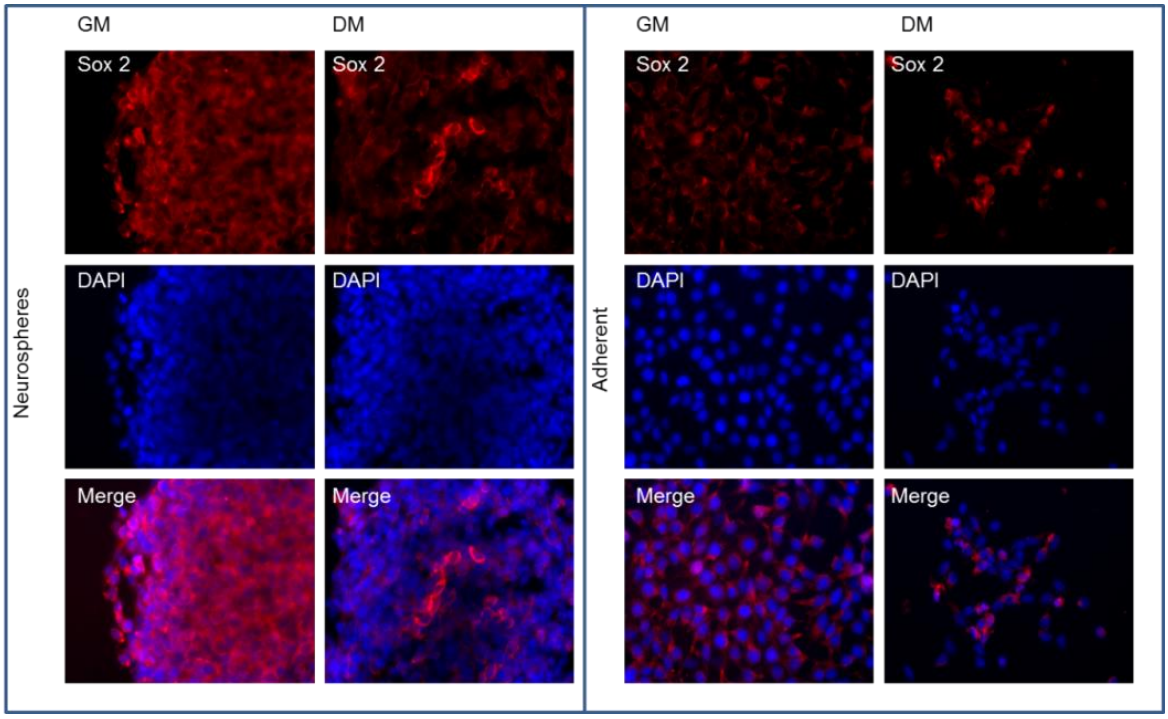

Figure 44. Immunostaining for Sox2. The distribution of Sox2-positive cells inside neurospheres in DM mirrored the distribution of MB-detected Sox2-positive cells, being inner core localized. Adherent cells cultured in GM highly expressed Sox2 with cytoplasmic localization of the protein. During differentiation, protein levels decreased, which positively correlated with the data from qRT-PCR.

4. Discussion

By applying MB-technology for the detection of Oct4, Sox2 and Nanog mRNA, we visualized a population of cells displaying a stem cell signature in LUHMES-derived neurospheres. Moreover, the use of MBs allowed for the detection of endogenous Oct4, Sox2 and Nanog in stem cells within the neurospheres, rather than exogenously expressed signal from a genetic manipulation. Stem cell markers-positive cells were found in the center of the spheres cultured in DM, while cells in the periphery showed signs of neuronal development. LUHMES cells grown as monolayer did not demonstrate significant Oct4 and Nanog expression, suggesting that cells growing as neurospheres are subjected to different

microenvironmental conditions, such as differences in growth factor levels and pO_2. However it is not clear if downstream processes in reverting cells to pluripotent stage are induced and further experiments are required to detect the differentiation potential of LUHMES derived neurospheres.

We chose three archetypal stem cell markers as the focus of this study, Oct4, Sox2, and Nanog. Oct4 (Oct3/4 or POU5F1) is a member of the Oct-family of POU transcription factors. Sox2 belongs to the Sox gene family, which are HMG box transcription factors that interact functionally with POU domain proteins. Nanog is a transcription factor, a key regulator of pluripotency in embryonic stem cells. However, Sox2 is associated with multipotent and unipotent stem cells, while Oct3/4 and Nanog are exclusively expressed in pluripotent stem cells. While Sox2 is expressed in adult neuronal stem cells and is retained in some populations of differentiating neurons [16, 17, 18], the expression of Oct4 in NSCs is still demonstrated in the literature [19]. A few studies clearly show that Oct4 is expressed at both the mRNA and protein level in "naïve" mouse [20, 21, 22, 23] and human neurospheres [24], and that expression drops during differentiation. Nanog is expressed in neurospheres derived from glioblastoma cells [25], but also in human fetal cortical and striatal derived neurospheres [24].
The relatively slow rate of proliferation and physiological senescence in culture make the use of human neural stem cells cumbersome under some experimental and pre-clinical settings. The immortalization of hNSC with the *v-myc* gene showed to generate stem cells with enhanced proliferative capacity, which greatly facilitates the study of NSCs in vitro and in vivo [26]. *v-myc* increases the pool of self-renewing cells and shift towards a more primitive cellular identity but without affecting the differentiation marker expression. Thus *v-myc* does not block differentiation, but delays cell cycle exit [27]

Two different studies [28, 29] aimed to show the relationship of *c-myc* to the core pluripotency factors Oct4 and Sox2. The authors demonstrated that although there are many genes that are common target for Oct4 and Sox2, the genes that *c-myc* targets only a fraction of these genes. *c-myc* binding regions also have distinctive histon marks. A functional distinction between the *myc* binding sites and the sites to which Oct4 and Sox2 binds was also revealed [28]. None of the *myc* localization sites had enchancer activity suggesting the idea that *myc* functions in a way that distinct from the other pluripotent factors [29, 30]. Expression of Oct4 in monolayer growing cells was not detected suggesting that induction of

Oct4 expression in neurospheres is likely not an artefact from *v-myc* overexpression in LUHMES but is influence by the cell environment and 3D architecture of the neurosphere.

Neurospheres cultures represent a heterogeneous system with respect to the size of the clusters, and the proliferative, differentiation, and developmental potential of parental clone-forming cells. Suslov et al. [3.] proposed a hypothetical model for the relationship between neurosphere size and the maturation level of clone-forming cells (figure 45).

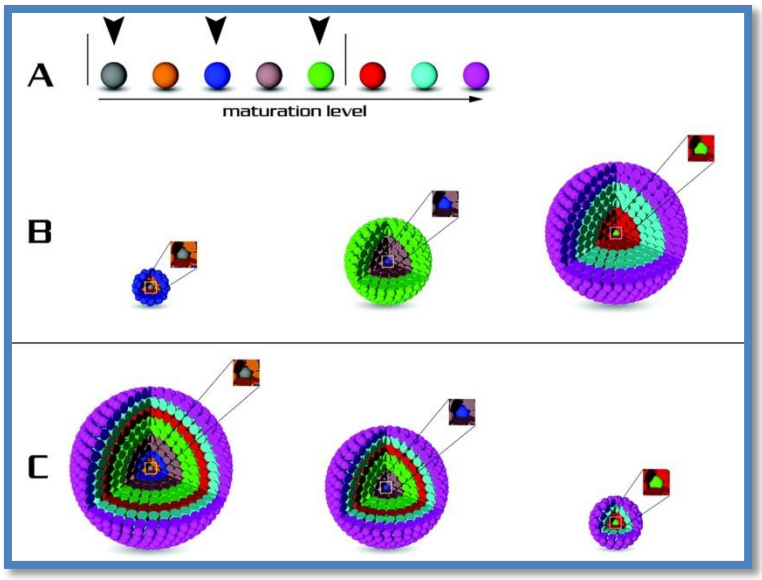

Figure 45. Hypothetical model for the relationship between neurosphere size and maturation level of clone-forming cells. (A) A row of eight (arbitrary number) cells with varying developmental potential is arranged and color-coded according to presumed maturation level. Five cells within the upright lines can give rise to neurospheres. In this group, the gray cell represents the most immature and the green cell is the most mature clonogenic cell. Three clone-forming cells are depicted (arrowheads); in B and C, alternative architectures of neurospheres are arranged according to the clonogenic potential of the parental cell. (B) In this scenario, the stem cell is less proliferatively active than the progenitor cell. In this model, the most mature (green) cell gives rise to the largest size clone, and the smallest neurosphere contains descendants (e.g., orange and blue cells) from the most immature clonogenic (gray) cell. (C) In this case, the stem cell is more proliferatively active than the progenitor cell. This represents a situation in which the smallest sphere arises from the green neurosphere-forming cell and the largest clone from the more immature gray cell. Both of these simplified models underscore a notion that molecular phenotypic heterogeneity of neurospheres might reflect differences in the developmental potential of distinct stem/progenitor cell groups that co-exist in the brain. (Suslov et al., PNAS, 2002).

Their findings suggest that the size of a clone might reflect responsiveness to growth factors and the proliferation/differentiation status of the parental clone-forming stem/progenitor cell. In this model, cells with varying developmental potential were proposed. Clone-forming cells able to give rise to neurospheres demonstrating different stages of maturation were distinguished and proposed to have a different arrangement within the neurosphere architecture. The most immature clonogenic cells were suggested to be localized in the core of the neurosphere, while progenitor and differentiated cells were located at the shell. This hypothetical model is in agreement with the experimental results shown here (Figures 39 and 41). Based on the MB signal it was observed that cells positive for stem cell markers were present in the core of the neurosphere, where access of differentiation stimuli is restricted. Results from qRT-PCR verified the expression of Oct4, Sox2 and Nanog in LUHMES derived neurospheres, confirming the existence of a cell population with a stem cell profile (Figure 42).

Proliferation and multipotentiality of CNS precursors are enhanced *in vitro* when cultured under hypoxic conditions [31]. The culture of human mesencephalic precursors at low oxygen tensions promotes their proliferation [32]. Oxygen tension in the neural niche functions to maintain stem cell self-renewal and the undifferentiated state. A hypoxic microenvironment facilitates stemness and prevents NSCs from differentiating unless changes in redox status, or other local cues, mobilize the NSC population to proliferate, differentiate, or migrate. It has also been shown that Oct4 is a specific target gene of hypoxia-inducible factor (HIF) [33], mechanistically linking how stem cells may sense hypoxic conditions in their niches, and how low pO_2 can modify stem cell function directly [34].

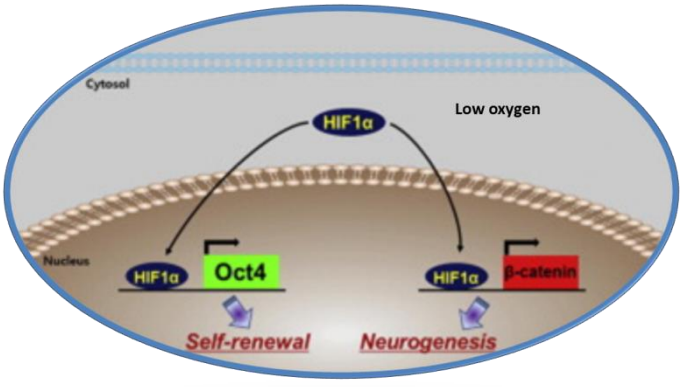

Figure 46. Proposed model of HIF and Oct4-mediated control of neural differentiation (modified from Choi et al., Biomaterials 2011; 32: 7013-7022)

This is one reasonable explanation why cells under hypoxic conditions within the center of neurospheres express Oct4 and Nanog, in contrast to adherent LUHMES. We speculated that neurosphere like growth, could provide the necessary stimuli that lead to reversion to a more immature state. Takehara et al. [22] demonstrated a drastic down-regulation of Oct4 expression only after transferring the NSCs to adherent conditions. Further, low pO_2, together with a growth factor gradient across individual neurospheres modulate the expression further. It was demonstrated that hypoxia is involved in pathological processes in cancer genesis by promoting reprograming and de-differentiation of tumor cells. It leads to more immature cell type that are highly aggressive, chemotherapy resistant and thus with poor clinical prognosis. One study of mouse brain tumor model [25] demonstrate Oct4 expression in both monolayer and neurosphere conditions. On the other hand, expression of Nanog was detected only in neurospheres. Authors explained increasing in proliferation and invasion of brain tumor cells grown as neurospheres compared to monolayer cells with coincided expression of both stem cell markers in neurospheres. Alternatively, differentiation of cells in the center of neurospheres is inhibited under the conditions existing in the spheres. This might be an explanation as to why cells with stem cell characteristics are localized in the inner core of neurosphere when they are exposed to DM. Oct 4 and perhaps Nanog induction by hypoxia would explain why qRT-PCR data did not show decreases in Oct 4 expressions in cells in neurospheres.

5. Conclusion

A deep understanding of how NSCs behave *in vitro* and *in vivo* must be achieved before the practical and safe use of these cells can be applied to human beings for therapeutic benefit. Identifying the different cell types within neurospheres, and tracking these cell populations separately to determine whether there are separate stem cell niches, is the next challenge. Our study shows that cell migration and specific niche formation within neurospheres is a real dynamic process that might be influenced by many factors, including composition of the extracellular matrix, growth factors, pO_2, and neurosphere heterogeneity.

References

1. Bez A, Corsini E, Curti D, et al. Neurosphere and neurosphere forming cells: morphological and ultrastructural characterization. Brain research 2003; 993: 18-29.
2. Altman J, Autoradiographic and histological studies of postnatal neurogenesis. IV. Cell proliferation and migration in the anterior forebrain with special reference to persisting neurogenesis in the olfactory bulb. J. Comp. Neurol. 1969; 137: 433-457.
3. Suslov O N, Kukekov V G, Ignatova T N, et al. Neural stem cell heterogeneity demonstrated by molecular phenotyping of clonal neurospheres. PNAS 2002; 22: 14506-14511.
4. Pacey L, Stead S, Gleave J, et al. Neural stem cell culture: neurosphere generation, microscopical analysis and cryopreservation.
5. Hill E J, Woehrling E K, Prince M, et al. Differentiating human NT2/D1 neurospheres as a versatile in vitro 3D model system for developmental neurotoxicity testing. Toxicology 2008; 249: 243-250.
6. Binello E, Qadeer Z A, Kothar H P, et al. Stemness of the CT-2A immunocompetent mouse brain tumor model: Characterization in vitro. Journal of cancer 2012; 3: 166-174. 10.7150/jca.4149.
7. Deleyrolle L P, Rietze R L, Reynolds B A. The neurosphere assay, a method under scrutiny. Acta Neuropsychiatrica 2008; 20: 2-8, 10.1111/j.1601-5215.2007.00251.x.
8. Wan F, Zhang S, Xie R, et al. The utility and limitations of neurosphere assay, CD 133 immunophenotyping and side population assay in glioma stem cell research. Brain Pathology 2010; 20: 877-889.
9. Pastrana E, Silva-Vargas V, Doetsch F. Eyes wide open: A critical review of sphere-formation as an assay for stem cells. Cell Stem Cell 2011; 10.1016/j.stem.2011.04.007.
10. Wang T Y, Sen A, Behie L, et al. Dynamic behavior of cells within neurospheres in expanding populations of neural precursors. Brain Research. 2006; 10.1016/j.brainres.2006.05.110.
11. Chen A, Rhee W J, Bao G, et al. Delivery of molecular beacons for live-cell imaging and analysis of RNA. RNA detection and visualization: Methods and Protocols, Methods in Molecular Biology, vol. 714, Jefferey E. Gerst (ed.); 10.1007/978-1-61779-005-8_10.

12. Lotharius J, Barg S, Wiekop P, et al.. Effect of mutant α-synuclein on dopamine homeostasis in a new human mesencephalic cell line. The Journal of Biological Chemistry 2002; 277: 38884-38894.
13. Atlasi Y, Mowla S J, Ziaee S A M, et al. OCT4 spliced variants are differentially expressed in human pluripotent and nonpluripotent cells. Stem Cells 2008; 26: 3068-3074.
14. Lee J, Kim H K, Rho J Y, et al. The human OCT-4 isoforms differ in their ability to confer self-renewal. J. Biol. Chem. 2006; 281: 33554-33565.
15. Saxe J P, Tomilin A, Schöler H R, et al. Post-translational regulation of Oct4 transcriptional activity. PLoS One 2009; 4: 1-9.
16. Pevny L H, Nicolis S K. Sox 2 roles in neural stem cells. The International Journal of Biochemistry & Cell Biology 2010; 42: 421-424.
17. Graham V, Khudyakov J, Ellis P, et al. Sox 2 functions to maintain neural progenitor identity. Neuron 2003; 39: 749-765.
18. Brazel C Y, Limke T L, Osborne J. K., et al. Sox 2 expression defines a heterogeneous population of neurosphere-forming cells in the adult murine brain. Aging Cell 2005; 4: 197-207.
19. Liedtke S, Stephan M, Kögler G. Oct 4 expression revisited: potential pitfalls for data misinterpretation in stem cell research. Biol. Chem. 2008; 389: 845-850.
20. Okuda T, Tagawa K, Qi M-L, et al. Oct-3/4 repression accelerates differentiation of neural progenitor cells in vitro and in vivo. Molecular Brain Research 2004; 132: 18-30.
21. Chin J-H, Shiwaku H, Goda O, et al. Neural stem cells express Oct-3/4. Biochemical and Biophysical Research Communications 2009; 388: 247-251.
22. Takehara T, Teramura T, Onodera Y, et al. Potential existence of stem cells with multiple differentiation abilities to three different germ lineages in mouse neurospheres. Stem Cells and Development 2009; 18: 1433-1440.
23. Lee S-H, Jeyapalan J N, Appleby V, et al. Dynamic methylation and expression of Oct 4 in early neural stem cells. Journal of Anatomy 2010; 217: 203-213.
24. Massa D, Pillai R, Monni E, et al. Expression analysis of pluripotency-associated genes in human fetal cortical and striatal neural stem cells during differentiation. Translational Neuroscience 2012; 3: 242-248.

25. Binelo E, Qadeer ZA, Kothari HP, Emdad L,Germano IM. Stemness of the CT-2A immunocompetent mouse brain tumor model: characterization in vitro. Journal of Cancer 2012; 3: 166-167.
26. De Filipps L, Ferrari D, Nodari L R, Amati B, Snyder E, et al. (2008) Immortalization of human neural stem cells with the c-myc mutant T58A. PLOS ONE 3(10): e3310
27. Kerosuo L, Piltti K, Fox H, Angers-Loustau A, Häyry V, et al. (2008) Myc increases self-renewal in neural progenitor cells through Miz-1. J Cell Sci 121: 3941-50
28. Chen X, Xu H, Yuan P, Fang F, Huss M, et al. (2008) Integration of external signaling pathways with the core transcriptional network in embryonic stem cells. Cell 133: 1106-17
29. Kim J, Chu J, Shen X, Wang J, Orkin SH (2008) An extended transcriptional network for pluripotency of embryonic stem cells. Cell 132: 1049-61
30. Chambers I, Tomlinson SR (2009) The transcriptional foundation of pluripoency. Development 136: 2311-22

31. Santilli G, Lamorte G, Carlessi L, et al. Mild hypoxia enhances proliferation and multipotency of human neural stem cells. PLoS ONE 5, 2010, e8575.
32. Storch A, Paul G, Csete M, et al. Long-term proliferation and dopaminergic differentiation of human mesencephalic neural precursor cells. Exp. Neurol. 2001; 170: 317-325.
33. Mohyeldin A, Garzón-Muvdi T, Quiñones-Hinojosa A. Oxygen in stem cell biology: a critical component of the stem cell niche. Cell Stem Cell 2010; 10.1016/j.stem.2010.07007.
34. Covello K L, Kehler J, Yu H, et al. HIF-2 alpha regulates Oct-4: effects of hypoxia on stem cell functions, embryonic development, and tumor growth. Genes Dev. 2006; 20: 557-570.

Chapter VII. General Discussion

1. Cellular models

In this work, it was demonstrated the usability of MBs for detecting and tracing time dependent, dynamic processes inside individual living cell as well cell clusters. Moreover we applied designed MBs in a biological study focused on differentiation of neural stem cells into dopamine neurons as well as reprogramming of somatic cells like ASC and MSC into pluripotent stem cells. As it is seen on figure 47 cell colonies or 3D clusters with different differentiation potential (totipotent, pluripotent or multipotent) obtain similar morphology. For example embryoid bodies and neurospheres are 3D cellular clusters. However, EBs can give rise to all germ layers, i.e. they are pluripotent. In contrast neurospheres can develop into neural and glial cells and thus they are determined as multipotent. Moreover ESC and iPSC obtain similar characteristics such as colonies morphology, capacity for self-renewal and differentiation, EB and teratoma formation etc. However as it was described before (Chapter V) not all iPSC are bona fide and they display different stages of reprograming. Detection and tracing the on-going processes during differentiation and reprograming as regards to expression of quintessential set of genes are of very high importance especially when reprogrammed cells will be used in therapy in humans.

LUHMES cell line showed to be a suitable model for study neural differentiation but also reverting into more immature stage caused by neurosphere like growth. We demonstrated formation of cell population inside neurospheres displaying immature characteristics and expressing pluripotent markers Oct4 and Nanog (however we did not determine differentiation potential of this population) caused only by the specific environment inside neurosphere. Although LUHMES are v-myc immortalized and thus dos not represent "natural" stem cells they are an appropriate model for MBs study cell behaviour within 3D cell clusters like neurosphere and they response to different environmental stimuli. Moreover, expression of Oct4 and Nanog were not detected in LUHMES grown as monolayer suggesting that pluripotent markers expression is induced by the specific environment and architecture of 3D cluster and not artefact from v-myc expression.

Non-differentiated adherent LUHMES show some characteristics associated with immature cells. They express Sox2 mRNA and it was dramatically lost at d5 of differentiation. Other stem cell markers like polysialylated neural cell adhesion molecule (PSA-NCAM) and PAX 3

(a marker for migrating neuroblasts) were also detected [1]. Moreover they express neuronal progenitors marker nestin and its expression remains after differentiation. Additionally the proliferating d0 cells expressed neuronal markers and several dopaminergic features, thus they already have a definite neuronal commitment. After 6 days in differentiation medium, additional neuronal and dopaminergic features are up-regulated, including TH, which is found in differentiated dopaminergic neurons [1]. LUHMES cell line show to be heterogeneous in respect of gene expression of neural stem cell, progenitors and neuronal markers. It seems to be a good and versatile cellular model to follow up- and down regulation of gene expression. Moreover, fast neurosphere formation allowed MBs tracking individual cell behavior within 3D cell population.

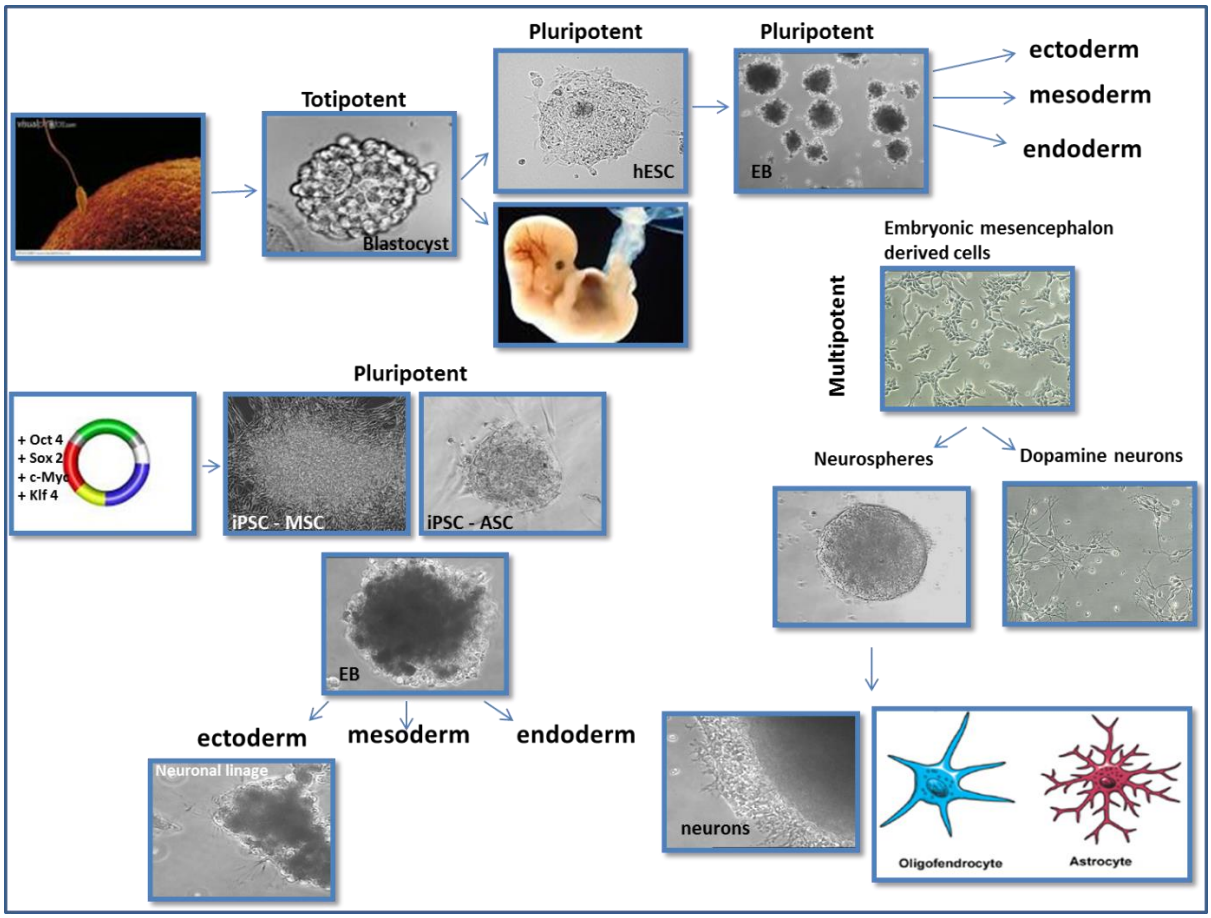

Figure 47. Cellular models used in the study. Cells with different differentiation potential display similar morphology. LUHMES showed that can differentiate into mature neurons but also step back in maturity forming neurospheres with stem cell signature cell population. It was demonstrated that cells can be reprogram into immature stage by transfecting with plasmid coding for pluripotent markers, but also spontaneously induced by the environmental conditions within neurospheres.

2. Considerations for MBs application in live cell gene expression detection

In contrast to hybridization in solution where the physicochemical conditions are simplified, hybridization of MBs to mRNA in living cells is complicated by the formation of secondary structures in mRNA molecules, RNA-binding proteins, and the degradation of the probes due to enzymes with nuclease activity [2]. If the target sequence has a double-stranded structure MBs compete with RNA strands, while when the target is a binding site for proteins, MBs compete with RNA-binding proteins in order to hybridize. These factors could make target sequence inaccessible to MBs in spite of unique probe sequence design. Software programs such as mFOLD and Beacon Designer can predict the formation of secondary structures so that these sequences can be avoided during the selection of probes in the design process. The prediction of protein binding sites in the target is more complicated due to only limited data existing for RNA-binding proteins [2]. Competition with RNA or RNA-binding proteins can result in a significant decrease in signal level due to inefficient hybridization between the MB and the target sequence. To overcome this, many studies have used 2'-O-methyl RNA MBs in order to increase affinity for the target mRNA [3]; in addition, a modified backbone is less vulnerable to nuclease activity. On the other hand, the formation of double-stranded RNA can lead to RNA silencing, and therefore influence cellular function. In this study, MBs with 2'-deoxy and 2'-O-methyl backbones were tested. Probe-target hybridization did not have any measurable effect on cell physiology including gene expression, self-renewal, or differentiation. Other authors [4, 5] have also successfully used non-modified MBs in their living cell studies, although over a shorter length of time. This suggests that it is a matter of choice for individual researchers to use either 2'-deoxy or 2'-O-methyl modified bases in the design of their MBs, although modified backbone MBs may be more appropriate in studies tracking gene expression over prolonged periods of time.

False positive signals due to MB-protein interaction and degradation are further limitation that reduces the usability of MBs in live cell imaging applications. Chen et al. [6] observed that MBs with non-modified backbones incubated with phosphodiesterase I and II show a small increase in fluorescence. They concluded that the fluorochrome and quencher conjugated on each end of MBs limit exonuclease activity. However, MBs are highly sensitive to degradation by S1 endonucleases, and Mung Bean endonucleases that cleave the

hairpin loops. Single-strand binding (SSB) proteins also cause significant increases in fluorescence. Although SSB proteins and nucleases are present in the cell cytoplasm, previous studies have shown that there are fewer DNA-protein interactions in the cytoplasm compared to the nucleus, and that the nuclease activity is in fact low [6]. MBs remain in their quenched hairpin conformation when localization is limited to the cytoplasmic compartment. Our data showed signal retained in the cytoplasm with perinuclear localization, but not within nucleus (Chapter IV). This pattern of expression and the appearance of signal at different time points during development suggest that these do not represent false-positive signals, but are due to specific hybridization between MB and target sequence.

One limitation that needs to be considered could be the theoretical decrease in the MB signal through dilution during cell division, especially in rapidly dividing cells and for highly express genes. Differentiated neurons are out of cell cycle and decreases in signal intensity due to MB dilution are therefore not observed. We were able to detect an increasing number of Sox2 and Oct4-positive cells in neurospheres grown in GM. Oct4 and Sox2 are not highly expressed genes in NSCs, an observation supported by our qRT-PCR data, and thus do not necessarily use up all the MBs in the intracellular pool that exists after transfection. This pool will be diluted after each cell division; however, as long as the pool of MB is larger than the pool of target mRNA, the MB will be able to emit maximum signal proportional to the amount of transcript. When the pool of MB inside the cell is smaller than the pool of target mRNA, the MB can emit a signal, but it will be weaker and not proportional to the true level of transcript. At some point, the MB will be too diluted and signal lost despite the cells expressing a high number of target molecules. It is possible that some of the Sox2 and Oct4-negative cells in neurospheres grown in growth medium are indeed Sox2 and Oct4 positive. However, transfected MBs remain a very powerful tool for use with cells that do not divide extensively, such as stem cells after induction, while their use might be limited and transient in rapidly dividing cells.

It is difficult to predict how many beacons penetrate each cell during transfection, and cell-to-cell variations in MB delivery might exist [5]. However, our transfection diffusion model demonstrates that a steady-state concentration is reached inside the cell after only a few seconds. After subtracting the volume of the nucleus, which is not pierced by MBs, the

average cell is predicted to contain 56000 beacons. It is a large pool of MBs which exists in the cell after transfection, and not all MBs are used up, especially in the case of genes with low expression as it was mentioned above. Therefore all mRNAs targeted by MBs should be saturated, and the signal intensity detected from individual cells in the same developmental stage should be relatively equal. We detected different signal patterns and intensities of the same MB between cells in the same stage of differentiation (Chapter IV). This might be explained not by variation in the number of penetrating MBs inside each cell, but by noise in gene expression, i.e. the variation in the number of copies of mRNA between cells due to the fundamentally stochastic nature of the biochemistry of gene expression.
MB intensity was positively correlated with quantification of gene expression by qRT-PCR, supporting the conclusion that detection of gene expression using MBs accurately reflects cellular mRNA levels.
As described by Sholz et al. [1], undifferentiated LUHMES grown as monolayer initially express Sox2 mRNA which dramatically decreases by day 5 after differentiation. The cognate protein follows the same expression profile. The signal from the Sox2-MB shows fluctuations in intensity during differentiation, but was halved at day six (Chapter VI). This suggests that the MB was able to recover from the "open" to "closed" state. However, the signal from the Sox2-MB did not disappear completely, suggesting that Sox2 was still expressed in differentiated neurons. These findings are supported by our qRT-PCR results and immunocytochemistry, as well as other published data [7, 8]. This suggests that MBs can detect not only up-regulation, but also down-regulation in gene expression.

It was possible to observe a decrease in Sox2 expression level upon differentiation as well as increasing in the expression of neuronal markers using MBs. Thus MBs may be used quantitatively for some applications. However, the dynamic range of MBs appears inferior to qRT-PCR, since Sox2-MBs could only detect a 2-fold reduction in Sox2 mRNA expression, while qRT-PCR demonstrated a 20-fold decrease in Sox2 mRNA levels (see Chapter IV). Moreover qRT-PCR results demonstrated no changes in gene expression of Oct4 and Nanog between neurospheres in GM and DM. Simultaneously the number of Oct4 and Nanog MB positive cells in GM significantly increased while the number of positive cells in neurospheres in DM did not increase over the time. This discrepancy between the results suggest that the total number of Oct4/Nanog cells in neurospheres in GM is higher than DM but with lower mRNA expression on single cell level. The opposite – MB positive cells in DM neurospheres are less but with higher expression of both markers. Thus both methods are

complementary and provide information about gene expression on two different levels – individual cell (MBs) and whole population (qRT-PCR). While qRT-PCR is a quantitative method, MBs retain spatial and temporal information which is lacking in destructive technologies such as qRT-PCR, such that they can track over time which part of the sphere population is expressing the gene of interest, and monitor it at a single cell level. GFP–reporter constructs are widely used to track which cells express certain genes, but they require recombinant technology which is time consuming and can result in changes to the regulation of gene loci, which may not accurately reflect the wild type endogenous expression. MBs employ a rapid methodology which does not require lengthy, and sometimes impossible genetic modifications, since they measure cytoplasmic mRNA expression. They may inhibit translation or cause changes the metabolism of the mRNA, leading to functional differences in cells transfected with MBs. However, in our experiments using MBs, we did not observe any kinetic differences in differentiation or proliferation compared to untransfected cells.

Despite all the disadvantages described, we show here that MBs are a powerful tool for the spatiotemporal detection of gene expression inside living cells. Measurements can be performed at the single cell level, allowing for the study of changes in mRNA expression and localization in the same cell. In contrast to widely used GFP–reporter constructs, MBs represent a rapid method for targeting endogenous gene expression without genetic modifications.

3. Perspectives and conclusions

Simultaneous transfection with MBs targeting for stem cell and differentiation markers and tracing the changes in gene expression of both markers during differentiation is the next challenge. Follow the real time distribution and behavior of different cell populations within 3D clusters will give invaluable information about the events occurring during development and differentiation. For this application MBs should be designed with fluorochromes with distinct emission specters (e.g. red and green) to differentiate the signals.

It was demonstrated that using transfected MBs is easy, rapid and relatively cheap way to detect gene expression in living cells. Signal can be detected only one hour after transfection and it is stable for more than 14 days when a modified backbone probes are used. Cells do

not need to be modified genetically and they demonstrate high viability after transfection. MBs do not affect physiological processes in cells. MBs could track gain-of-expression but also loss-of-expression during differentiation. This suggests that they can regenerate from a hybridized open state to a non-hybridized closed state inside cells and reused. Thus it seems that fluctuation in gene expression can be also detected.

References

1. Scholz D, Pöltl D, Genewsky A, et al. Rapid, complete and large-scale generation of post-mitotic neurons from the human LUHMES cell line. Journal of neurochemistry 2011; 10.1111/j.1471-4159.2011.07255.x.
2. Rhee W. J., Santangelo P. J., Jo H., Bao G. Target accessibility and signal specificity in live-cell detection of BMP-4 mRNA using molecular beacons. Nucleic Acids Reserch 2008, vol. 36, no. 5, DOI: 10.1093/nar/gkn039.
3. Tsourkas A., Behlke M. A., Bao G. Hybridization of 2'-O-methyl and 2'-deoxy molecular beacons to RNA and DNA targets. Nucleic Acids Research 2002, vol. 30, no 23, 5168-5174.
4. Lennon F. E., Hermann C. D., Olivares-Navarrete R., Rhee W. J., Schwartz Z., Bao G., Boyan B. D. Use of molecular beacons to image effects of titanium surface microstructure on β1 integrin expression in live osteoblast-like cells. Biomaterials 2010; 31 7640-7647.
5. Desai H. V., Voruganti I. S., Jayasuriya C., Chen Q., Darling E. M. Live-cell, Temporal gene expression analysis of osteogenic differentiation in adipose-derived stem cells. Tissue Engineering 2013; vol. 19, no. 1-2, pp. 40-8.
6. Chen A. K., Behlke M.A., Tsourkas A. Avoiding false-positive signals with nuclease-vulnerable molecular beacons in single living cells. Nucleic Acids Research 2007, vol. 35, no 16, DOI: 10.1093/nar/gkm593.
7. Pevny L H, Nicolis S K. Sox 2 roles in neural stem cells. The International Journal of Biochemistry & Cell Biology 2010; 42: 421-424.
8. Graham V, Khudyakov J, Ellis P, et al. Sox 2 functions to maintain neural progenitor identity. Neuron 2003; 39: 749-765.

Appendix 1

Elsevier Editorial System(tm) for Biomaterials
Manuscript Draft

Manuscript Number: jbmt24366

Title: Dynamic tracking of expression of neuronal markers in living human neurons detected using molecular beacons

Article Type: FLA Original Research

Section/Category: Biomaterials at the Nanoscale for Diagnostic Systems (BND)

Keywords: Molecular beacons; Transfection diffusion model; Gene expression; Imaging

Corresponding Author: Mrs Mirolyuba Ilieva,

Corresponding Author's Institution: DTU

First Author: Mirolyuba Ilieva

Order of Authors: Mirolyuba Ilieva; Paolo Della Vedova; Ole Hansen, Professor; Martin Dufva, Associate Professor

Abstract: Monitoring gene expression is an important tool for elucidating mechanisms of cellular signaling, especially when gene expression is followed in real time in living cells. In order to monitor gene expression during nerve cell development, molecular beacon (MB) probes targeting markers representing different stages of neuronal differentiation were designed and synthesized as 2'-O-methyl RNA backbone oligonucleotides. MBs targeted against GAPDH mRNA were designed and used as a positive control. MBs were transfected into human mesencephalic cells (LUHMES) using streptolysin-O-based membrane permeabilization. Mathematical modeling and simulations predicted that approximately 56000 MB copies were transfected into each cell over a few seconds. Gene expression was detected at different time points using fluorescence microscopy. Nestin and NeuN were expressed approximately 35% of LUHMES cells grown in growth medium, and in 80-90% of cells after differentiation. MAP2 and tyrosine hydroxylase mRNAs were expressed 48 and 72h post induction of differentiation. In contrast, GAPDH mRNA was detected in >95% of cells. The gene expression changes measured using MBs were confirmed using qRT-PCR. These results suggest that MBs are simple to use living cell sensors, and particularly useful for dynamically studying gene expression.

Dynamic tracking of expression of neuronal markers in living human neurons detected using molecular beacons

Mirolyuba Ilieva[1*], Paolo Della Vedova[1], Ole Hansen[1,2], Martin Dufva[1]

[1]*Department of Micro- and Nanotechnology, Technical University of Denmark,DTU Nanotech, Building 345E, DK-2800 Kgs. Lyngby, Denmark.*

[2]*CINF - Center for Individual Nanoparticle Functionality, Technical University of Denmark, DK-2800 Kgs. Lyngby, Denmark.*

*Corresponding Author: Mirolyuba Ilieva, Department of Micro- and Nanotechnology, Technical University of Denmark, Ørsteds Plads 345 Ø, building 344, 2860 Kgs. Lyngby, Tel. +45 45258159, Fax. +45 45 88 77 62, miil@nanotech.dtu.dk, www.nanotech.dtu.dk

Abstract

Monitoring gene expression is an important tool for elucidating mechanisms of cellular signaling, especially when gene expression is followed in real time in living cells. In order to monitor gene expression during nerve cell development, molecular beacon (MB) probes targeting markers representing different stages of neuronal differentiation were designed and synthesized as 2'-O-methyl RNA backbone oligonucleotides. MBs targeted against GAPDH mRNA were designed and used as a positive control. MBs were transfected into human mesencephalic cells (LUHMES) using streptolysin-O-based membrane permeabilization. Mathematical modeling and simulations predicted that approximately 56000 MB copies were transfected into each cell over a few seconds. Gene expression was detected at different time points using fluorescence microscopy. Nestin and NeuN were expressed approximately 35% of LUHMES cells grown in growth medium, and in 80-90% of cells after differentiation. MAP2 and tyrosine hydroxylase mRNAs were expressed 48 and 72h post induction of differentiation. In contrast, GAPDH mRNA was detected in >95% of cells. The gene expression changes measured using MBs were confirmed using qRT-PCR. These results suggest that MBs are simple to use living cell sensors, and particularly useful for dynamically studying gene expression.

Key words: Molecular beacons; Transfection diffusion model; Gene expression; Imaging;

Introduction

The ability to detect RNAs in individual live cells allows investigators to exactly pinpoint when a gene is turned on and off in response to a stimulus. Detecting and measuring gene expression has traditionally been limited to the use of technologies such as DNA microarrays, reverse-transcription polymerase chain reaction (RT-PCR), northern blotting, and fluorescence *in situ* hybridization (FISH), all of which examine gene expression in lysed or chemically-fixed cell populations. In contrast to these destructive methods, green fluorescent protein labeling (GFP) can be used to track gene expression in living cells. However, GFP and other similar reporter systems cannot measure endogenous mRNA expression in living cells, since a) the GFP gene must be fused to the promoter region of interest in order to function, b) GFP/promoter constructs might be integrated into the host genome or be transfected as plasmids, and c) the GFP gene product is not necessarily processed in the same way as the native gene in terms of transcription, maturation, or translation, which can lead to errors in measurement [1,2]. In practical experimental terms, GFP reporter systems require genetic modification of the cell and are time and labor consuming, and sometimes impossible to realize.

Molecular beacon technology was first described in 1996 by Tyagi & Kramer. Molecular beacons (MBs) are stem-loop forming oligonucleotides with a fluorochrome on one end, and a quencher on the other that recognize and report the presence of specific nucleic acids in homogeneous solutions

[3]. When a closed-state MB hybridizes to a specific nucleic acid target via a specific recognition sequence, the stem breaks and the MB unfolds into an open state. The fluorochrome is quenched in the closed, but not in the open state. Therefore, MBs are ideally suited to monitoring gene expression of specific genes inside living cells. However, to date, only a handful of reports describe the use of MBs for monitoring gene expression in living cells. Bratu et al. [4] used MBs to visualize the distribution and transport of oskar mRNA in Drosophila oocytes, while Santangelo *et al.* used MBs to analyze the distribution and transport of mRNA in intracellular organelles [5], and elegantly demonstrated that both mRNAs for GAPDH and K-Ras are localized in mitochondria. The combination of protein detection with antibodies and mRNA detection with MBs has been used to detect and isolate rare cancer stem cells from populations of normal cells, using fluorescence activated cell sorting (FACS) [6]. MBs targeted against the Oct4 mRNA transcription factor, which is highly expressed in embryonic and cancer stem cells, were introduced into mouse carcinoma cell line without affecting cell function; the fluorescent signal from Oct4 mRNA-targeting MBs provided clear discrimination between undifferentiated and retinoic acid-differentiated cells. Recently, MBs targeted against Sox2 mRNA were used as the sole discriminator to sort mouse embryonic and neural stem cells [7], and Sox2 mRNA-positive cells formed neurospheres more efficiently than Sox2 mRNA-negative cells. The clinical and diagnostic utility of MBs has been demonstrated in a feasibility study on bladder cancer [8], in which MBs were used to detect survivin mRNA, which is specifically expressed in bladder cancer cell lines. However, the MB-

based assay produced some false positive results, which compromised its immediate use for routine diagnosis. Further clinical diagnostic development is required.

MBs have also been used to monitor expression of two microRNAs (miR-26a and miR-206) during myogenesis [9]. This study used two MBs with different dyes and quenchers, allowing simultaneous visualization of both miRNAs during myogenesis. Real-time changes in β1-integrin expression in osteoblasts in response to surface modification were tracked with MBs over short periods of time; this study was particularly powerful since changes in mRNA localization were visualized in the same live cells [10]. Finally, MBs were used to monitor the temporal gene expression of osteogenic markers, including alkaline phosphatase, type I collagen and osteocalcin during differentiation of adipose-derived stem cells [11].

Despite this broad range of uses of MBs inside living cells, the routine application of MBs in cell research, especially in dynamic studies of gene expression, still appears to be a challenge for many investigators. The aim of this work was to demonstrate the utility of MBs for studying molecular events inside living cells, particularly to detect and dynamically trace changes in gene expression during differentiation of stem cells into neural lineage. We describe the design and use of MBs towards GAPDH, NeuN, MAP, nestin, and tyrosine hydroxylase (TH) mRNAs to track neural stem cell progression from neuronal progenitors, via mature neurons, into highly specialized dopaminergic neurons. Time lapse imaging of growing and differentiating cells allowed us to

determine the differentiation status of each cell in the population throughout a seven-day experiment.

Materials and methods

Cell culture and media

LUHMES (Lund human mesencephalic cell line, ATCC, CRL-2927) are a subclone of the tetracycline-controlled, v-myc-overexpressing human mesencephalic-derived cell line MESC2.10 immortalized with a LINX v-myc retroviral vector, as described by Lotharius et al. [12], but which possess robust dopaminergic characteristics [13]. Undifferentiated cells were cultured and expanded in cell culture flasks pre-coated with Geltrex®, which is a reduced growth factor basement membrane extract purified from murine Engelbreth-Holm-Swarm tumor (Invitrogen). The flasks were coated by incubating for 1 h at 37°C with Geltrex® diluted 1:100 in phosphate buffered saline (PBS). Cultures were maintained in growth medium (GM), consisting of advanced DMEM/F12 (Sigma), 1x N2 supplement (Gibco), 2 mM L-glutamine, 1% penicillin/streptomycin, and 40 ng/ml recombinant basic fibroblast growth factor (bFGF; Invitrogen). Cells were maintained at 37°C in a humidified atmosphere with 5% CO_2.

HeLa Tet-On® Advanced cells (631155, Clontech) were cultured in DMEM/F12 supplemented with 10% fetal bovine serum (FBS), penicillin 100 U/ml and streptomycin 100 µg/ml.

Differentiation of LUHMES

The differentiation process was initiated by adding differentiation medium (DM) consisting of advanced DMEM/F12, 1x N2 supplement, 2 mM L-glutamine, 1 mM dbcAMP (Sigma), 1 µg/ml tetracycline (Sigma), and 2 ng/ml recombinant human glial cell-derived neurotrophic factor (GDNF; R&D Systems).

Design of molecular beacons

mRNA-targeting MBs were designed using Beacon Designer 7.9 (Premier Biosoft). The target sequence for each MB was analyzed using Human Genome BLAST (http://blast.ncbi.nlm.nih.gov/Blast.cgi) to minimize the risk of non-specific binding to unrelated mRNA. The program was used to avoid cross homology, repeats, and low complexity regions based on expect (E)-value and percentage identity. The E-value is the number of hits expected with similar or better score, and it depicts the significance of the match (an E-value of 0 indicates complete homology). Regions with E-value greater than the target value were avoided. Percentage identity is the percentage of identical bases between query and subject sequence in an alignment. A percentage identity of 100 indicates complete homology. The regions with percentage identity

greater than the percentage identity criterion (default = 98 for the human genome) were avoided. Regions not satisfying both the E-value and the percentage identity criteria were avoided.

It is important to design the MB in an area of the target with minimal secondary structure formation. This helps prevent the template from preferentially annealing to itself faster than to the MB. The program identified and avoided template sequence predicted to give rise to significant secondary structures.

The parameters for MB design were set to ensure that the search succeeded in finding the best possible sequence. The length of the MBs was between 18 and 30 bp. The melting temperature (T_m) values of the probes were calculated using the nearest neighbor thermodynamic calculation with Santa Lucia values [14]. The parameters were set as follows: hairpin maximum d*G* (the free energy of the most stable alternate hairpin that is acceptable) 4 -kcal/mol; self-dimer maximum d*G* (the free energy of the most stable self-dimer that is acceptable) 7 -kcal/mol; cross-dimer maximum d*G* (the free energy of the most stable cross-dimer that is acceptable in a multiplex reaction) 7 -kcal/mol; run/repeat maximum five bp/dinucleotide probes with single (e.g. AAAAA) runs or dinucleotide (e.g. ATATATATAT) repeats of length greater than the specified value were discarded. After selecting a probe sequence, two complementary arm sequences were added, one on each side of the probe sequence. The stem region of the MBs was five bp long, with a CG content of 80%.

All calculations performed with this program used the following conditions: temperature for beacon free energy calculation 55°C, monovalent ion concentration 100 mM, free Mg^{2+} concentration 3 mM, and target concentration 250 nM.

In Beacon Designer the search algorithm calculates all the properties of every possible probe within the allowed length and positional boundaries, and rates them. This rating determines how well the designed oligonucleotide meets the search parameters relative to the tolerance limits specified for each parameter. The parameters used in the rating are maximum hairpin d*G*, maximum self-dimer d*G*, maximum run/repeat length, and maximum cross-dimer d*G* and T_m; if all parameters are exactly on target, the rating is 100. The rating of the probe depends on two factors: how close the probe is to the target value of each parameter, and how tightly the tolerances (permissible value of variation acceptable by the program from a pre-set standard value) are specified. Highly rated probes have most or all parameters near their ideal values, and are very likely to work well. For the MB probe search the quality of the designed probe is displayed as 'best' (rating greater or equal to 75), 'good' (rating between 74 and 50), 'poor' (rating below 50), or 'not found'. Only MBs with a 'best' rating were chosen for synthesis and further evaluation.

MBs were synthesized with an 2'-O-methyl RNA backbone, Cy3 molecule attached to the 5'-end, and black hole quencher 2 (BHQ-2) attached to the 3'-end (Eurofins MWG Operon). The sequences of the MBs used in the study are listed in Table 1. MBs were diluted in RNase/DNase free dH_2O to yield stock concentrations of 100 µM, and stored at -20°C.

Toxin-based membrane permeabilization

MBs were introduced into the cytoplasm of living cells using toxin-based membrane permeabilization using streptolysin-O (SLO, Sigma), which is a bacterial exotoxin that reversibly forms pores in the cell surface [15]. SLO at a concentration 1 µg/ml was activated with the reducing agent tris(2-carboxyethyl)phosphine hydrochloride solution (TCEP, Sigma), at a final concentration 5 mM for at least 30 min at 37°C. Cells were washed with Dulbecco's PBS (DPBS) without Ca^{2+} and Mg^{2+}, trypsinized for 3 min at 37°C, and collected by centrifugation for 5 min at 190 x g. The activated SLO was diluted in serum free medium (Opti-MEM) to concentrations between 1 and 800 ng/ml, and mixed with MB (2 µM final concentration). Cells ($1x10^5$) were incubated with the SLO/MB mixture in a final volume of 100 µl for approximately 15 min. Afterwards, the permeabilized cells were resealed by washing in DPBS containing Ca^{2+} and Mg^{2+}, and plated in 12-well plates precoated with Geltrex® and containing GM. The differentiation process was started 24 h after plating by exchanging GM for DM.

HeLa cells were transfected as a monolayer with 230 ng/ml (17 U/ml) activated SLO. Cells ($1x10^5$) were washed three times with pre-warmed DPBS and incubated with toxin and MB (2 µM final concentration) in 200 µl Opti-MEM for 15 min. Cells were washed three times with DPBS containing Ca^{2+} and Mg^{2+} and complete growth medium was added.

Detection of cellular viability

Cellular viability was detected using calcein-propidium iodide staining. Medium from each well was carefully removed and cells were incubated for 30 min with 3 µM calcein AM (live cell dye) and 2.5 µM propidium iodide (dead cell dye) diluted in warm 1x DPBS without Ca^{2+} and Mg^{2+}.

Imaging and image analysis

Phase contrast and fluorescent images were acquired using a Carl Zeiss Axio Vision 4.8.2 equipped with ApoTome Imaging system, 40x/0.75 Plan-Neofluar objective, HBO lamp, and a Zeiss Axiocam MRm B/W camera. The same exposure time and filter set (43 HE Ds Red 538-570 nm) were used for all experiments. Single-cell image analysis was performed using ImageJ software (http://rsb.info.nih.gov/ij/). A region of interest (ROI) was drawn around the cells and the total fluorescent intensity (FI) measured. The background fluorescence was detected by drawing a ROI in an area outside the cell of interest, and the total FI measured. In ImageJ, the total fluorescence intensity is reported as integrated density (ID), which is the sum of the values of the pixels in the selection. The background measurement of FI was subtracted from the cellular measurement [15]. Cells expressing the gene of interest were calculated as the number of cells with positive fluorescent signal emitted from each specific MB per 100 counted cells.

Quantitative polymerase chain reaction

Total RNA was isolated from cultured cells using the RNeasy Mini Kit (Qiagen). Cells were lysed directly on the dish. The lysates were collected and purified according to the manufacturer's instructions. Single-stranded cDNA was prepared from total RNA using random RT primers under standard conditions using MultiScribe Reverse Transcriptase (Applied Biosystems). The cDNA from each sample was diluted and used for real-time PCR analysis for quantification of neuronal marker expression. TaqMan assays (Invitrogen) for target genes were used as follows: GAPDH (ID Hs03929097_g1), nestin (ID Hs00707120_s1), MAP2 (ID Hs00258900_m1), NeuN (RBFOX3 ID Hs01370653_m1), and TH (ID Hs00165941_m1). PCR amplifications were performed in duplicate using the Chromo4 Real-Time Detection system (BioRad) at 95°C for 10 s, followed by 40 cycles of 95°C for 5 s and 60°C for 30 s. To quantify the relative expression of each gene, the C_t (threshold cycle) values were normalized to the C_t value of GAPDH (e.g. $\Delta C_t = C_t(\text{target}) - C_t(\text{GAPDH})$). All experiments included negative controls containing no cDNA template.

Statistical analysis

Results are expressed as mean ± standard error of the mean (SEM). qPCR was analyzed using a Student's t-test (n=5). Analyses were performed using Graph Pad Prism v.6 (GraphPad Software Inc., CA, USA).

Results

Introduction of MBs into cells

Cell viability and transfection efficiency were investigated as a function of SLO concentration ranging from 1 ng/ml (corresponding to 0.07 U/ml) to 800 ng/ml (corresponding to 59.7 U/ml). Transfection efficiency was evaluated using a MB targeting GAPDH mRNA. Cell viability was evaluated using calcein/propidium iodide staining. An SLO concentration of 17 U/ml (230 ng/ml) was determined to be the optimal concentration, with 75% of the cells showing signal from MB targeting GAPDH 24 h post-transfection, and >95% cell viability (Figure 1A). However, GAPDH expression was detected as early as 1 h post transfection (earliest time point investigated) suggesting that hybridization to target is a rapid process. Moreover, cells showed no defects in growth or differentiation and they exhibited the same morphology as non-transfected cells (untransfected cells are shown in Figure 1B, and transfect cells are shown in the brightfield images in Figure 5). An SLO concentration of 17 U/ml (230 ng/ml) was therefore used in further experiments.

The transport of MBs into cells during transfection is a diffusion process, whereby the MBs diffuse through open pores in the cell membrane. In order to estimate the number of MBs that are effectively transfected into the cells, two simplified diffusion models were used. The cells were assumed to be spherical with a radius $a = 5$ μm, a cell membrane $x_m = 10$ nm thick, and in the membrane $N_p \simeq 600$ pores (2 pores per μm^2) with a pore radius of $a_p = 15$ nm open during transfection [16]. MBs were modeled as solid spheres with a radius of $a_b = 2.5$ nm, and a concentration $C_0 = 2$ μM was used in a medium with a viscosity $\eta = 0.85 \times 10^{-3}$ Pa s at 300 K; the

viscosity of the cell interior was assumed to be identical.

Diffusion problems in dilute systems are governed by Fick's first and second laws, as shown in equations (1) and (2), respectively:

$$\boldsymbol{J} = -D\nabla \mathrm{C}, \tag{1}$$

where C is the concentration, $\boldsymbol{J}$ is the diffusion flux density, and D the diffusivity. Fick's second law is a conservation law:

$$\frac{\partial C}{\partial t} = -\nabla \cdot J \simeq D\nabla^2 C, \tag{2}$$

where *t* is time. The approximation is valid if the diffusivity is constant. The diffusivity of the MBs may be estimated using the Stokes-Einstein equation:

$$D = \frac{k_{\mathrm{B}} T}{6\pi\eta a_b}, \tag{3}$$

where η is the viscosity of the medium, k_{B} is Boltzmann's constant, and T the absolute temperature.

A direct evaluation at 300 K yields a diffusivity of $D = 100\ \mu m^2 s^{-1}$ that agrees well with values in the literature [17].

The real diffusion problem is a complicated 3D problem; however, the different length scales involved in the problem suggest that approximations can be made. Using typical diffusion times of $t_d = \lambda^2/(2D)$, where λ is the characteristic length scale, results in diffusion times for the pore regions that are five orders of magnitude lower than the diffusion times relevant to the cell scale, and therefore a quasi steady-state approximation may be applied to the pore regions. Furthermore, the pores are so far apart that they hardly interact during the diffusion process. As a result, we can estimate the diffusion flux through a single pore by the net flux I that results from: 1) the quasi steady-state diffusion to a disc of radius $a_p - a_b$ (to compensate for the finite size of the MBs), 2) the steady state diffusion through a tube of radius $a_p - a_b$ and length x_m, and 3) the quasi steady-state diffusion from a disc of radius $a_p - a_b$ to the cell interior. The fluxes 1) and 3) are given by $I_{1,3} = 4(a_p - a_b)D\Delta C_{1,3}$, where $\Delta C_{1,3}$ is the concentration difference that drives the flux [18]. The flux 2) is $I_2 = \left[\pi(a_p - a_b)^2/x_m\right]D\Delta C_2$, where the symbols are the same as above. The three fluxes are identical and the sum of concentration differences is $\Delta C_1 + \Delta C_2 + \Delta C_3 = C_0 - C_c$, where C_c is the concentration inside the cell, which is considered approximately uniform. As a result, the flux through a single pore is:

$$I_p = \left(\frac{2}{4(a_p-a_b)D} + \frac{x_m}{\pi(a_p-a_b)^2 D}\right)^{-1}(C_0 - C_c), \tag{4}$$

and the total flux through all pores is N_p times larger. Integrating Fick's second law, equation (2) over the volume $V = \frac{4}{3}\pi a^3$ of the cell yields:

$$\frac{\partial C_c}{\partial t} = \frac{N_p I_p}{V} = \frac{3DN_p(a_p-a_b)^2}{2a^3[\pi(a_p-a_b)+2x_m]}(C_0 - C_c) \equiv \frac{C_0-C_c}{\tau_c}, \tag{5}$$

where τ_c is the time constant relevant for the transfection

$$\tau_c = \frac{2a^3[\pi(a_p-a_b)+2x_m]}{3DN_p(a_p-a_b)^2}. \tag{6}$$

With the parameters given, the resulting time constant is $\tau_c \simeq 0.53$ s. The solution to equation (4) is obtained by

$$C_c = C_0\left(1 - \exp\frac{-t}{\tau_c}\right), \tag{7}$$

and within a few time constants (a few seconds) the concentration of MBs saturates at C_0.

In an alternative approach, we may use a mean field approximation and calculate an effective diffusivity D_e of MBs in the porous membrane [19]:

$$D_e = D\,\frac{\varepsilon(1-\delta)}{\tau}, \tag{8}$$

where ε is the porosity (i.e. the ratio of total pore volume to total membrane volume), δ is the constrictivity (i.e. the ratio of the radius of the diffusing particle to the pore radius), and τ is the tortuosity, which corrects for the curvature of the pores. Since the pores are short and straight we take $\tau = 1$, and then the effective diffusivity is estimated as $D_e \simeq 0.12\ \mu m^2 s^{-1}$, approximately three orders of magnitude smaller than the diffusivity in the free fluid. With this model, the time constant may be estimated from

$$\tau_{c2} = \frac{V}{4\pi a^2}\frac{x_m}{D_e} = \frac{a x_m}{3 D_e}, \tag{9}$$

and a numerical value of $\tau_{c2} \simeq 0.14\ s$ is estimated, which is lower than the first estimate, which we regard as more reliable. At such low porosity, the mean field approximation may not be sufficiently accurate since the effects of diffusion to and from the pores are excluded from the model, and in the first model these effects are seen to be dominant; this is the cause for a difference by a factor of three in magnitude of the two time constants. In both cases, the transfection is completed within a few seconds, well in advance of the closing of the pores after 15 min of transfection, and the concentration reaches the final value of $C_0 = 2\ \mu M$.

We also performed a Finite Element Model (FEM) simulation using COMSOL 4.2 (http://www.comsol.com) to verify the first diffusion model, with Figure 2 showing the simulated average concentration of MBs inside the cell as a function of transfection time. In the FEM model, a cone segment of the spherical cell with exactly one pore was used to represent a $1/N_p$ fraction of the cell volume. The cone region was extended far into the free fluid volume in order to also represent a $1/N_p$ fraction of that. Figure 2 also illustrates the results of the analytical model using the calculated time constant of $\tau_{c2} \simeq 0.53\,\mathrm{s}$ as the solid line; the agreement between the FEM simulation and the analytic model is almost perfect.

Given the cell size and the MB concentration, the number of MBs in the cell becomes approximately 56000 if the cell volume is corrected for the volume of the nucleus (approximately 10%), where MBs do not penetrate. Bustin [20] found that there are about 10^8 mRNA copies of GAPDH per microgram of total RNA. Assuming that there is about 4 pg total RNA per cell, there would be about 400 GAPDH mRNA copies per cell, indicating that there is about 100-fold more MB than possible target.

Direct experimental verification of the diffusion model by tracking the fluorescence during transfection is difficult due to the high background from MBs in the medium. Therefore we instead tracked the decay of fluorescence from cells loaded with MBs after a second treatment with SLO to re-open pores and thus allow out-diffusion of MBs from the loaded cells to an initially MB free

medium. The adherent cell line HeLa was transfected using the SLO protocol (material and methods) with MB towards TH, but without a quencher attached. The pores were closed and cells were washed three times and incubated for 1 h to let cells recover while hybridization was not expected since TH is not expressed in this particular cell line. The cells were fluorescent as expected and had their normal morphology (data not shown) after transfection. At this point the cells were again treated with SLO reagent to re-open the pores and the fluorescent decay from the cells was monitored by time laps microscopy for 20 minutes. Figure 3 shows the fluorescence emission from a representative cell. After about 10 minutes, the fluorescence reached the base line level suggesting that all the transfected fluorescent MBs had diffused out of the cells. The resulting time constant (~200 s) however was much longer than that expected from the theoretical model. This suggests that other factors may dominate the transfection kinetics than diffusion of MBs over the membrane or that the parameters (number of pores and pore size) used in the diffusion model are incorrect.

Gene expression of neuronal markers detected by MBs

MBs targeted against mRNAs specific for neural progenitors (nestin), mature neurons (NeuN and MAP2), and highly specialized dopamine neurons (TH) were delivered into embryonic midbrain neurons (LUHMES). MBs targeting GAPDH were used as a control. Cells were left to attach to culture plates for 24 h after transfection in GM supplemented with bFGF. 24 h after transfection, the

differentiation process was induced by switching GM to DM containing dbcAMP, tetracycline, and GDNF. The measurement of fluorescence was commenced 24 h after transfection, and images were taken every 24 h for 192 h. The patterns of fluorescence signal emitted from cells varied (Figure 4), and included small dotted signals (Figure 4 A1 and B1), more compact punctate signals (Figure 4 A2 and B2), or widespread cytoplasmic cluster-like fluorescence (Figure 4 A3 and B3). The last pattern was more often observed in differentiated cells, due to the compact cell body and tight perinuclear cytoplasmic organization. Non-differentiated cells showed signals in the lamellipodia and cell body space (Figure 4 A2), while differentiated cells showed only cell body-localized MB signals (Figure 5). All signal categories were included in the analysis when the calculating percentage of positive cells (see below). Large bright signals were interpreted as false positives, being emitted from morphologically dead cells (Figure 4 C). These false positive signals were excluded from the analysis.

Figure 5 shows images of the signals emitted from MBs taken 24 h post-transfection, and 168 h after induction of differentiation. GAPDH MBs were used as transfection control, and approximately 75% of cells were positive 24 h post-transfection. Nestin, an intermediate filament protein expressed in dividing cells during the early stages of development of the CNS, and nuclear protein antigen (NeuN), were also detected 24 h after transfection in about 40% of cells (Figure 5 and Figure 6). In contrast, no MAP2 and TH expression was detected in cells 24 h post induction of

differentiation (Figures 5 and 6). Expression of MAP2 was present in 30% of cells 48 h post induction of differentiation (Figure 6), while the first TH-positive cells appeared 72 h post induction (Figure 6). The number of cells positively expressing neuronal markers reached their maximum at different time points as follows: 85% nestin and NeuN-positive cells 120 h post induction, 85% MAP2-positive cells 144 h post induction, and 70% TH-positive cells 192 h post induction.

The intensity of the nestin-MB signal increased about two-fold compared to point-of-induction levels. The maximum increase in nestin-MB signal was observed 120 h post induction. A slight decrease in the signal was detected 192 h after induction. The signal intensity changes observed for NeuN-MB were similar. However, the maximal signal of NeuN was observed 168 h post induction (Figure 7). In contrast, no signal was recorded for MAP2-MB and TH-MB 24 h post induction. The MAP2-MB signal plateaued 120 h post induction, while TH-MB signal plateaued 72-96 h post induction. MAP2-MB signal intensity decreased slightly 192 h post induction, while TH levels remained constant.

Correlation between qRT-PCR and MB signal intensities

To corroborate the results using different MBs, qRT-PCR was used to measure the respective mRNA expression before and 168 h after differentiation. GAPDH was used as an internal positive

control. Expression of nestin and NeuN was detected in non-differentiated cells, and it significantly increased after seven days of differentiation (Figure 8). In contrast, expression of the neuronal markers MAP2 and TH was not detected in non-differentiated cells, but was later expressed, corroborating the accuracy of the measurements made using MBs (Figures 5, 6, and 7).

Discussion

Since MBs were first described, their multiple applications in detecting gene expression by targeting RNA inside living cells have only been exploited in a limited number of studies. Here we described the use of a panel of MBs targeting molecular markers specific for the progressive stages of neuronal differentiation, and demonstrate that MBs can be used as a routine gene expression assay, as well as a reporter gene technology.

The design of MBs requires careful consideration, in particular with regards to target specificity. Our results suggest that the detected signals are specific, since signal from MBs targeting different markers during differentiation following the correct biological sequence. The expression of the housekeeping gene GAPDH (constant expression), the progenitor marker nestin (expressed during the early stages of differentiation of neuronal progenitors), and the neuronal nuclear antigen NeuN were all detected. The total number of positive cells for each marker differed, as expected. Thus, the number of GAPDH positive cells was twice the number of cells positive for the neuronal

markers. Following differentiation, signal from the mature neuron marker MAP2 was detectable. Finally, TH expression was detected 72 h after differentiation was induced, as described by Scholz et al [21]. All these findings were corroborated by qRT-PCR.

In contrast to hybridization in solution where the physicochemical conditions are simplified, hybridization of MBs to mRNA in living cells is complicated by the formation of secondary structures in mRNA molecules, RNA-binding proteins, and the degradation of the probes due to enzymes with nuclease activity [22]. If the target sequence has a double-stranded structure MBs compete with RNA strands, while when the target is a binding site for proteins, MBs compete with RNA-binding proteins in order to hybridize. These factors could make target sequence inaccessible to MBs in spite of unique probe sequence design. Software programs such as mFOLD and Beacon Designer can predict the formation of secondary structures so that these sequences can be avoided during the selection of probes in the design process. The prediction of protein binding sites in the target is more complicated due to only limited data existing for RNA-binding proteins [22]. Competition with RNA or RNA-binding proteins can result in a significant decrease in signal level due to inefficient hybridization between the MB and the target sequence. To overcome this, many studies have used 2'-O-methyl RNA MBs in order to increase affinity for the target mRNA [23]; in addition, a modified backbone is less vulnerable to nuclease activity. On the other hand, the formation of double-stranded RNA can lead to RNA silencing, and therefore influence cellular

function. In this study, MBs with 2'-O-methyl backbones were tested. Probe-target hybridization did not have any measurable effect on cell physiology including gene expression, self-renewal, or differentiation. Other authors [10,11] have successfully used non-modified MBs in their living cell studies, although over a shorter length of time. This suggests that it is a matter of choice for individual researchers to use either 2'-deoxy or 2'-O-methyl modified bases in the design of their MBs, although modified backbone MBs may be more appropriate in studies tracking gene expression over prolonged periods of time.

False positive signals due to MB-protein interaction and degradation are a further limitation that reduces the usability of MBs in live cell imaging applications. Chen et al. [24] observed that MBs with non-modified backbones incubated with phosphodiesterase I and II show a small increase in fluorescence. They concluded that the fluorochrome and quencher conjugated on each end of MBs limit exonuclease activity. However, MBs are highly sensitive to degradation by S1 endonucleases, and Mung Bean endonucleases that cleave the hairpin loops. Single-strand binding (SSB) proteins also cause significant increases in fluorescence. Although SSB proteins and nucleases are present in the cell cytoplasm, previous studies have shown that there are fewer DNA-protein interactions in the cytoplasm compared to the nucleus, and that the nuclease activity is in fact low [24]. MBs remain in their quenched hairpin conformation when localization is limited to the cytoplasmic compartment. Our data show signal retained in the cytoplasm with perinuclear localization, but not

within nucleus (Figure 4). This pattern of expression and the appearance of signal at different timepoints during development suggest that these do not represent false-positive signals, but are due to specific hybridization between MB and target sequence.

One limitation that needs to be considered could be the theoretical decrease in the MB signal through dilution during cell division, especially in rapidly dividing cells and for highly expressed genes. Differentiated neurons are out of cell cycle and decreases in signal intensity due to MB dilution are therefore not observed.

It is difficult to predict how many beacons penetrate each cell during transfection, and cell-to-cell variations in MB delivery might exist [11]. However, our COMSOL simulation demonstrates that a steady-state concentration is reached inside the cell after only a few seconds. After subtracting the volume of the nucleus, which is not pierced by MBs, the average cell is predicted to contain 56000 beacons. This suggests that a pool of MBs exists in the cell after transfection, and not all MBs are used up, especially in the case of genes with low expression. Therefore all mRNAs targeted by MBs should be saturated, and the signal intensity detected from individual cells in the same developmental stage should be relatively equal. We detected different signal patterns and intensities of the same MB between cells in the same stage of differentiation (Figure 4). This might be

explained not by variation in the number of penetrating MBs inside each cell, but by noise in gene expression, i.e. the variation in the number of copies of mRNA between cells due to the fundamentally stochastic nature of the biochemistry of gene expression. MB intensity was positively correlated with quantification of gene expression by qRT-PCR, supporting the conclusion that detection of gene expression using MBs accurately reflects cellular mRNA levels.

The diffusion model suggests that within seconds MBs are moving into opened cells while the measured data suggest that steady state levels is reached after 10 minutes. While the discrepancy does not have any practical impact on a 15 minute transfection procedure, it points to other factors than diffusion of MBs affecting the speed of transfection. Firstly, the model takes into account only the diffusion process, assuming that all the pores are already open from the start. It is known from literature [25,26] that the pore formation involves the binding of streptolysin O molecules in arc- or ring- shaped structures comprising about 50-80 subunits that progressively form on the cellular membrane and cause lysis. This process depends on the SLO to cell concentration ratio. Furthermore, pore forming times between 10 s and 300 s have been recorded. Secondly, the pores exhibit a size distribution and 30 nm is considered an upper limit for the diameter. Hence, an overall smaller pore size could be used in the model resulting in a lower permeability. Third, in the model the entire surface of the cells contains pores, while the adherent HeLa cells likely only had pores on cell surfaces facing the medium since it is likely that surfaces facing the bottom are inaccessible by

SLO reagent and by MBs. Finally, the number of fully developed pores may be lower than assumed in the model. By contrast, the LUHMES cells are transfected in solution phase which of natural reasons provides pore formation all around the cells but also shorter diffusion distances of SLO reagents to the cells suggesting that LUHMES cells are more rapidly transfected than HeLa cells. In conclusion, the theoretical model shows that diffusion process alone is not a limiting factor and other time constants may play an important role in the transfection procedure. Despite that, since the standard transfection procedure was 15 minutes and all the MBs diffuse out of a HeLa cell in 10 minutes (figure 3); it is likely that LUHMES cells have the same concentration of MB inside as the concentration added to the medium. Based on this reasoning, it is likely that the calculated number of about 56000 MBs inside LUHMES cells after transfection is correct.

One significant advantage of *in situ* methodologies is the ability to gather spatial data on biological phenomena of interest. In these experiments, each cell appears follow its own course during differentiation; some cells express the genes of interest very early, while the percentage of neuronal marker-expressing cells increases more rapidly during the later stages of neurogenesis. This suggests that there are different expression pattern and population-level heterogeneity during neuronal differentiation. In contrast to PCR-based assays, which collect data from the differentiating population as a whole, MBs accurately measure expression of genes of interest on a single cell level. MBs can be used to repeatedly assess gene expression in the same cell population over time, which is not possible using the destructive methods.

Commonly utilized transfection methods for oligonucleotide delivery, such as lipid and dendrimer-based delivery methods, have often failed to deliver MBs into cells. MB-transfection agent complexes do not always dissociate efficiently once internalized, leading to brightly fluorescing punctate aggregates that interfere with fluorescent measurements. Furthermore, MB-transfection agent complexes can often lead to entrapment and degradation of the probes within endosome/lysosome compartments, thus increasing background signal. The transfection efficiency of neurons is particularly limited [27], and indeed LUHMES represent a particularly challenging system, since they cannot be transfected using standard methods, such as with lipo- or nucleofection. One routinely used method for direct introduction of MBs into the cytoplasmic compartment of living cells is toxin-based membrane permeabilization using streptolysin-O (SLO), as used in this study. Although it has been successfully used to deliver MBs into a wide variety of cell types, including human dermal fibroblasts, stem cells, and cancer cells [15], SLO is not a popular method for neuronal transfection. Here we show that the SLO-membrane permeabilization delivery method is a rapid, efficient, and gentle method for the delivery of MBs into neurons. Cells viability was high and the transfection efficiency nearly 100%.

Despite all the disadvantages described, we show here that MBs are a powerful tool for the spatiotemporal detection of gene expression inside living cells. Measurements can be performed at

the single cell level, allowing for the study of changes in mRNA expression and localization in the same cell. In contrast to widely used GFP–reporter constructs, MBs represent a rapid method for targeting endogenous gene expression without genetic modifications.

Conclusions

We designed MBs targeting multiple factors in order to profile cells during neuronal differentiation, and optimized the method for delivering MBs to living neurons. Our simulations show that during transfection the concentration of MBs reach a steady state after few seconds and that we end up with 100-fold more MB than possible target. MBs offer significant advantages over traditional techniques because they allow for real-time imaging of individual cells and preserve spatial information. They overcome the need to lyse cells for qPCR, or fix cells for molecular imaging techniques such FISH. Time-consuming and technically challenging genetic manipulations are not required.

Acknowledgements

This work was supported by FTP grant 09-070568, and partly supported by The Danish National Research Foundation's Center for Individual Nanoparticle Functionality (DNRF54).

References

[1] Dobek GL., Zhang X, Balazs DA, Godbey WT. Analysis of promoters and expression-targeted gene therapy optimization based on doubling time and transfectability. The FASEB Journal 2011;25:3219-28.

[2] Lee JY, Colinas J, Wang JY, Mace D, Ohler U, Benfey P. Transcriptional and posttranscriptional regulation of transcription factor expression in Arabidopsis roots. PNAS 2006;103:6055–60.

[3] Tyagi S, Kramer FR. Molecular beacons: probes that fluoresce upon hybridization. Nat Biotechnol 1996;14:303-8.

[4] Bratu DP, Cha BJ, Mhlanga MM, Kramer FR, Tyagi S. Visualizing the distribution and transport of mRNAs in living cells. PNAS 2003;100:13308-13.

[5] Santangelo PJ, Nix B, Tsourkas A, Bao G. Dual FRET molecular beacons for mRNA detection in living cells. Nucleic Acids Res 2004;32:e57.

[6] Rhee WJ, Bao G. Simultaneous detection of mRNA and protein stem cell markers in live cells. BMC Biotechnology 2009;9:30.

[7] Larsson HM., Lee ST, Roccio M, Velluto D, Lutolf MP, Frey P, Hubbell JA. Sorting live stem cells based on Sox 2 mRNA expression. PLOS ONE 2012;7:e49874.

[8] Zhao J, Wang ZQ, Wang XY, Yang XJ, He D. Preliminary Study of diagnostic utility of molecular beacons in bladder cancer. Urology 2010;76:512.e8-512.e13.

[9] Kang WJ, Cho YL, Chae JR, Lee JD, Choi KJ, Kim S. Molecular beacon – based bioimaging of multiple microRNAs during myogenesis. Biomaterials 2011;32:1915-22.

[10] Lennon FE, Hermann CD, Olivares-Navarrete R, Rhee WJ, Schwartz Z, Bao G, Boyan BD. Use of molecular beacons to image effects of titanium surface microstructure on β1 integrin expression in live osteoblast-like cells. Biomaterials 2010;31:7640-47.

[11] Desai HV, Voruganti IS, Jayasuriya C, Chen Q, Darling EM. Live-cell, temporal gene expression analysis of osteogenic differentiation in adipose-derived stem cells. Tissue Engineering 2013;19:40-8.

[12] Lotharius J, Barg S, Wiekop P, Lundberg C, Raymon HK, Brundin P. Effect of mutant α-synuclein on dopamine homeostasis in a new human mesencephalic cell line. J Biol Chem 2002;277:38884-94.

[13] Lotharius J, Falsig J, van Beek J, Payne S, Dringen R, Brundin P, Leist M. Progressive degeneration of human mesencephalic neuron-derived cells triggered by dopamine-dependent oxidative stress is dependent on the mixed-lineage kinase pathway. J Neurosc 2005;25:6329-42.

[14] SantaLucia Jr. A unified view of polymer, dumbbell, and oligonucleotide DNA nearest-neighbor thermodynamics. PNAS 1998;95:1460-65.

[15] Chen A, Rhee W J, Bao G, Tsourkas A. Delivery of molecular beacons for live-cell imaging and analysis of RNA. RNA detection and visualization. In: Jefferey E. Gerst, editors. Methods and Protocols, Methods in Molecular Biology 2011;714:159-174.

[16] Keyel PA, Loultheva L, Roth R, Salter RD, Watkins SC, Yokoyama WM, Heuser J. Streptolysin O clearance through sequestration into blebs that bud passively from the plasma membrane. J Cell Sci 2011;124:2414-23.

[17] Lukacs GL, Haggie P, Seksek O, Lechardeur D, Freedman N, Verkman AS. Size-dependent DNA mobility in cytoplasm and nucleus. J Biol Chem 2000;275:1625-9.

[18] Carslaw HS, Jaeger JC. Conduction of heat in solids. In: London: Oxford University Press 2nd Ed. 1959. p. 215.

[19] Grathwohl P. Diffusion in natural porous media: Contaminant transport, sorption/desorption and dissolution kinetics. In: Kluwer Academic 1998. p. 29-34.

[20] Bustin SA. Absolute quantification of mRNA using real-time reverse transcription polymerase chain reaction assays. J Mol Endocrinol 2000;25:169–93.

[21] Scholz D, Pöltl D, Genewsky A, Weng M, Waldmann T, Shildknecht S, Leist M. Rapid, complete and large-scale generation of post-mitotic neurons from the human LUHMES cell line. J Neurochem 2011;119:957-71.

[22] Rhee WJ, Santangelo PJ, Jo H, Bao G. Target accessibility and signal specificity in live-cell detection of BMP-4 mRNA using molecular beacons. Nucleic Acids Res 2008;36:e30.

[23] Tsourkas A, Behlke MA, Bao G. Hybridization of 2'-O-methyl and 2'-deoxy molecular beacons to RNA and DNA targets. Nucleic Acids Res 2002;30:5168-74.

[24] Chen AK, Behlke MA, Tsourkas A. Avoiding false-positive signals with nuclease-vulnerable molecular beacons in single living cells. Nucleic Acids Res 2007;35:e105.

[25] Niedermeyer W. Interaction of streptolysin-O with biomembranes: kinetic and morphological studies on erythrocyte membranes. Toxicon 1985;23:425–39.

[26] Palmer M. et al. Streptolysin O: A Proposed Model of Allosteric Interaction between a Pore-Forming Protein and Its Target Lipid Bilayer. Biochemistry 1998;37:2378–2383.

[27] Karra D, Dahm R. Transfection techniques for neuronal cells. J Neurosci 2010;30:6171-7.

Figure legends

Figure 1. (A) Cells treated with 17 U/ml SLO and stained with calcein/PI for detection of cell viability after toxin-based membrane permeabilization. Live cells are stained in green, dead cells are stained in red. (B) Morphology of non-transfected LUHMES on Geltrex® in GM (left) and DM (right).

Figure 2. The average concentration of MBs in the cell as a function of transfection time. Results from a COMSOL FEM model (dots) are compared to the analytical model (black line) with the time constant .

Figure 3. Fluorescence emission decay as a function of time for a representative HeLa cell after the second treatment with SLO. The resulting time constant is .

Figure 4. Different MB signal patterns observed in LUHMES cells grown in GM 24 h after transfection (A) and 168 h post differentiation (B). A1, B1 - dotted signals; A2, B2 - compact punctate shape; A3, B3 - cluster-like fluorescence. (C) C1 - Big bright fluorescent clusters originating from apoptotic cells (artifact). This pattern of signal was excluded from calculations of

the number of positive cells and signal intensity. C2 - Morphology of apoptotic cell with blebbing. The signal shown is using GAPDH-MBs.

Figure 5. Signals from molecular beacons targeting housekeeping gene expression of GAPDH, intermediate filament protein, and markers for neuronal progenitors (nestin), microtubule-associated protein 2 (MAP2), neuronal nuclear antigen (NeuN), and tyrosine hydroxylase (TH). Cells were SLO transfected and seeded in growth medium (GM), containing 40 ng/ml bFGF. The differentiation process was started 24 h later culturing in differentiation medium (DM) supplemented with dbcAMP, tetracycline, and GDNF.

Figure 6. Percentage of cells expressing the neuronal markers nestin, MAP2, NeuN, and TH. Results are presented as mean ± standard error of the mean (SEM).

Figure 7. Integrated density of MBs targeting the neuronal markers. Data are displayed as mean ± standard error of the mean.

Figure 8. Analysis of mRNA expression levels of neuronal markers using qRT-PCR in non-differentiated and dopamine-like differentiated LUHMES. Expression was normalized to GAPDH mRNA expression. Data are expressed as mean ± SEM. **P<0.01, ***P<0.001.

Molecular beacon	Sequence	GenBank numbers
GAPDH	CGCUC AGUUGGUGGUGCAGGAGG GAGCG	NM_002046.3
Nestin	CGCUCUCUCACUACCUCCACAUCCUUGAGCG	NM_006617
NeuN	CGCUC UCCCAUUCAGCUUCUCCCG GAGCG	NM_001082575.1
MAP	CGCUCGUUGUCUCUGGCUGAGAAACUAA GAGCG	NM_002374.3
TH	CGCUCACACCUUCACAGCUCGGGA GAGCG	NM_199292.2

*Stem sequence is underlined

Table 1: The molecular beacon sequences used within this study

Figure_1.tiff
Click here to download high resolution image

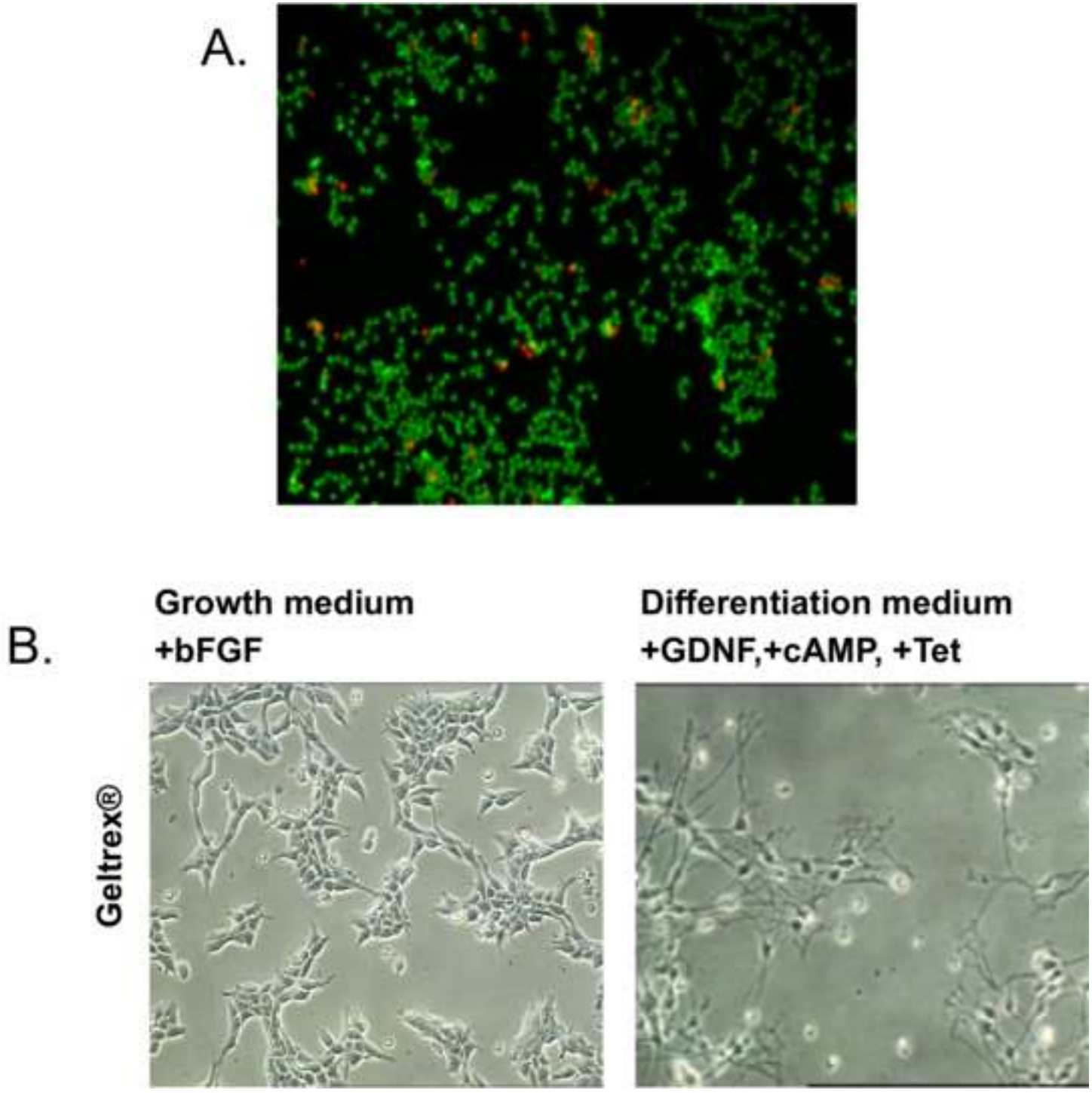

Figure_2.tiff
Click here to download high resolution image

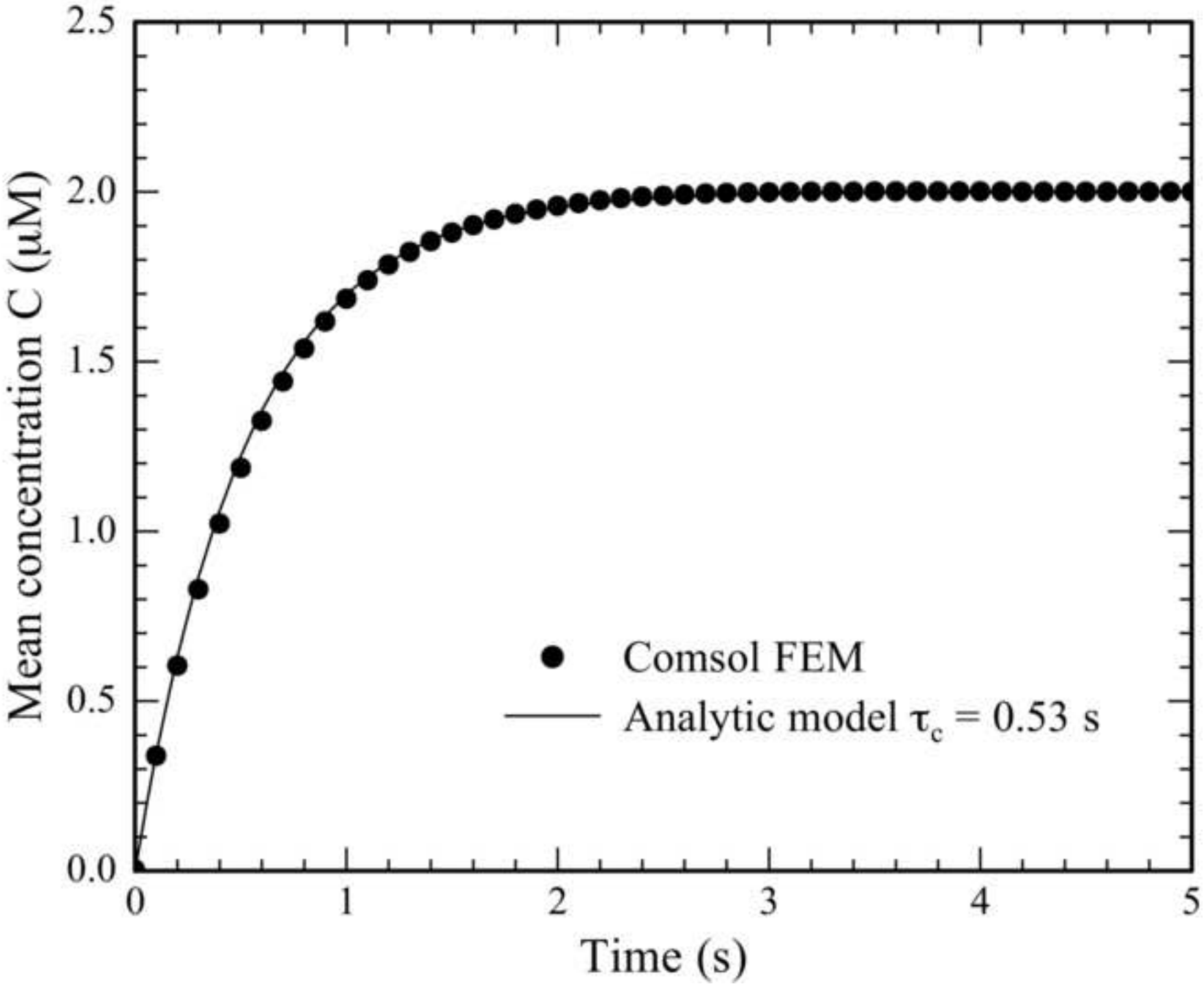

Figure_3.tif
Click here to download high resolution image

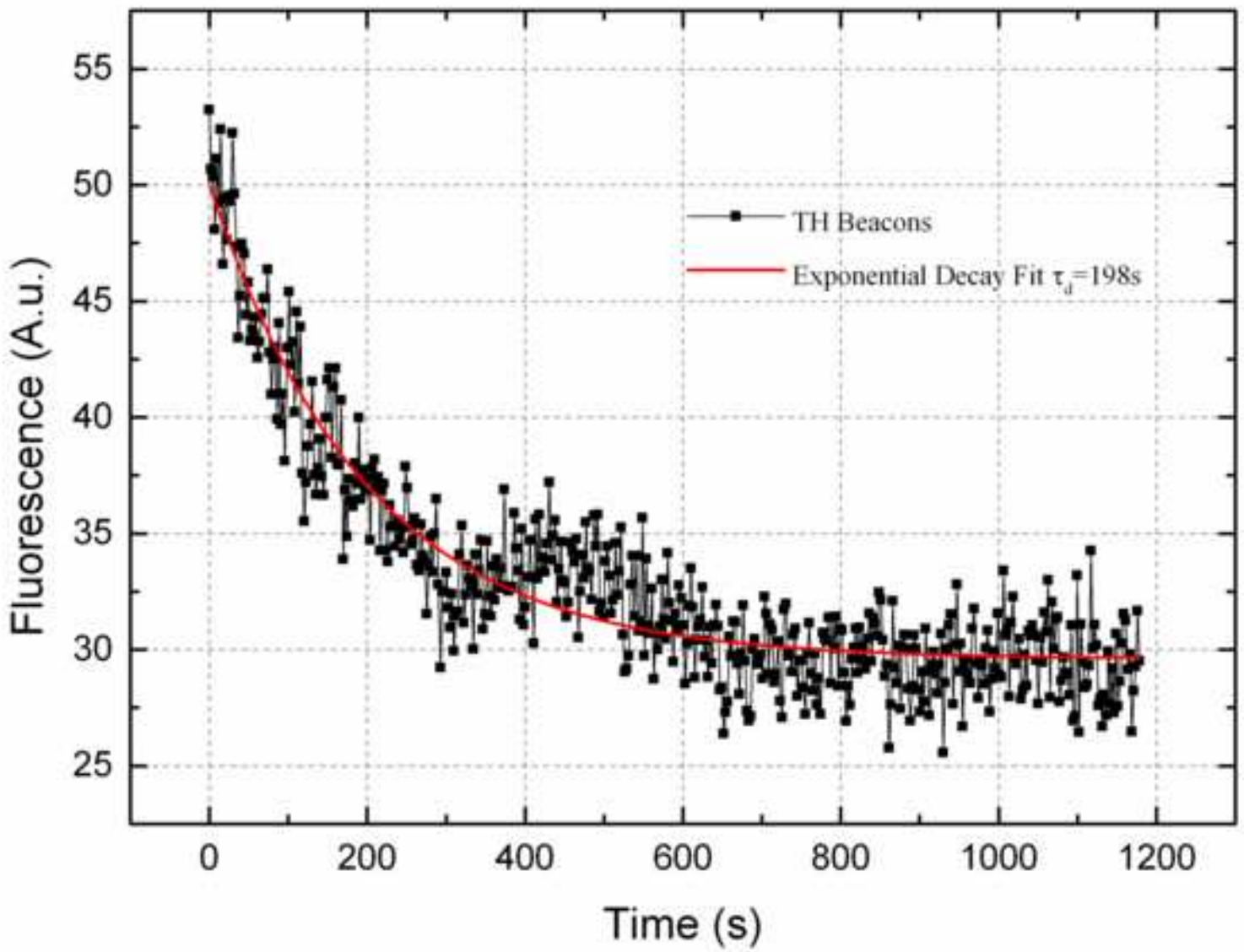

Figure_4.tiff
Click here to download high resolution image

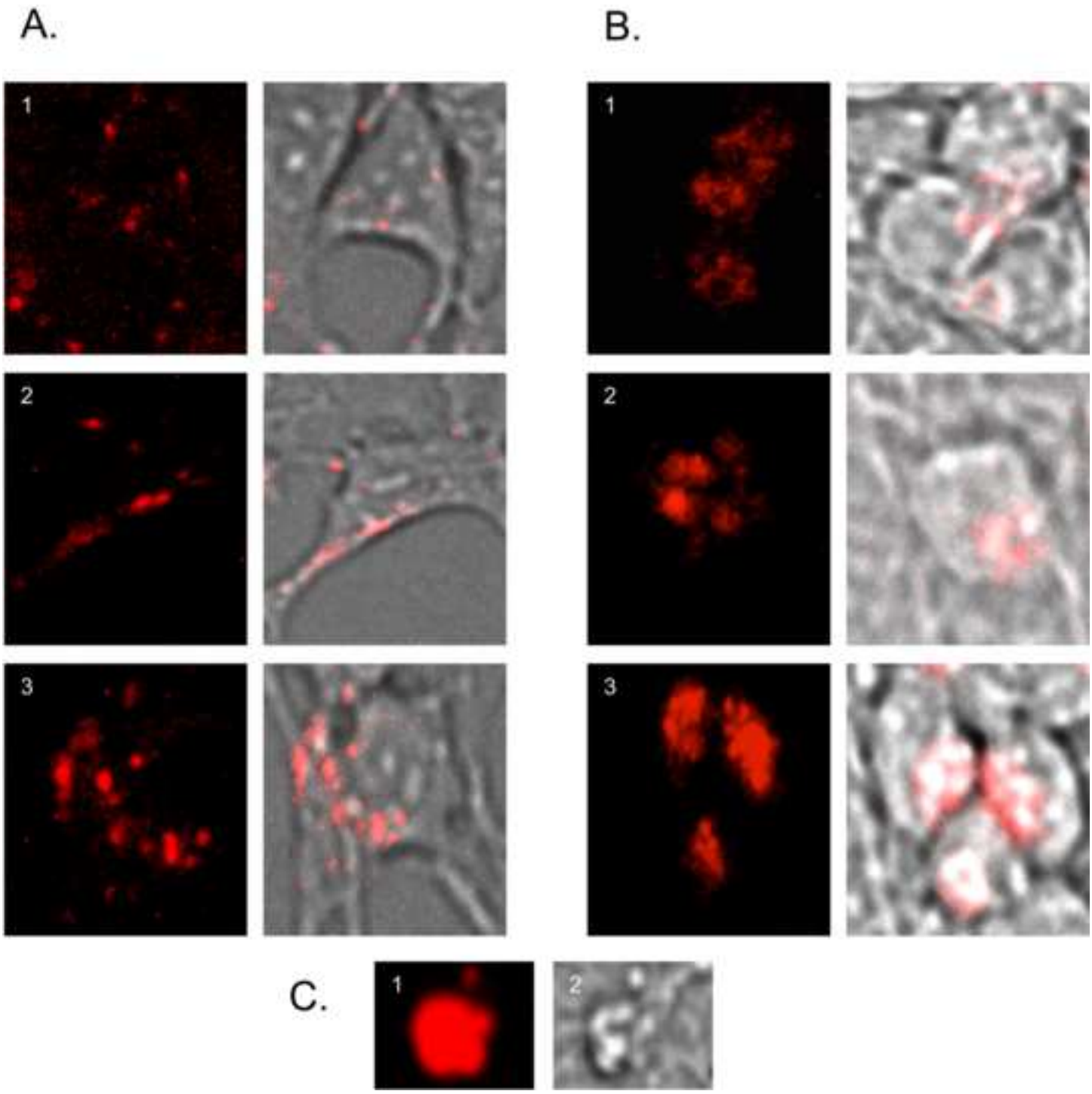

Figure_5.tiff
Click here to download high resolution image

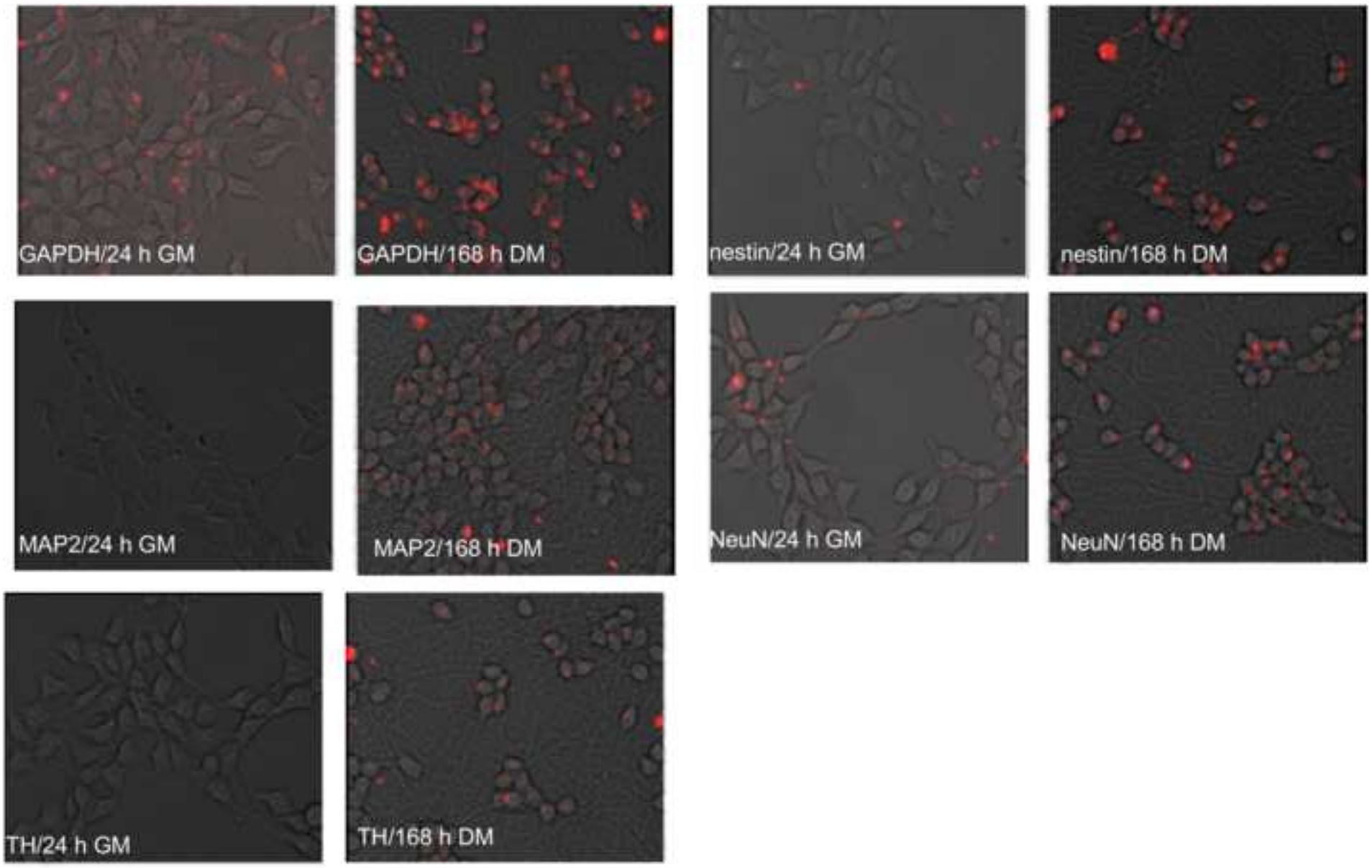

Figure_6.tiff
Click here to download high resolution image

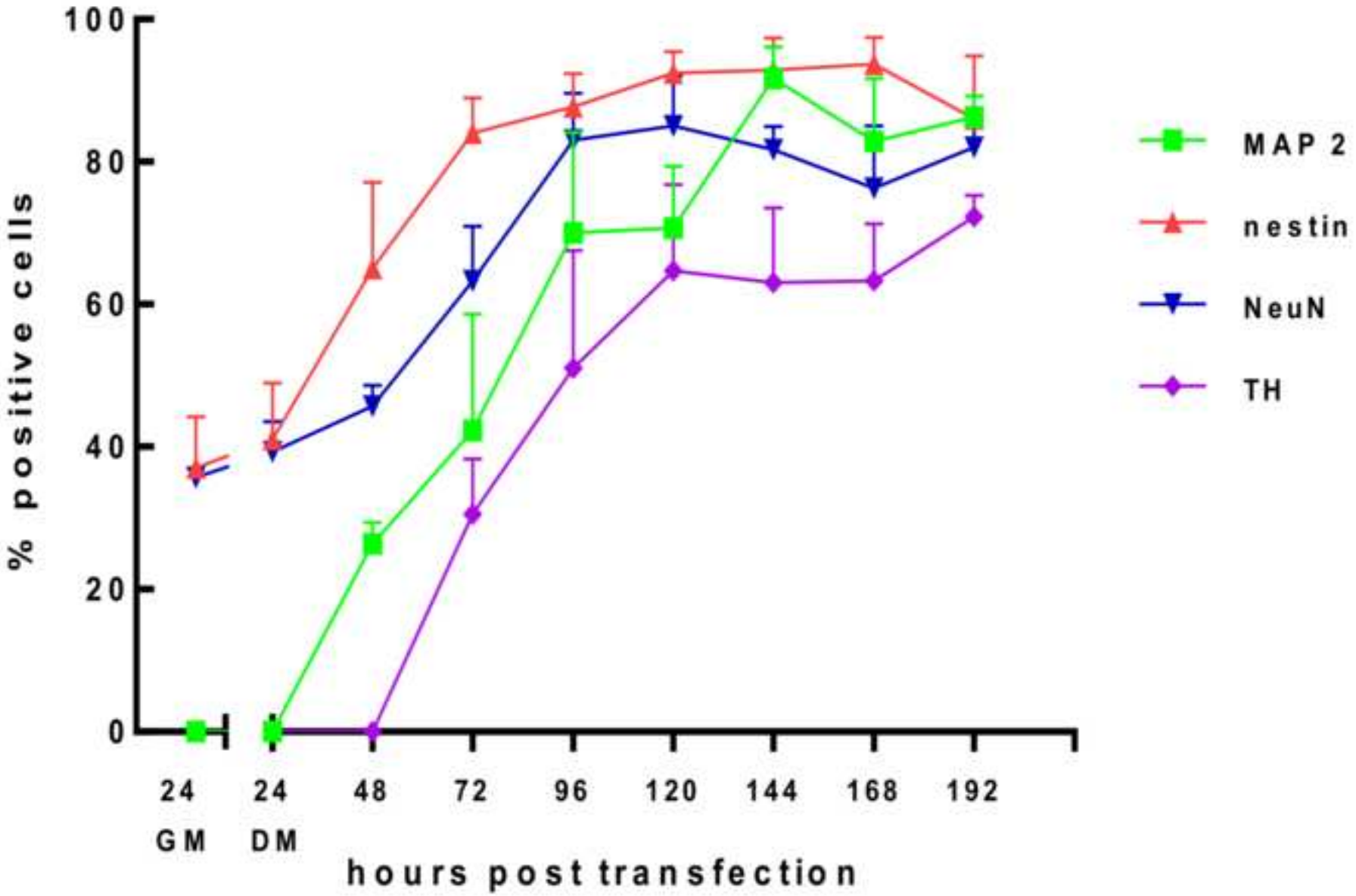

Figure_7.tiff
Click here to download high resolution image

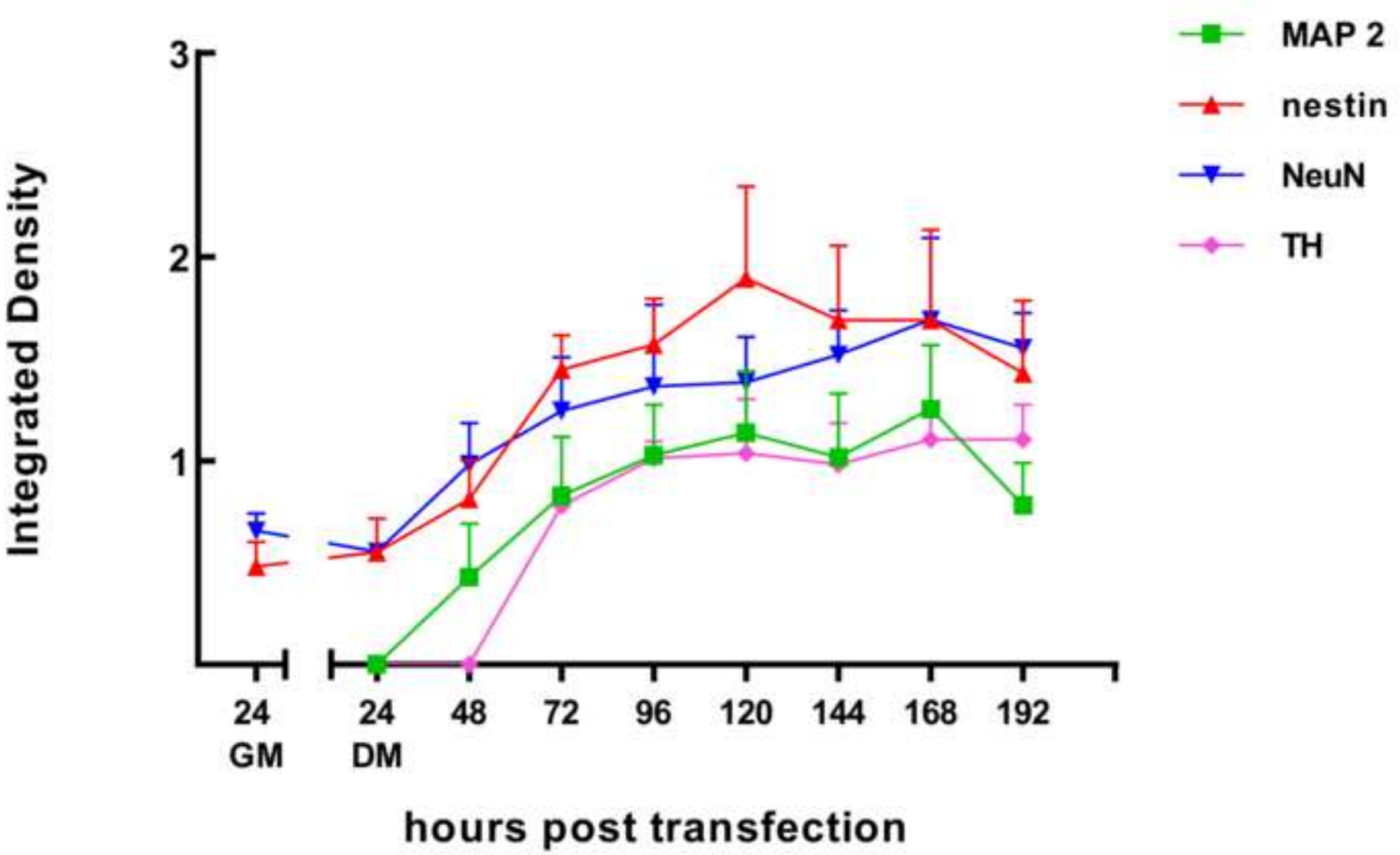

Figure_8.tiff
Click here to download high resolution image

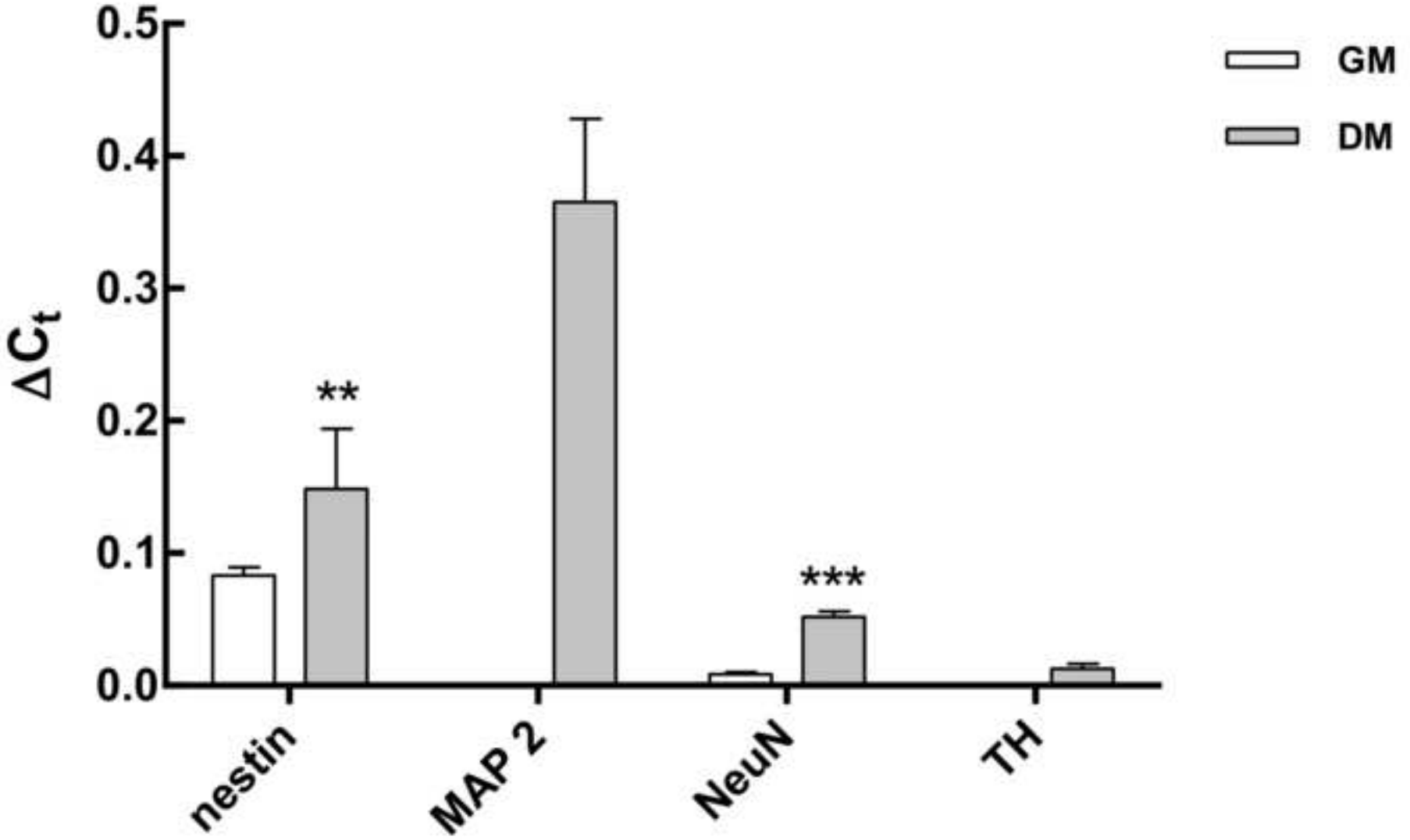

Appendix 2

Running title: Tracking stem cells inside neurospheres

Title: **Sox2 and Oct4 mRNA-expressing cells, detected by molecular beacons, localize to the center of neurospheres during differentiation**

Mirolyuba Ilieva, Martin Dufva

Department of Micro- and Nanotechnology, Technical University of Denmark, DK-2800 Kgs. Lyngby

Author contributions:

Mirolyuba Ilieva: Conception and design, Collection and/or assembly of data, Data analysis and interpretation, Manuscript writing, Final approval of manuscript

Martin Dufva: Conception and design, Financial support, Administrative support, Data analysis and interpretation, Manuscript writing, Final approval of manuscript

Corresponding Author: Martin Dufva, Department of Micro- and Nanotechnology, Technical University of Denmark, Ørsteds Plads 345 Ø, building 344, 2860 Kgs. Lyngby, Tel. +45 45 25 63 24, Fax. +45 45 88 77 62, martin.dufva@nanotech.dtu.dk, www.nanotech.dtu.dk

Acknowledgments: This work was financially supported by the Danish Research Council, Grant-no FTP-09-070568.

Key words: Molecular beacons, neurospheres, gene expression, time-laps miscroscopy, cell tracking, Oct4/Sox2.

Abstract

Neurospheres are used as a popular *in vitro* assay to measure the properties of neural stem cells. Stem cells retain their phenotype inside the spheres, and differentiate at the periphery, which provides an effective model for studying the role of stem cells in tissue heterogeneity and the effect of the cellular microenvironment. To investigate the molecular and phenotypic heterogeneity of neurospheres, molecular beacons (MBs) targeted against the stem cell markers Oct4 and Sox2 were designed, and synthesized with a 2'-O-methyl RNA backbone. Oct4 and Sox2 MBs were transfected into human embryonic mesencephalon derived cells, which spontaneously form neurospheres when grown on poly-L-ornitine/fibronectin matrix and medium complemented with bFGF. Tracking Oct4 and Sox2 gene expression using MBs and quantitative image analysis every day for seven days showed that the Oct4 and Sox2 mRNA-expressing cells cluster in the centre of neurospheres cultured in differentiation medium. In contrast, cells at the periphery of the differentiating spheres developed neurite outgrowths, indicating terminal differentiation. Neurospheres cultured in growth medium contained Oct4 and Sox2-positive cells distributed throughout the entire sphere, and no differentiating neurones. Gene expression of Sox2 and Oct4 mRNA detected by MBs correlated well with gene and protein expression measured by qRT-PCR and immunostaining, respectively. These experimental data support the theoretical model that stem cells cluster in the centre of neurospheres, and demonstrate the use of MBs for the spatial localization of specific gene-expressing cells within heterogeneous cell populations.

Introduction

Stem cells are found in most tissues and are characterized by their ability to self-renew and undergo differentiation into specialized effector cells. These properties make stem cells

crucial for maintaining tissue homeostasis, and for tissue repair after injury; they are therefore of great interest for their potential therapeutic use, and their contribution to pathological processes such carcinogenesis. Stem cells exist in either a quiescent or activated state, and have the ability to switch between these states [1]. The progeny of stem cells have also been shown to have the ability to revert back to stem cells [2].

Neural stem cells (NSCs) are tissue-specific stem cells that have the capacity for proliferation, self-renewal, and the ability to produce a large family of differentiated functional progeny [3]. NSCs exist in specialized 'niches' in the adult mammalian brain, including in humans, and continuously generate new neurons that functionally integrate into neural circuits [4]. Experimentally, long-term culture systems are based either on cell growth in monolayers, or as neurospheres, which are free floating clonal cell aggregates. *In vitro* growth of NSCs as neurospheres allows for continuous propagation of potentially heterogeneous populations of NSCs and their progenitors, and exhibit intra-clonal neural cell-lineage diversity containing, in addition to NSCs, neuronal and glial progenitors at different stages of differentiation [5]. Neurosphere formation assays are widely used as a model for neuronal development, and for studying neurogenesis [6]. They have also been used to characterize the factors and molecular mechanisms controlling stem cell properties, and to find the gene expression signatures that characterize different cell populations [7, 8].

However, the following limitations of neurospheres mean that they are insufficient on their own to definitively prove the existence of a stem cell population within the clusters [9,10]. First, multiple populations of more committed progenitor cells, as well as stem cells, can give

rise to neurospheres. Second, most of stem cells are in the quiescent stage, which is incompatible with neurosphere formation. Third, cells within the neurosphere can shuttle between quiescent and activated states, and even more committed progenitors can revert back to a more primitive state [11]. Furthermore, the neurosphere is a dynamic structure and therefore tracking cellular movements within neurospheres is important for their complete characterization, since cell-cell or cell-environment interactions may have a significant impact on NSC differentiation, and contribute to the heterogeneity of the neurosphere [12]. It is therefore important to employ time lapse microscopy when using the neurosphere forming assay, in order to accurately and confidently detect cells with stem cell characteristics within the clusters, and track their behavior when exposed to different stimuli.

With these limitations in mind, the following questions arise: do neurospheres contain cells with a stem cell signature; what is the distribution of cells within the clusters (i.e. do they formed niches); what is their fate during differentiation; and, most importantly from an experimental point of view, how can cells be tracked in real time without affecting cell viability and differentiation? Although a universal stem cell marker does not exist, one of the most meaningful measures of 'stemness' is the expression of transcription factors such as Oct4 and Sox2. However, the detection of expression of these genes in living cells usually requires fusion of Oct4 or Sox2 gene promoters with a reporter gene, such as green fluorescent protein (GFP). Instead of using genetic manipulation, transcription factor gene expression can also be detected using molecular beacon (MB) technology, in which the presence of specific mRNAs are detected after transfection [13, 14, 15, 16]. MBs are hairpin oligonucleotides with fluorescent dye on one end, and quencher attached to the other. The sequence within the loop is complementary to the desired target mRNA [17]. When the MB hybridizes to the target, the

fluorochrome separates from the quencher, and a signal can be detected. Recently, MBs targeted against Sox2 were applied to the sorting of cells isolated from mouse brains in order to generate neurospheres with high efficiency from the isolated Sox2-MB positive cells [18].

In this study we investigate, as a function of time, the location of Oct4 and Sox2 mRNA-positive cells within neurospheres grown in either growth medium (GM) or in differentiation medium (DM). For the first time we demonstrate that MBs can be used to determine the exact location of Oct4/Sox2 positive cells inside living neurospheres, allowing us to confirm a model of stem cell distribution within differentiating neurospheres.

Materials and methods

Cell culture and media

LUHMES (Lund human mesencephalic cell line, ATCC, CRL-2927) are a subclone of the tetracycline-controlled, v-myc-overexpressing human mesencephalic-derived cell line MESC2.10. For neurosphere formation, cells were cultured in cell culture flasks coated with 50µg/ml poly-L-ornitine (Sigma) overnight at room temperature (RT), followed by coating with 1µg/ml human fibronectin (Sigma) in H_2O for at least 3h at 37°C. Adherent monolayer cells were cultured in cell culture flasks coated with Geltrex®, a reduced growth factor basement membrane extract purified from murine Engelbreth-Holm-Swarm tumor (Invitrogen), diluted 1:100 in PBS for 1h at 37°C. Cultures were maintained in growth medium (GM) consisting of Advanced DMEM/F12 (Sigma) containing 2mM L-glutamine, 1x N2 supplement (Gibco), 1% penicillin/streptomycin, and 40ng/ml recombinant bFGF (Invitrogen), at 37°C in a humidified atmosphere containing 5% CO_2 .

The human embryonic stem cell (hESC) line BG01V (ATCC, SCRC-2002) was propagated on Mitomycin C-treated mouse embryonic fibroblasts (ATCC, MEF SCRC-1040) in complete GM DMEM/F12 containing 2mM L-glutamine, 1x MEM non-essential amino acid solution (Gibco), 0.1mM 2-mercaptoethanol (Sigma), 4ng/ml bFGF (Invitrogen), 5% knockout serum replacement (Invitrogen), 15% fetal bovine serum (FBS), and 1% penicillin/streptomycin. The medium was change daily. Cells were adapted to grow on Geltrex®-coated flasks and the final experiments were performed on this cell growth matrix.

Differentiation of LUHMES

Differentiation was initiated by adding DM consisting of advanced DMEM/F12, 1x N2 supplement, 2mM L-glutamine, 1mM dbcAMP (Sigma), 1µg/ml tetracycline, and 2ng/ml recombinant human GDNF (R&D system).

Molecular beacons

mRNA-targeting MBs were designed using Beacon Designer 7.9 (Premier Biosoft). To avoid cross hybridization and formation of secondary structures, the target sequence for each MB was analyzed using BLAST (http://blast.ncbi.nlm.nih.gov/) and mFOLD (downloadable from http://mfold.rna.albany.edu/). MBs were synthesized with an 2'-O-methyl RNA backbone, a Texas Red molecule attached to the 5' end, and a black hole quencher 2 (BHQ2) attached to the 3' end (Eurofins MWG Operon). The sequences of the MBs used were: Oct4 (NM_203289) - CGCUC UCAUUCACCCAUUCCCUGUU GAGCG; Sox2 (NM_003106.3) - CGCUC CGCCGCCGAUGAUUGUUAUUAU GAGCG (underlined sequences indicate the stem formation sequences). MBs were diluted in RNase/DNase free dH_2O to yield stock concentrations of 100µM, and stored at -20°C.

Transfection of MBs into LUHMES cells for monolayer growth

MBs were introduced into the cytoplasm of living cells by toxin-based membrane permeabilization using Streptolysin O (SLO, Sigma). Prior to use, SLO (1 µg/ml) was activated with Tris (2-carboxyethyl) phosphine hydrochloride solution (TCEP, Sigma) at a final concentration 5mM, for at least 30 min at 37°C. Adherent LUHMES cells were washed with Dulbecco's phosphate-buffered saline (DPBS) without Ca^{2+} and Mg^{2+}, and trypsinized for 3 min at 37°C. The cell suspension was centrifuged for 5 min at 190 x g to collect the cells. The cells were resuspended in Opti-MEM medium. 1 x 10^5 cells were incubated with activated SLO at a concentration of 17 U/ml (230ng/ml) and MBs (2µM) in a final volume 100µl for approximately 15 min. Permeabilized cells were resealed by washing in DPBS containing Ca^{2+} and Mg^{2+}, and plated on Geltrex®-coated dishes in GM. The differentiation process was started 24 h after plating by exchanging the GM with DM.

Transfection of MBs into neurospheres

1x10^5 cells were seeded on poly-L-ornitin/fibronectin-coated 12 well plates for neurosphere formation. Neurospheres were transfected 72h after neurosphere formation. Free-floating neurospheres were collected by centrifugation for 5 min at 190 x g, and then incubated with the mixture containing 17U/ml TCEP-activated SLO, and 2µM MBs for 15 min at 37°C.

Transfection of MBs into hESC

hESCs growing on MEF were treated with collagenase IV solution in DMEM/F12 at a concentration of 0.5 mg/ml (or ~200U/ml) for 45 min. When the majority of the hESC colonies detached, an appropriate volume of DMEM/F12 was added and the cell suspension was collected. Cells were centrifuged for 5 min at 200 x g at 25°C, the cells re-suspended in Opti-MEM, and the procedure for transfection of adherent LUHMES was followed. Finally, cells were plated on Geltrex®-coated dishes in complete hESC medium.

Cell viability assays

Cellular viability after SLO-mediated transfection was detected by calcein/propidium iodide staining. The medium from each well was carefully removed and cells were incubated for 30 min with 3μM calcein AM (live dye), and 2.5μM propidium iodide (dead dye), diluted in warm 1x DPBS without Ca^{2+} or Mg^{2+}.

Quantitative real-time polymerase chain reaction (qRT-PCR)

Total RNA from adherent cells or neurospheres was isolated using the RNeasy Mini kit (Qiagen). Adherent cells were lysed directly on the dish, while neurospheres were collected by centrifugation prior to the addition of lysis buffer. The lysates were collected and purified according to the manufacturer's instructions. Single-stranded cDNA was prepared from total RNA using random RT primers under standard conditions using MultiScribe Reverse Transcriptase (Applied Biosystems). The cDNA from each sample was diluted and used for RT-PCR analysis based on the Taqman assay (Invitrogen), for quantification of expression of Oct4 (ID Hs04260367_gH) and Sox2 (ID Hs01053049_s1), with GAPDH (ID Hs03929097_g1) used as an internal positive control. qPCR amplifications were performed in duplicate using the Chromo4 Real-Time PCR Detection system (BioRad) at 95°C for 10s, followed by 40 cycles of 95°C for 5s and 60°C for 30s. In order to quantify the relative expression of the gene, the C_t (threshold cycle) values were normalized to the C_t value of GAPDH (e.g $\Delta C_t = C_t$(Oct 4)-C_t(GAPDH)). All experiments included negative controls of no cDNA in the reaction mixture.

Immunocytochemistry

Neurospheres were grown in 8-well LabTek Permanox chamber slides (Nunc, Roskilde, Denmark), precoated with poly-L-ornitin/fibronectin, while monolayers were cultured on

Geltrex®-coated chamber slides. Cells were fixed in 4% (v/v) formaldehyde in PBS containing 0.05M sucrose (v/v) and 0.4mM $CaCl_2$ for 20 min, and blocked with 1% (w/v) bovine serum albumin (BSA) in PBS. Overnight incubation with primary antibody diluted in PBS containing 5% (v/v) fetal calf serum (FCS), 50mM glycine, and 0.025% (v/v) Triton X100, was followed by incubation with secondary antibody for 1h at RT. The primary and secondary antibodies used in this study are listed in Table 1. DAPI (0.1 µg/ml) was added to the buffer in the last washing step in order to stain the nuclei.

Imaging and image analysis

Phase contrast and fluorescent images were acquired on the Carl Zeiss Axio Vision 4.8.2 equipped with the ApoTome imaging system, 10x/0.3 and 40x/0.75 Plan-Neofluar objective, HXB lamp, and a Zeiss Axiocam MRm B/W camera. The same exposure time and filter set (43 HE Ds Red 538-570 nm) were used for all experiments.

Single-cell image analysis was performed using ImageJ software. A region of interest (ROI) was draw around the cell and the total fluorescence intensity was measured. The background fluorescence was detected by drawing a ROI in an area outside the cell of interest, and the total fluorescent intensity measured for this ROI. In ImageJ the total fluorescent intensity is reported as integrated density (ID), which is the sum of the values of the pixels in the selection. The background fluorescent intensity was subtracted from the cellular measurement as previously described [19].

Statistical analysis

Results are expressed as mean ± standard error of the mean (S.E.M.). qPCR results were analyzed using a Student's t-test (n=5). Analyses were performed using GraphPad Prism v6 (GraphPad Software Inc., CA, USA).

Results

LUHMES-derived neurospheres express both stem cell markers Oct4 and Sox2. According to the original description by Lotharius et al. (the depositor of the LUHMES cell line in ATCC), LUHMES cells grow as a monolayer on plates pre-coated with poly-L-ornitine/fibronectin [20]. Under these conditions, we observed consistently that the cells detached and formed free-floating neurospheres. In contrast, LUHMES cells grown on Geltrex® formed a monolayer. We therefore had the means to study LUHMES cells in monolayers and neurospheres, and compare differences in the biological properties between the two. In order to find out whether cells in neurospheres are expressing Oct4 or Sox2 mRNA respectively and how these cells reorganize during differentiation, MBs targeting Oct4 and Sox2 mRNAs were designed and synthesized with a 2'-O-methyl RNA backbone. The utility of MBs targeting Oct4 and Sox2 was first verified by introducing them into a hESC cell line, which is known to highly express Oct4 and Sox2, and is therefore a good positive control for the method. Cells were examined 24h after transfection and signal from both beacons was detected (Figure 1). MBs were next introduced into LUHMES cells by SLO-mediated membrane permeabilization. We confirmed that this method did not adversely affect cell viability within neurospheres by measuring cell viability using calcein/propidium iodide staining, which showed that cells maintain viability after SLO transfection (data not shown) with overall very low numbers of apoptotic cells observed; most of the dead cells were found

outside neurospheres, and apoptosis and necrosis was not observed in the inner core of the neurospheres. In addition to demonstrating that MBs do not promote cell death, this also confirmed that fluorescence inside the neurospheres is specific for MB's and is not autofluorescence from dead or dying cells. Monolayers of LUHMES showed >95% viability after the transfection procedure (data not shown).

The signal from the Sox2-targeting MB was detected both in cells growing as monolayer, and in cells growing as neurospheres (Figures 2A and 3A). In contrast, Oct4 was expressed in cells growing in neurospheres, but not expressed in cells growing as monolayers (Figures 2B and 3B). These results demonstrate that cells growing in neurospheres express the pluripotent state-related gene Oct4 in addition to the neuronal stem cell marker Sox2. 24h after SLO transfection, cells positive for Oct4 and Sox2 were localized on the surface of the neurosphere (Figure 2). This preference for this localization pattern is likely due to transfection being more efficient in cells localized on the surface of the nerospheres rather in the middle of the neurpheres. Cells positive for Oct4 and Sox2 mRNA, respectively, was found exclusively in the center of the spheres after 24h culture in DM. By contrast, cells positive for Oct4 and Sox2 respectively, were diffusely spread within neurospheres after 24h culture in GM (figures 2A and B). It was observed that both the number of Oct4 and Sox2-positive cells, and the absolute number of cells, increased with time in the spheres grown in GM. It was difficult to determinate the number of the respective Oct4 and Sox2 positive cells within neurospheres in DM because they formed tight clusters in the center. Neurospheres cultured in DM either proliferated (4C inset) or showed distinct signs of differentiation of cell at the rim of the spheres (Figure 4D inset). However, cells positive for Oct4 and Sox2 respectively were in all of them localized to the inner core of neurosphere (figures 2 and 4). Significant decrease in

signal intensity of Sox2/Oct4 MBs with the time was not detected suggesting stability of the reporter fluorophore to photobleaching or depletion of the transfected MB pool.

The intensity of Sox2-MB signal in adherent neurons was measured using image analysis (Figure 3C), and it was found to be high 24h after transfection, and decreased 24h after the start of the differentiation process. The signal intensity fluctuated during culture in DM, and was halved compared to initial values after 144 h. Oct4 was not expressed, precluding an equivalent analysis.

Using MB to track Oct4 mRNA expressing cells inside neurospheres during differentiation.

Oct4 mRNA expression was followed over time in neurospheres during the process of differentiation. To get obtain 3D spatial resolution, images of neuropheres were captured as z-stacks with a Zeiss Apotome and assembled into a 3D representation. As it was mentioned before, some of the neurospheres attached to the bottom of the plate when exposed to DM. The neurospheres were of varying size from small (50µm in diameter) to large (200µm in diameter). Cells located at the rim of the sphere formed long neurites and differentiated into cells with neuronal morphology (Figures 4B and 4D inset). Other neurospheres grew in size instead of showing features of differentiation (Figure 4C inset). Fusion between growing neurospheres was also seen (Figure 4A inset). In all cases, 24h after switching to DM, Oct4-mRNA positive cells were organized in the center of the neurospheres (Figure 4). The cells at the periphery of some neurospheres showed clear evidence of neural outgrowths, indicating that these cells differentiate under these conditions.

qRT-PCR and immunocytochemical analysis of stem cell markers.

qRT-PCR detection of transcript, and immunofluorescence staining of Sox2 and Oct4 proteins, were used to verify the results observed using MBs to visualize Sox2/Oct4 in LUHMES cells. qRT-PCR confirmed that neurospheres expressed both Sox2 and Oct4 mRNA (Figure 5). No significant differences in Oct4 expression levels were found between growing and differentiated neurospheres. Oct4 expression was barely detectable in either differentiating or growing LUHMES cells grown in monolayers. In contrast, significant Sox2 expression was detected in both neurospheres and adherent cells in GM. Sox2 expression dramatically decreased during differentiation of adherent cells and neurospheres, the latter showing less pronounced decreases in expression. Both Sox2-MB and qRT-PCR were therefore able to detect decreases in Sox2 expression.

Staining with antibodies targeted against Oct4 demonstrated protein expression in neurospheres, but not in monolayer cultures (Figures 6A), corroborating the qRT-PCR and MB results. Moreover, The Oct4 protein was localized in the cytoplasm of the neurosphere cells cultured in differentiation medium. Due to the high cell number in neurospheres grown in GM, it was difficult to determine the intracellular localization of the Oct4 protein under this condition. It has been described previously [21, 22] that two splice variants of Oct4 exist, Oct4A and Oct4B, with nuclear and cytoplasmic localization domains, respectively. Oct4A is restricted to stem cells, whereas Oct4B can be detected also in various nonpluripotent cell types [23]. The antibody used in this study detects both isoforms.

Sox2 protein was detected under all growth conditions with cytoplasmic localization (Figure 6B). A decrease in number of Sox2 protein-positive cells was observed in both monolayer cultures and neurospheres after exposure to DM. These results again corroborate the qRT-PCR and Sox2-MB results. Both Oct4 and Sox2-positive immunostained cells in neurospheres grown in DM showed a distribution of staining similar to the signal detected by MBs, namely being localized mainly in the center of the cluster.

Discussion

By applying MB-technology for the detection of Sox2 and Oct4 mRNA, we visualized a population of cells displaying a stem cell-like gene expression in LUHMES-derived neurospheres. Oct4 and Sox2 mRNA-positive cells were found in the center of the spheres cultured in DM, while cells in the periphery showed signs of neuronal development. Sox2 was expressed in monolayers of LUHMES cells and Sox2 mRNA expression decreased upon differentiation. By contrast, LUHMES cells grown as monolayer did not demonstrate significant Oct4 expression, suggesting that cells growing as neurospheres are subjected to different microenvironmental conditions, such as differences in growth factor levels and pO_2. This change of environment appears to induce Oct4 mRNA expression in the LUHMES cells. It is however unclear at this stage if the Oct4 positive cell population has any pluripotent characteristics.

We chose two archetypal stem cell markers as the focus of this study, Oct4 and Sox2. Oct4 (Oct3/4 or POU5F1) is a member of the Oct-family of POU transcription factors. Sox2 belongs to the Sox gene family, which are HMG box transcription factors that interact

functionally with POU domain proteins. Both genes play a key role in regulating stem cell pluripotency and differentiation. However, Sox2 is associated with multipotent and unipotent stem cells, while Oct3/4 is exclusively expressed in pluripotent stem cells. While Sox2 is expressed in adult neuronal stem cells and is retained in some populations of differentiating neurons [24, 25, 26], the expression of Oct4 in NSCs is still demonstrated in the literature [27]. A few studies clearly show that Oct4 is expressed at both the mRNA and protein level in "naïve" mouse [28, 29, 30, 31] and human neurospheres [32], and that expression drops during differentiation. The results of Massa et al. [32] based on qRT-PCR demonstrated dramatic decrease of Oct4 expression in cortical neurospheres after the first week of differentiation. In contrast striatum derived neurospheres expressed the same level of Oct4 before and after one week of differentiation [32]. This corroborates our qRT-PCR results were no significant difference in Oct4 expression in neurospheres in GM and DM was detected. Immunostaining suggest that there were overall fewer Oct 4 positive cells but also fewer cells in total in neurospheres cultured in DM as compared with corresponding neurospheres cultured in GM (Figure 6) which supports the QRT-PCR data that overall Oct4 expression is not decreasing when switching from GM to DM.

Functionally, hypoxia promotes proliferation and multipotentiality of CNS precursors [33] and promotes proliferation of human mesencephalic precursors [34]. Oct 4 expression may therefore be upregulated inside the neurosphere due to the low O_2 tension inside neuropheres [35] . It has also been shown that Oct4 is a specific target gene of hypoxia-inducible factor-2α (HIF-2α) [36], mechanistically linking how stem cells may sense hypoxic conditions in their niches, and how low pO_2 can modify stem cell function directly [37]. This is one reasonable explanation why cells under hypoxic conditions within the center of neurospheres increase expression of Oct4, in contrast to adherent LUHMES. Oct 4 induction by hypoxia would

explain why qRT-PCR data did not show decreases in Oct 4 expressions in cells in neurospheres. However, 24h post transfection, Oct4 (and Sox2) mRNA positive cells were located at the surface of the neurospheres indicating that sphere formation is triggering the induction of Oct4 while low O_2 tension might further increase the expression. The small number of cells positive for Oct4 and Sox2 mRNA respectively indicate that differentiation is suppressed inside the neurospheres.

Neurospheres cultures represent a heterogeneous system with respect to the size of the clusters, and the proliferative, differentiation, and developmental potential of parental clone-forming cells. Suslov et al. [5] proposed a hypothetical model for the relationship between neurosphere size and the maturation level of clone-forming cells. Their findings suggest that the size of a clone might reflect responsiveness to growth factors and the proliferation/differentiation status of the parental clone-forming stem/progenitor cell. In this model, cells with varying developmental potential were proposed. Clone-forming cells able to give rise to neurospheres demonstrating different stages of maturation were distinguished and proposed to have a different arrangement within the neurosphere architecture. The most immature clonogenic cells were suggested to be localized in the core of the neurosphere, while progenitor and differentiated cells were located at the shell. This hypothetical model is in agreement with the experimental results shown here (Figures 2A, 2B, and 4). Based on the MB signal it was observed that cells positive for Oct4 and Sox2 were present in the core of the neurosphere, where access of differentiation stimuli is restricted. Results from qRT-PCR and immunostaining verified the expression of Oct4 and Sox2 in the centre of neurospheres (Figure 5).

The relatively slow rate of proliferation and physiological senescence in culture make the use of human neural stem cells cumbersome under some experimental and pre-clinical settings. The immortalization of hNSC with the *v-myc* gene showed to generate stem cells with enhanced proliferative capacity, which greatly facilitates the study of NSCs in vitro and in vivo [38]. *v-myc* increases the pool of self-renewing cells and shift towards a more primitive cellular identity but without affecting the differentiation marker expression. Thus *v-myc* does not block differentiation, but delays cell cycle exit [39]

Two different studies [40, 41] aimed to show the relationship of *c-myc* to the core pluripotency factors Oct4 and Sox2. The authors demonstrated that although there are many genes that are common target for Oct4 and Sox2, the genes that *c-myc* targets only a fraction of these genes. *c-myc* binding regions also have distinctive histon marks. A functional distinction between the *myc* binding sites and the sites to which Oct4 and Sox2 binds was also revealed [40]. None of the *myc* localization sites had enchancer activity suggesting the idea that *myc* functions in a way that distinct from the other pluripotent factors [41, 42]. Expression of Oct4 in monolayer growing cells was not detected suggesting that induction of Oct4 expression in neurospheres is likely not an artefact from *v-myc* overexpression in LUHMES but is influence by the cell environment and 3D architecture of the neurosphere.

As described by Sholz et al. [43], several precursor cell markers were examined in LUHMES on d0 (undifferentiated) and d5/6 (differentiated) after differentiation indication using qPCR and immunocytochemistry. We also find that undifferentiated LUHMES expressed Sox2 mRNA and immunostaining confirmed the expression of the cognate protein. The protein was exclusively localization in the cytosol on d0 and was partly lost at d5 (Figure 6B). The results of MB Sox2 (Fig 2A) and qRT-PCR (Figure 5) measurements supported immunocytchemistry data (Figure 6B). The fact that the undifferentiated adherent LUHMES

cells retain some phenotypic features usually associated with immature cells was also confirmed by staining of polysialylated neural cell adhesion molecule (PSA-NCAM), which was positive on d0 for all cells and still positive for some cells on d5 [43].

Small structures resembling the whip-like appendages called primary cilia were frequently observed (Figure 3A and B upper bright field). Similar structures have for instance been found on stem cells. LUHMES cells are *v-myc* immortalized and thus genetically altered and perhaps it is not the best representative cellular model for study normal gene expression involved in lineage analysis and fate determination of NSCs. However, the genuine multipotentiality of the source cells (human embryonic mesencephalon tissue), their strict growth factor dependence, fast neurosphere formation, and their rapid proliferation arrest after differentiation induction, make them a suitable model system for this study. We were able to trace one particular cell population within cell cluster and thus prove the concept for usability of molecular beacons for live, time dependent, 3D monitoring of gene expression.

Cells in neurosphere are regarded as multipotent in their ability to generate all major neuronal phenotypes [32]. However, it was not possible to firmly conclude the differentiation potential capacity of the Oct 4 positive cells inside neurospheres formed by LUHMES cells. However, the expression of the Oct4 gene suggests, but does not prove, that these cells have stepped back in maturity functionally.

The signal from the Sox2-MB shows fluctuations in intensity during differentiation, but was halved at day six (Figure 3C.). This suggests that the MB was able to recover from the "open" to "closed" state. However, the signal from the Sox2-MB did not disappear

completely, suggesting that Sox2 was still expressed in differentiated neurons. These findings are supported by our qRT-PCR results and immunocytochemistry, as well as other published data [24, 25]. We were able to detect an increasing number of Sox2 and Oct4-positive cells in neurospheres grown in GM. Oct4 and Sox2 are not highly expressed genes in NSCs, an observation supported by our qRT-PCR data (Figure 5), and thus do not necessarily use up all the MBs in the intracellular pool that exists after transfection. This pool will be diluted after each cell division; however, as long as the pool of MB is larger than the pool of target mRNA, the MB will be able to emit maximum signal proportional to the amount of transcript. When the pool of MB inside the cell is smaller than the pool of target mRNA, the MB can emit a signal, but it will be weaker and not proportional to the true level of transcript. At some point, the MB will be too diluted and signal lost despite the cells expressing a high number of target molecules. It is possible that some of the Sox2 and Oct4-negative cells in neurospheres grown in growth medium (Figures 2 and 3, respectively) are indeed Sox2 and Oct4 positive. However, transfected MBs remain a very powerful tool for use with cells that do not divide extensively, such as stem cells after induction, while their use might be limited and transient in rapidly dividing cells.

The use of MBs as a tool for following differentiation is uncommon, and there are further limitations. For instance, it is difficult to know how many beacons penetrate each cell during transfection, and also whether each cell takes up an equal amount of probe [44]. However, since it was possible to observe a decrease in Sox2 expression level upon differentiation using the Sox2-MB, they may be used quantitatively for some applications (Figure 3C). However, the dynamic range of MBs appears inferior to qRT-PCR, since Sox2-MBs could only detect a 2-fold reduction in Sox2 mRNA expression, while qRT-PCR demonstrated a 20-fold decrease

in Sox2 mRNA levels. Nevertheless, MBs retain spatial information which is lacking in destructive technologies such as qRT-PCR, such that they can track over time which part of the sphere population is expressing the gene of interest, and monitor it at a single cell level. GFP–reporter constructs are widely used to track which cells express certain genes, but they require recombinant technology which is time consuming and can result in changes to the regulation of gene loci, which may not accurately reflect the wild type endogenous expression. MBs employ a rapid methodology which does not require lengthy, and sometimes impossible genetic modifications, since they measure cytoplasmic mRNA expression. However, they may inhibit translation or cause changes the metabolism of the mRNA, leading to functional differences in cells transfected with MBs. However, in our experiments targeting Sox2 and Oct4 using MBs, we did not observe any kinetic differences in differentiation or proliferation compared to untransfected cells.

Conclusion

A deep understanding of how NSCs behave *in vitro* and *in vivo* must be achieved before the practical and safe use of these cells can be applied to human beings for therapeutic benefit. Identifying the different cell types within neurospheres, and tracking these cell populations separately to determine whether there are separate stem cell niches, is the next challenge. Our study shows that cell migration and specific niche formation within neurospheres is a real dynamic process that might be influenced by many factors, including composition of the extracellular matrix, growth factors, pO_2, and neurosphere heterogeneity. Moreover we suggest a potentially very useful technique for cell detection and tracing inside 3D structures based on their gene expression profile.

Acknowledgments The financial support from the Danish Research Council, Grant-no FTP-09-070568 is gratefully acknowledged.

Disclosure of potential conflicts of interests. The authors have declared that no potential conflicts of interests exist.

References

1. Li L, Clevers H (2010) Coexistence of quiescent and active adult stem cells in mammals. Science 327: 542-545
2. Davies EL, Fuller MT (2008) Regulation of self-renewal and differentiation in adult stem cell linages: lessons from the Drosophila male germ line. Cold Spring Harb. Symp Quant Biol 73: 137-145
3. Bez A, Corsini E, Curti D, Biggiogera M, Colombo A, et al.(2003) Neurosphere and neurosphere forming cells: morphological and ultrastructural characterization. Brain Res 993: 18-29
4. Altman J (1969) Autoradiographic and histological studies of postnatal neurogenesis. IV. Cell proliferation and migration in the anterior forebrain with special reference to persisting neurogenesis in the olfactory bulb. J Comp Neurol 137: 433-457
5. Suslov O N, Kukekov V G, Ignatova T N, Steindler D (2002). Neural stem cell heterogeneity demonstrated by molecular phenotyping of clonal neurospheres. PNAS 22: 14506-14511
6. Pacey L, Stead S, Gleave J, Tomczyk K, Doering L (2006) Neural stem cell culture: neurosphere generation, microscopical analysis and cryopreservation. Nat Prot DOI: 10.1038/nprot.2006.215

7. Hill EJ, Woehrling EK, Prince M, Coleman MD (2008) Differentiating human NT2/D1 neurospheres as a versatile in vitro 3D model system for developmental neurotoxicity testing. Toxicology 249: 243-250
8. Binello E, Qadeer ZA, Kothari HP, Emdad L, Germano I M (2012) Stemness of the CT-2A immunocompetent mouse brain tumor model: Characterization in vitro. Journal of cancer 3: 166-174. 10.7150/jca.4149
9. Deleyrolle LP, Rietze RL, Reynolds BA (2008) The neurosphere assay, a method under scrutiny. Acta Neuropsychiatrica 20: 2-8, 10.1111/j.1601-5215.2007.00251.x
10. Wan F, Zhang S, Xie R, Gao B, Campos B, et al. (2010) The utility and limitations of neurosphere assay, CD 133 immunophenotyping and side population assay in glioma stem cell research. Brain Pathol 20: 877-889
11. Pastrana E, Silva-Vargas V, Doetsch F (2011) Eyes wide open: A critical review of sphere-formation as an assay for stem cells. Cell Stem Cell 10.1016/j.stem.2011.04.007
12. Wang T Y, Sen A, Behie LA, Kallos AS (2006) Dynamic behavior of cells within neurospheres in expanding populations of neural precursors. Brain Res 10.1016/j.brainres.2006.05.110
13. Bratu D, Cha B-J, Mhlanga M M, Kramer FR, Tyagi S (2003) Visualizing the distribution and transport of mRNAs in living cells. PNAS 23: 13308-13313
14. Rhee W J, Santangelo Ph J, Jo H, Bao G (2008) Target accessibility and signal specificity in live-cell detection of BMP-4 m RNA using molecular beacons. Nucleic Acids Res 10.1093/nar/gkn039

15. Santangelo Ph, Nitin N, LaConte L, Woolums A, Bao G (2006). Live-cell characterization and analysis of a clinical isolate of bovine respiratory syncytial virus, using molecular beacons. J Virol 2006; 80 (2): 682-88
16. Rhee W J, Bao G (2009) Simultaneous detection of mRNA and protein stem cell markers in live cells. BMC Biotechnology 9:e30
17. Tyagi S, Kramer FR (1996) Molecular beacons: probes that fluoresce upon hybridization. Nat Biotechnol 14: 303-8
18. Larsson HM, Tae Lee S, Roccio M, Velluto D, Lutolf P, et al.(2012) Sorting live stem cells based on Sox2 mRNA expression. PLOS ONE 7: e49874
19. Chen A, Rhee WJ, Bao G, Tsourkas A Delivery of molecular beacons for live-cell imaging and analysis of RNA. RNA detection and visualization: Methods and Protocols, Methods in Molecular Biology, vol. 714, Jefferey E. Gerst (ed.); 10.1007/978-1-61779-005-8_10
20. Lotharius J, Barg S, Wiekop P, Lundberg C, Raymon HK, et al.(2002) Effect of mutant α-synuclein on dopamine homeostasis in a new human mesencephalic cell line. J Biol Chem 277: 38884-38894
21. Atlasi Y, Mowla SJ, Ziaee SAM, Gokhale PJ, Andrews PW (2008) OCT4 spliced variants are differentially expressed in human pluripotent and nonpluripotent cells. Stem Cells 26: 3068-74
22. Lee J, Kim H K, Rho JY, Han YM, Kim J (2006) The human OCT-4 isoforms differ in their ability to confer self-renewal. J Biol Chem 281: 33554-65
23. Saxe JP, Tomilin A, Schöler HR, Plath K, Huang J (2009) Post-translational regulation of Oct4 transcriptional activity. PLOS ONE 4: 1-9

24. Pevny L H, Nicolis S K. (2010) Sox 2 roles in neural stem cells. Int J Biochem Cell Biol 42: 421-424

25. Graham V, Khudyakov J, Ellis P, Pevny L (2003) Sox 2 functions to maintain neural progenitor identity. Neuron 39: 749-765

26. Brazel CY, Limke TL, Osborne JK, Miura T, Cai J, et al. (2005) Sox 2 expression defines a heterogeneous population of neurosphere-forming cells in the adult murine brain. Aging Cell 4: 197-207

27. Liedtke S, Stephan M, Kögler G. (2008) Oct 4 expression revisited: potential pitfalls for data misinterpretation in stem cell research. Biol. Chem. 389: 845-850

28. Okuda T, Tagawa K, Qi M-L, Hoshio M, Ueda H, et al. (2004)Oct-3/4 repression accelerates differentiation of neural progenitor cells in vitro and in vivo. Mol Brain Res 132: 18-30

29. Chin J-H, Shiwaku H, Goda O, Komuro A, Okazawa H (2009) Neural stem cells express Oct-3/4. Biochem Biophys Res Commun 388: 247-251

30. Takehara T, Teramura T, Onodera Y, Kishigami S, Matsumoto K et al. (2009) Potential existence of stem cells with multiple differentiation abilities to three different germ lineages in mouse neurospheres. Stem Cells Devt 18: 1433-1440

31. Lee S-H, Jeyapalan JN, Appleby V, Noor DAM, Sottile V, et al. (2010) Dynamic methylation and expression of Oct 4 in early neural stem cells. J of Anat 217: 203-213

32. Massa D, Pillai R, Monni E, Kokaia Z, Diana A (2012) Expression analysis of pluripotency-associated genes in human fetal cortical and striatal neural stem cells during differentiation. Transl Neurosc 3: 242-248

33. Santilli G, Lamorte G, Carlessi L, Ferrari D, Rota Nodari L, et al. (2010) Mild hypoxia enhances proliferation and multipotency of human neural stem cells. PLOS ONE 5, e8575

34. Storch A, Paul G, Csete M, Boehm BO, Carvey PM, et al. (2001) Long-term proliferation and dopaminergic differentiation of human mesencephalic neural precursor cells. Exp Neurol 170: 317-325

35. Fercher A, Zhdanov AV, Papkovsky DB. O2 imaging in biological specimens. 2012, Phosphorescence Oxygen-sensitive probes, Springer Briefs in Biochemistry and Molecular biology. ISBN 978-3-0348-0525-4

36. Mohyeldin A, Garzón-Muvdi T, Quiñones-Hinojosa A (2010) Oxygen in stem cell biology: a critical component of the stem cell niche. Cell Stem Cell 2010; 10.1016/j.stem.2010.07007

37. Covello K L, Kehler J, Yu H, Gordan JD, Arsham AM et al (2006) HIF-2 alpha regulates Oct-4: effects of hypoxia on stem cell functions, embryonic development, and tumor growth. Genes Dev. 20: 557-570

38. De Filipps L, Ferrari D, Nodari L R, Amati B, Snyder E, et al. (2008) Immortalization of human neural stem cells with the c-myc mutant T58A. PLOS ONE 3(10): e3310

39. Kerosuo L, Piltti K, Fox H, Angers-Loustau A, Häyry V, et al. (2008) Myc increases self-renewal in neural progenitor cells through Miz-1. J Cell Sci 121: 3941-50

40. Chen X, Xu H, Yuan P, Fang F, Huss M, et al. (2008) Integration of external signaling pathways with the core transcriptional network in embryonic stem cells. Cell 133: 1106-17

41. Kim J, Chu J, Shen X, Wang J, Orkin SH (2008) An extended transcriptional network for pluripotency of embryonic stem cells. Cell 132: 1049-61

42. Chambers I, Tomlinson SR (2009) The transcriptional foundation of pluripoency. Development 136: 2311-22

43. Scholz D, Pöltl D, Genewsky A, Weng M, Waldmann T (2011) Rapid, complete and large-scale generation of post-mitotic neurons from the human LUHMES cell line. J Neurochem 10.1111/j.1471-4159.2011.07255.x

44. Desai H V, Voruganti I S, Jayasuriya C, Chen Q, Darling EM (2012) Live-cell, Temporal gene expression analysis of osteogenic differentiation in adipose-derived stem cells. Tissue Eng 10.1089/ten.tea.2012.0127

Table 1. The primary and secondary antibodies used within this study.

Antibody	Host	Working dilution	Source	Cat No.
Primary antibodies				
Oct4	Rabbit	1:400	Cell Signaling Technology	#2750
Sox2	Goat	1:100	Santa Cruz Biotechnology, Inc.	Sc-17320
Secondary antibodies				
Alexa Fluor 488 anti-rabbit IgG	Goat	1:1000	Life Technologies	A-11008
FITC-conjugated anti-goat IgG	Rabbit	1:40	Dako Cytomation	F025002

Figures

Figure 1. Detection of A. Oct4 and B. Sox2 expression in human embryonic stem cells BG01V using MBs.

Figure 2. Detection of stem cells markers in neurospheres using MBs targeting **A** Sox2, and **B** Oct4. After 72h growth in GM, neurospheres were SLO-transfected with MBs for Oct4 and Sox2. Cells were kept in GM until 24h post-transfection, at which time the medium was switched to either GM or DM. Gene expression was detected 24, 48, 72, and 96h (i.e. 24, 48, and 72h after differentiation induction) after transfection.

Figure 3. Detection of Sox2 (**A**) and Oct4 (**B**) in adherent LUHMES using MBs. Brightfield and fluorescent photomicrographs taken 24h after transfection and 144h after induction of differentiation. **C.** Integrated density of Sox2 targeting MBs as function of time. Data is presented as mean ± S.E.M.

Figure 4. Tracking Oct4-positive cells inside neurospheres during differentiation. **A** 24h after initiation of differentiation, Oct4-positive cells are still diffusely spread in some neurospheres, while in others they start localizing to the inner core. **B** 48h later the neurospheres attach to the matrix and the cells located around the rim start to form neurites. Neurospheres demonstrate varying sizes and differentiation potential. **C** Fusion between neurospheres was seen, together with neurite formation. **D** In both cases, the MB-detected Oct4-positive cell population was located in the middle of neurospheres. Images were acquired with ApoTome Imaging system, 10x/0.3 Plan Neofluar objective and DsRed filter set.

Figure 5. qRT-PCR analysis of mRNA levels of Oct4 and Sox2 under different growth conditions. Cells grown as neurospheres in GM (white bar, N/G), cells grown as neurospheres in DM (gray bar, N/D), cells grown as monolayer in GM (hatched bar, A/G), and cells grown as monolayer in DM (black bar, A/D). Expression was normalized to GAPDH mRNA expression. Data is present as mean ± S.E.M. n = 5 ***$p<0.001$, ****$p<0.0001$ compared to monolayer cell growth, ++++$p<0.0001$ compared to cells cultured in growth medium.

Figure 6. Immunocytochemistry of **A** Neurospheres and adherent LUHMES stained for Oct4. Expression at the protein level was detected in neurospheres under both GM and DM culture conditions. Oct4-positive cells are diffusely spread within neurospheres when cultured in GM, and localized in the center of neurospheres in DM. Oct4 expression at the protein level was not detected in cells growing as a monolayer. **B** Immunostaining for Sox2. The distribution of Sox2-positive cells inside neurospheres in DM mirrored the distribution of MB-detected Sox2-positive cells, being inner core localized. Adherent cells cultured in GM highly

expressed Sox2 with cytoplasmic localization of the protein. During differentiation, protein levels decreased, which positively correlated with the data from qRT-PCR.

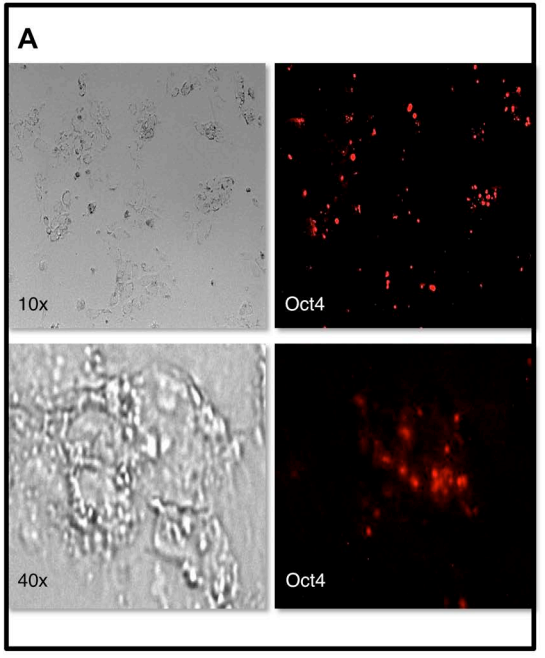
A
10x
Oct4
40x
Oct4

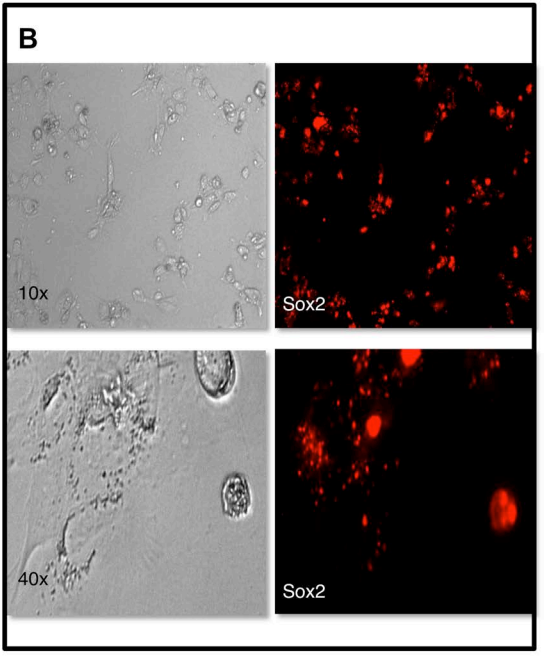
B
10x
Sox2
40x
Sox2

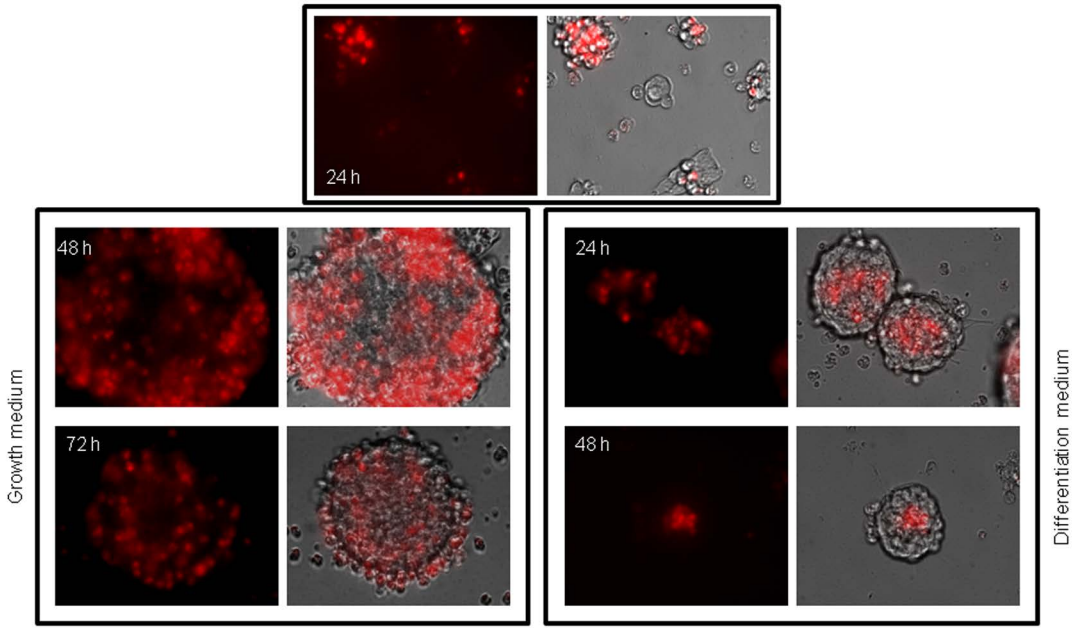
24 h
48 h
72 h
24 h
48 h
Growth medium
Differentiation medium

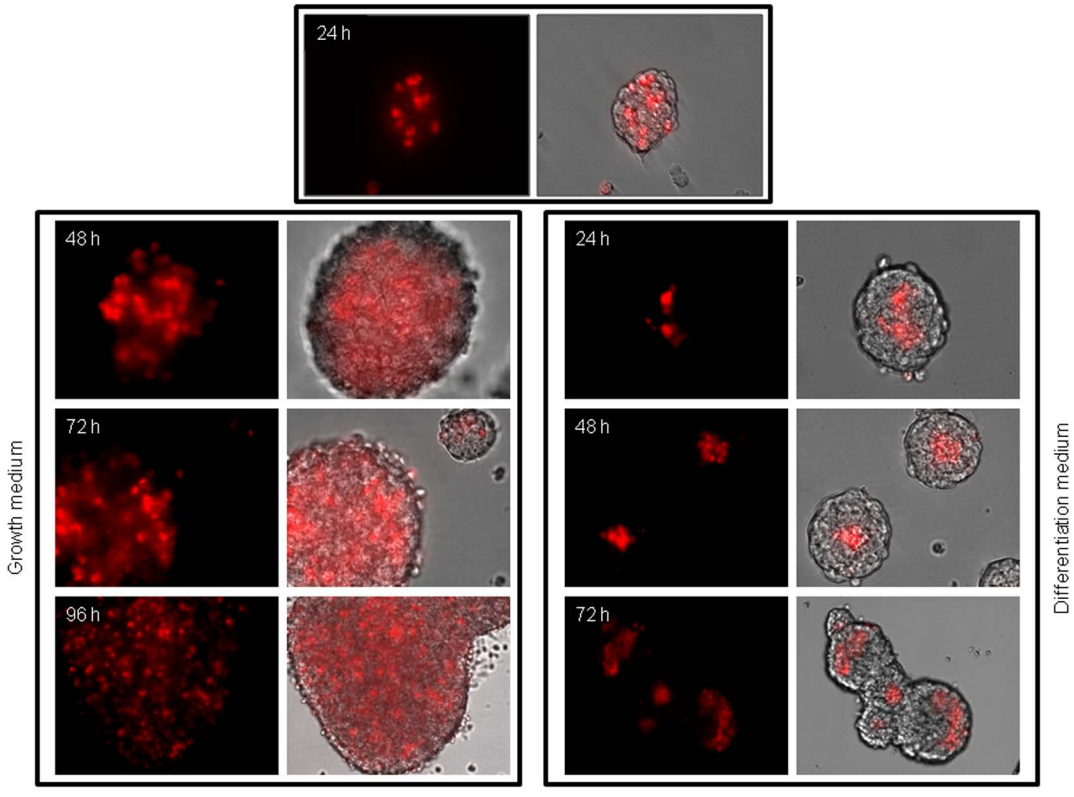
24 h
48 h
72 h
96 h
24 h
48 h
72 h
Growth medium
Differentiation medium

A.

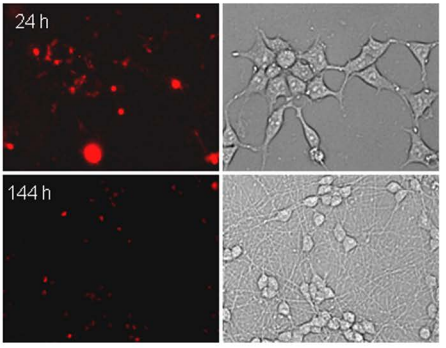
24 h
144 h

B.

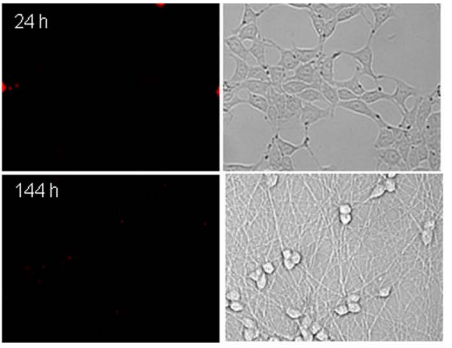
24 h
144 h

C.

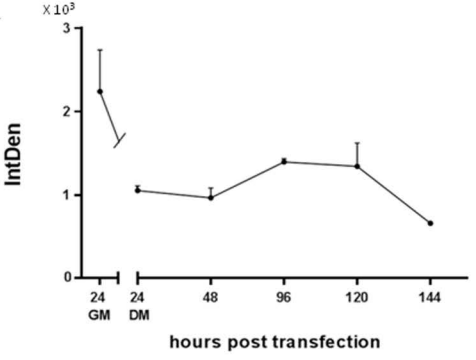
X 10³
3
2
1
0
IntDen
24
GM
24
DM
48
96
120
144
hours post transfection

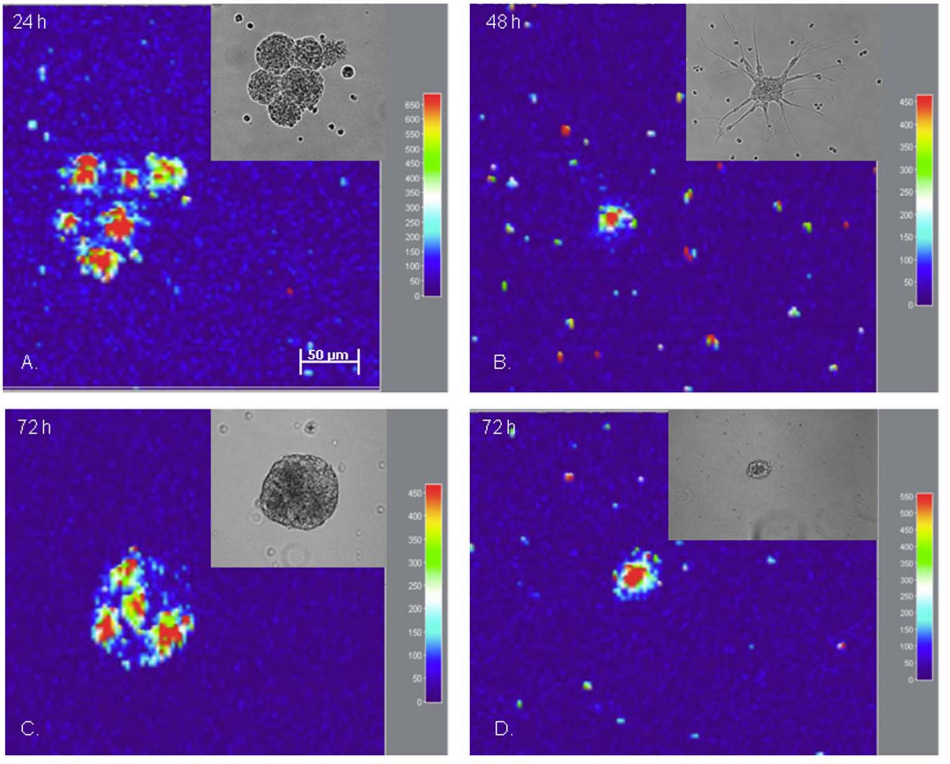
24 h
A.
50 µm
48 h
B.
72 h
C.
72 h
D.

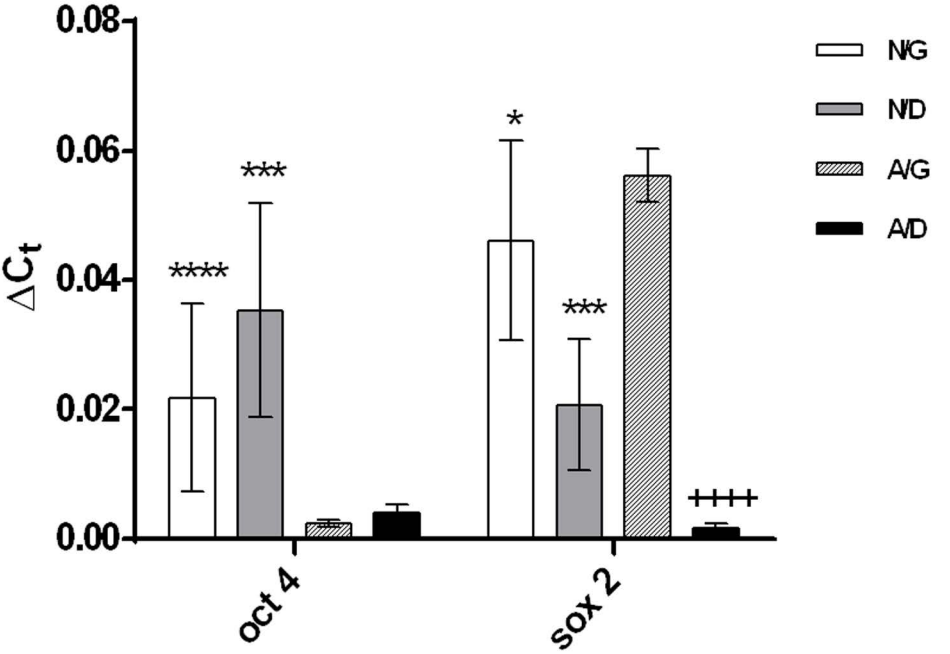
0.08
0.06
0.04
0.02
0.00
ΔCt
****
***
*
***
++++
oct 4
sox 2
N/G
N/D
A/G
A/D

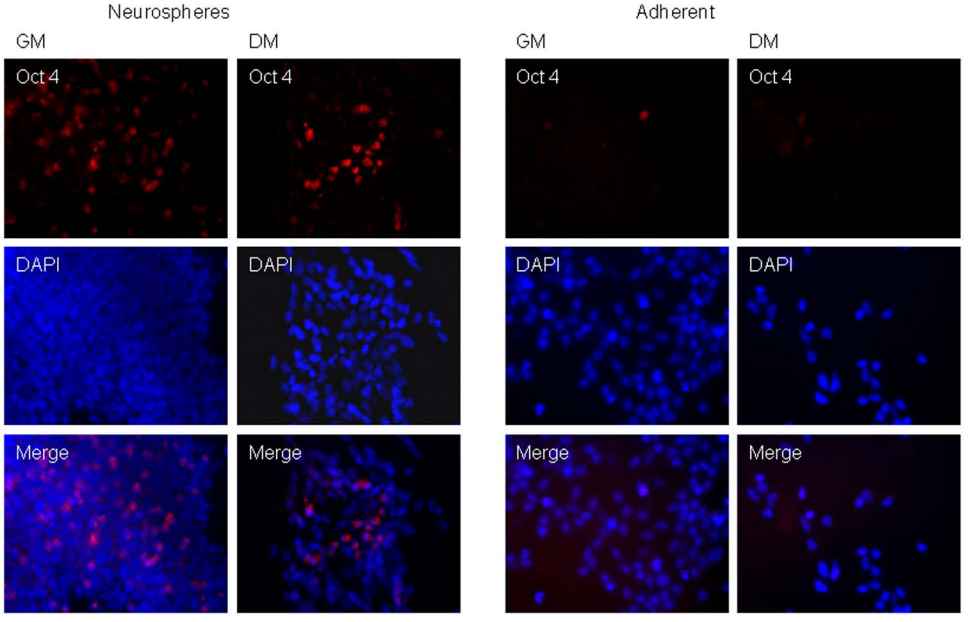
Neurospheres
Adherent
GM
DM
GM
DM
Oct 4
Oct 4
Oct 4
Oct 4
DAPI
DAPI
DAPI
DAPI
Merge
Merge
Merge
Merge

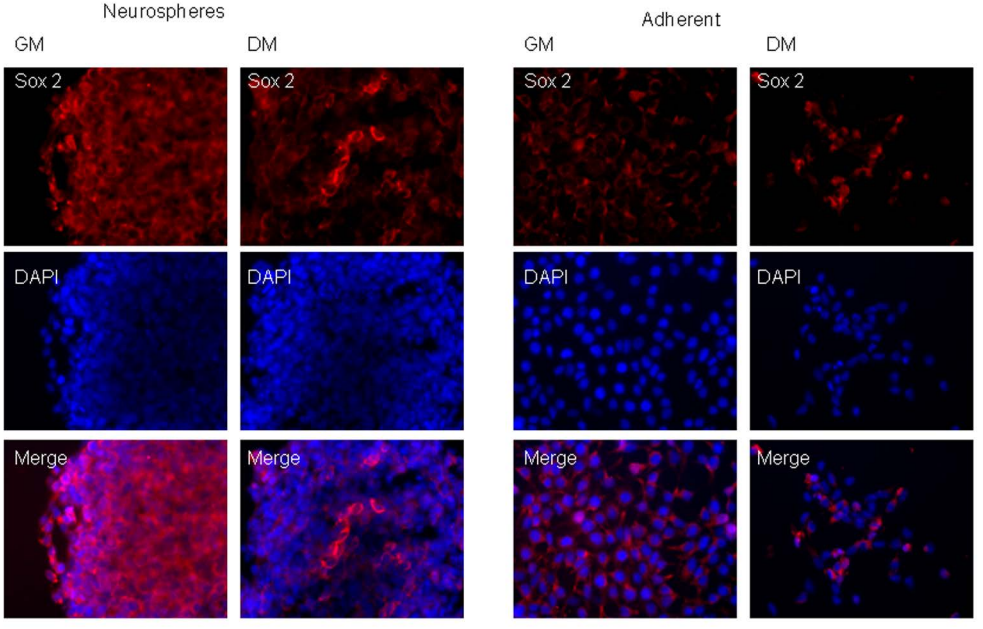
Neurospheres
Adherent
GM
DM
GM
DM
Sox 2
Sox 2
Sox 2
Sox 2
DAPI
DAPI
DAPI
DAPI
Merge
Merge
Merge
Merge

Appendix 3

Molecular beacon technology based sensor for real-time detection and tracking neural stem cell differentiation

Mirolyuba Ilieva, Paolo Della Vedova, Martin Dufva

Introduction

Molecular beacon (MB) technology is based on fluorescent resonance energy transfer (FRET) and complementary pairing principles. A stem-loop forming oligonucleotide with fluorochrom on one side and quencher on the other is a highly specific and sensitive sensor which can be introduced inside living cell. Hybridizing with specific target "closed" MB became in "open" state when the fluorescent dye and quencher separate and signal occurs. [1] Thus, it allows detection and monitoring of gene expression and following fundamental cellular events like differentiation, regeneration, and cancer genesis.

Materials and Methods

Molecular beacon probes for stem cell marker Sox 2, marker for differentiated neurons Tyrosine hydroxylase (TH) and house-keeping gene GAPDH were design and synthesized as DNA oligos or 2'-O-methyl RNA backbone and stem length of 5 bp.

Human mesencephalic cell line (LUHMES) were grown adherently on Matrigel or as neurospheres on fibronectin in medium containing bFGF. They can differentiate into morphologically and biochemically mature dopamine-like neurons. MBs were derived inside cells by Streptolysin O based membrane permeabilization [2]. 24 h after transfection of MB, growth medium was switched to differentiation medium. Gene expression was detected on different time points after transfection by fluorescent microscopy.

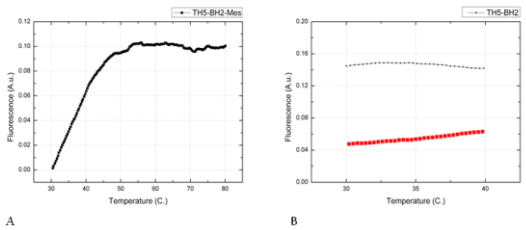

Fig 1. A. Melting and B. Hybridization curves of BHQ2/TAMRA DNA molecular beacon, 5 bp stem length.

Manuscript received August 10, 2012. This work was supported in part by the FTP project 09-070568. M.I, P. D. V., and M. D. are with with the DTU Nanotech, Technical University of Denmark, Oersted Plads, Building 345B, Kgs. Lyngby, DK-2800, Denmark e-mail: miil@nanotech.dtu.dk

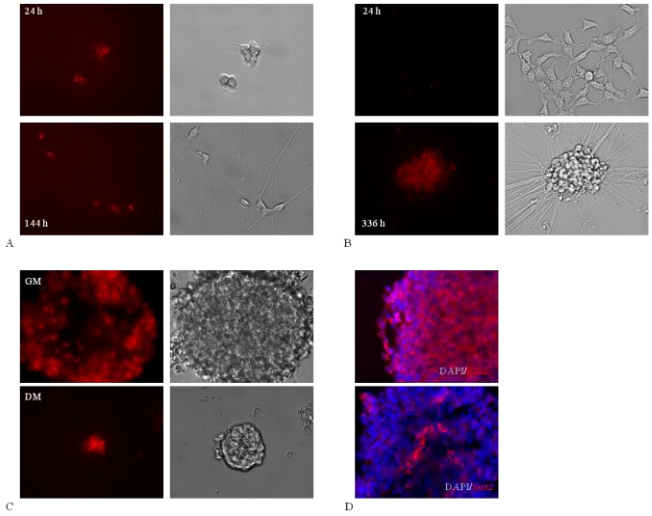

Fig 2. Detection of gene expression inside living cells. A. GAPDH – house-keeping gene with constant expression. MB – DNA/Texas red/BHQ2. B. Tyrosine hydroxylase (TH) – marker for specialized neural cells. Expression increasing upon differentiation. MB - 2'-O-methyl RNA backbone/Cy3/BHQ2. C. Sox 2 expression in neurospheres. Neural stem cells are localized in the center of the neurosphere. MB – DNA/Texas red/BHQ2. D. Immunostaining for Sox 2.

Results

A two-fold increase in the signal in the presence of the complementar oligo was detected (Fig 1B). A melting point of the stem of 40°C verifies that spontaneous opening of MB is not occurring inside the cells (Fig. 1A). The signal inside living cells is detectable 1 h after transfection and it is stable for up to 14 days. The MBs sensors were able to track gain-of expression of neural marker TH and loss-of-expression of stem cell marker Sox2, whereas house-keeping gene expression remains constant (Fig. 2). This suggests that the MBs can "regenerate" from open hybridized state to closed non-hybridized state inside cell. The gene expression change recorded with molecular beacon was confirmed by qPCR and immunostaining for the expression on protein level. The results suggest that MBs are simple to use sensors inside living cells and will be useful for studying transient and dynamic gene expression.

References

[1] S. Tyagi, FR. Kramer, "Molecular beacons: probes that fluoresce upon hybridization," *Nature Biotechnology*, 1996 Mar; 14(3): 303-8.

[2] A.K. Chen, et al., "Delivery of Molecular Beacons for Live-Cell imaging and Analysis of RNA," J. Gerst (ed.), RNA Detection and Visualization: Methods and protocols, Methods in Molecular Biology, vol 714.

Nanomachine based optical sensors

P. Della Vedova, M.Ilieva, O.Hansen and M.Dufva.

Introduction

Molecular beacons (MBs) are powerful biological probes that exhibit high selectivity and affinity and can be easily fabricated [1]. One of the major limitations of these probes is the inability to be restored to the sensing state after a hybridization reaction. Sensor regeneration is critical for online sensing.

Here we present a novel MB configuration, comprising a gold nanoparticle (GNP) acting simultaneously as a fluorescence quencher [2] and an actuator (nanosized heater) which is controlled remotely by an external microwave field [3]. Localized heating allows for control of the structure and chemical state of the MB. The novel gold-based MB nanomachine will allow regeneration and calibration of MB by melting hybridized targets off the machine. (Fig.1, left)

Materials and Methods

Gold nanoparticles are conjugated through an aminogroup to a MB having a flourochrome at the opposite end. MBs designed this way are carefully characterized by melting and hybridization curves to ensure optimal functionality (Fig. 2,B). Stem cells are transfected with these MBs and cultured in a custom made microfluidic system that includes an actuation coil and enables simultaneous observation of the fluorescence signal under the microscope (Fig.1, right).

Results

The interaction between the EM field and GNPs creates eddy currents on the surface of the metal particle, which becomes a highly localized point source of heat. Our simulations show that the heat is highly localized in the particle surroundings and the heat dissipates within 1-2 particle radii (Fig.2, A).

Our experiments show an increase in fluorescence after irradiation of the MBs (Fig2, C-D).

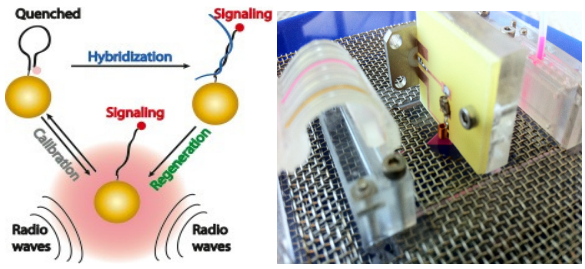

Fig. 1. Working principle of the nanomachine (left) and close-up of the microfluidic setup used in the experiment (right).

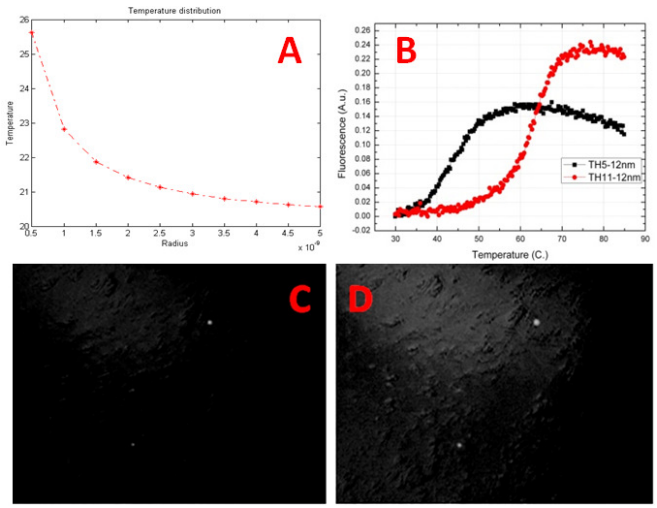

Fig. 2. (A)Temperature distribution around the nanoparticle, (B) melting curves of MB, (C-D) Fluorescence signal before (left) and after (right) irradiation.

The increase in fluorescence could be explained by the selective heating of the GNPs that causes melting the stem of the MB and therefore a displacement of the fluorophore quencher pair (Fig1. right).The control experiment has been performed using the same setup with a different kind of MBs in which the gold nanoparticle has been replaced by an organic quencher. In this case, no increase in fluorescence signal has been detected after irradiation with the EM field. Irradiation tests performed on liquid solutions containing different salt concentrations, show that bulk heating of the medium is not sufficient for MBs melting.

This tool opens new possibilities such as following down regulation of gene expression in living cells, something that cannot be done today because of technical limitation.

Manuscript received August 10, 2012. This work was supported by FTP grant number 09-070568.

P. Della Vedova, M. Ilieva, O. Hansen and M Dufva are with DTU Nanotech, Kgs.Lyngby, DK-2800, Denmark(phone: +45258159; e-mail: pdve@ nanotech.dtu.dk).

References

[1] S. Tyagi et al., «Molecular beacons: Probes that fluoresce upon hybridization», *Nat. Biotechnol.*, vol. 14, n°. 3, pagg. 303–308, Mar 1996.

[2] Lakowicz, J. R. *Principles of Fluorescence Spectroscopy,* 2nd ed.; Springer: New York, 1999.

[3] K. Hamad-Schifferli, et al., «Remote electronic control of DNA hybridization through inductive coupling to an attached metal nanocrystal antenna», *Nature*, vol. 415, n°. 6868, pagg. 152–155, Gen 2002.